LBL-12322

Lawrence Berkeley Laboratory
UNIVERSITY OF CALIFORNIA

Physics, Computer Science & Mathematics Division

EXTENSION OF GLIMM'S METHOD TO THE PROBLEM OF GAS FLOW IN A DUCT OF VARIABLE CROSS-SECTION

Simon KaMan Fok
(Ph.D. thesis)

December 1980

Prepared for the U.S. Department of Energy under Contract W-7405-ENG-48

DISCLAIMER

EXTENSION OF GLIMM'S METHOD TO THE PROBLEM OF GAS FLOW IN A DUCT OF VARIABLE CROSS-SECTION*

Simon KaMan Fok

Ph.D. Thesis

December 1980

Department of Mathematics and Lawrence Berkeley Laboratory
University of California
Berkeley, California 94720

*This work was supported in part by the Director, Office of Energy Research, Office of Basic Energy Sciences, Engineering, Mathematical, and Geosciences Division of the U.S. Department of Energy under contract W-7404-ENG-48.

Extension of Glimm's Method to the Problem of Gas Flow in a Duct of Variable Cross-section

by

Simon KaMan Fok

Abstract

Various numerical methods for extending Glimm's scheme to solve a nonlinear hyperbolic system of partial differential equations in one space variable of the form $\bar{u}_t + \bar{f}_x(\bar{u}) = \bar{g}(\bar{x},u)$ are described. The reason for considering Glimm's scheme rather than some finite difference schemes is because of its ability to pick out the correct weak solution of a given hyperbolic system of partial differential equations without requiring it to be written in conservation form. The numerical schemes we shall look at are (1) Generalized Glimm's scheme, (2) Glimm's scheme with Sod's operator splitting method, and (3) Liu's scheme. In particular, the inhomogeneous Burgers' equation and the problem of radial symmetic gas flow will be studied, and Sod's operator splitting method will be seen to be best among the three numerical schemes. Finally, gas flow in a duct of variable cross-section is discussed together with the classical Chisnell's formula which describes the changes in the speed of the shock with respect to the varying cross-sectional area. It will be shown that incorporating Chisnell's formula into Glimm's scheme (with operator splitting) and Liu's scheme can be done easily; moreover, the resulted schemes are

best in treating shock propagation problem in a duct of montonically decreasing and increasing cross-sectional area respectively. Thus, the case of a variable area duct can be handled by hybridizing Glimm's scheme (with operator splitting and Chisnell's formula) and Liu's scheme (with Chisnell's formula).

Acknowledgements

First, I would like to thank my thesis adviser Professor Alexandre J. Chorin whose constant encouragement is the key factor in the completion of this thesis. Also, I would like to thank him and Professor Paul Concus who made the two years stay in Lawrence Berkeley Laboratory both stimulating and enjoyable.

I would like to thank Dr. S.S. Lin, Dr. Philip Colella, Dr. James Lavita, and Professor Ole Hald whose advice has helped tremendously. Finally, I would like to thank Professor T. P. Liu without whom the programming of Liu's scheme would have proved impossible.

Lastly, my thanks go to Betty who make the completion of this thesis possible.

Table of Contents

Acknowledgements i

Table of Contents ii

Introduction 1

Chapter 1 Inhomogeneous Burgers' Equation

1.1 Preliminaries 5

1.2 Generalization of Glimm's Scheme 6

1.3 The Riemann Problem 8

1.4 Solution of the Riemann Problem for $u_t + (\frac{u^2}{2})_x = g(x,u)$ 9

1.5 The Method of Operator Splitting 20

1.6 Test Problems 22

1.7 Conclusions 30

Chapter 2 Radially Symmetric Gas Flows

2.1 Preliminaries 31

2.2 Liu's Construction 33

2.3 Operator Splitting 38

2.4 Point Blast Explosion 40

2.5 Test Problem 44

2.6 Conclusions 47

Chapter 3 Shock Propagation Down a Duct of Variable Cross-section

3.1 The Classical and Generalized Chisnell Formula 48

3.2 The Chisnell formula and the Numerical Schemes of Glimm and Liu 55

3.3 Test Problems 57

3.4 Conclusions 66

Chapter 4 Conclusions and Discussions 67

Illustrations 70

Bibliography 113

Introduction

We wish to extend Glimm's scheme for solving the following nonlinear hyperbolic system of partial differential equations in one space variable:

$$\bar{u}_t + \bar{f}_x(\bar{u}) = \bar{g}(x,\bar{u}) \quad , \tag{1}$$

with

$$\bar{u}(x,0) = \bar{u}_o(x) \quad , \tag{2}$$

where $\bar{u}(x,t)$: $Rx[0,\infty) \rightarrow R^N$ is the solution vector to be determined, and $\bar{f}$: $R^N xR^N$ is a C^2 mapping whose Jacobian matrix $D_u F = A(u)$ has N real distinct right eigenvalues $\lambda_1(u) < \ldots < \lambda_N(u)$ known as the characteristic velocities for system (1). Finally, $\bar{g}(x,\bar{u})$: $RxR^N \rightarrow R^N$ is called the source term for the problem, and the function $\bar{u}_o$: $R \rightarrow R^N$ is the given initial datum. If the source term $\bar{g}=0$, then (1) is called a hyperbolic system of conservation laws.

The following three examples are the special cases of (1) that we shall study closely in this thesis. Chapter 1 will concentrate on example 1 while examples 2 and 3 will be dealt with in chapters 2 and 3 respectively. Moreover, we are interested in each case initial data that immediately resolves into a shock wave.

Example 1. The inhomogeneous inviscid Burgers' equation:

$$\frac{\partial u}{\partial t} + \frac{\partial \frac{u^2}{2}}{\partial x} = g(x,u) \quad . \tag{3}$$

The single characteristic velocity for (3) is $\lambda(u)=u$.

Example 2. The best-known physical example of a hyperbolic system of the form (1) is the set of equations for an inviscid, non-heat-conducting, radially symmetric gas flow:

$$\frac{\partial}{\partial t}\begin{bmatrix}\rho\\ m\\ e\end{bmatrix} + \frac{\partial}{\partial x}\begin{bmatrix} m\\ \frac{m^2}{\rho}+p\\ \frac{m(e+p)}{\rho}\end{bmatrix} = \frac{(1-\alpha)}{x}\begin{bmatrix} m\\ \frac{m^2}{\rho}\\ \frac{m(e+p)}{\rho}\end{bmatrix} \qquad (4)$$

Here ρ is the density of the gas, u is the velocity, $m=\rho u$ is the momentum, p is the pressure, e is the energy per unit volume, α is a constant which is equal to 2 for cylindrical symmetry and 3 for spherical symmetry. Finally, we may write

$$e = \frac{p}{\gamma-1} + \frac{\rho u^2}{2} \quad ,$$

where γ is the ratio of specific heats (a constant greater than 1). The three characteristic velocities for the system are

$$\lambda_1(u) = u - c \quad , \lambda_2(u) = u \quad , \lambda_3(u) = u + c \quad , \qquad (5)$$

where $c = (\frac{\gamma p}{\rho})^{1/2}$ is the sound speed.

Example 3. Another well-known physical example is one-dimensional gas flow in a duct of given cross-sectional area A(x), where A(x) does not vary too rapidly. The equations are

$$\frac{\partial}{\partial t}\begin{bmatrix}\rho\\ m\\ e\end{bmatrix}+\frac{\partial}{\partial x}\begin{bmatrix}m\\ \frac{m^2}{\rho}+p\\ \frac{m(e+p)}{\rho}\end{bmatrix}=-\frac{A'(x)}{A(x)}\begin{bmatrix}m\\ \frac{m^2}{\rho}\\ \frac{m(e+p)}{\rho}\end{bmatrix} \tag{6}$$

Again, the characteristic velocities are given by (5).

The numerical schemes we shall use are: (1) A straightforward generalization of the random choice method introduced by Glimm [6] for a strictly hyperbolic system of conservation form and developed as a numerical method by Chorin[2]. (2) Glimm's scheme with Sod's operator splitting method[13]. (3) Liu's scheme[9]. One major advantage of such numerical schemes over other finite difference schemes is that they have the property of keeping shock fronts perfectly sharp.

The thesis is divided as follows. In chapter one, we shall describe a most natural way of generalizing Glimm's method to (1); also, Sod's operator splitting method will be introduced. As an illustration, we shall solve the inhomogeneous Burgers' equation using both methods, one of the major conclusion is that the generalized Glimm's method is not practical. In chapter two, Liu's scheme will be introduced. As an example, we look at the problem of a point blast explosion where again Sod's operator splitting method is shown to be best. Finally in chapter three, the classical formula of Chisnell[1] which describes the speed of a shock relative to the cross-sectional area A(x) of a variable area duct will be rederived in a more general setting. In general, Chisnell's formula is only good as a local result. This, however, fits into the structure of Glimm's scheme and Liu's scheme very well because these two schemes typically use local results from solu-

tions of Riemann problems (see section 1.3) to advance from one time level to the other. It will be seen that appropriate hybridization of Chisnell's formula with both Liu's scheme and Glimm's scheme with operator splitting is ideal for handling the problem of shock propagation in a variable area duct.

Then using numerical experiments in the following three chapters, we shall try to justify the following recommedations:

Problem	Recommeded numerical scheme
Inhomogeneous Burgers' equation	Glimm's scheme with operator splitting
Spherically symmetric gas flow	Glimm's scheme with operator splitting
Gas flow in a monotonic decreasing area duct	Glimm's scheme with operator splitting and Chisnell's formula
Gas flow in a monotonic increasing area duct	Liu's scheme with Chisnell's formula
Gas flow in a duct of variable cross-sectional area $A(x)$	For $A'(x)<0$, use Glimm's scheme with operator splitting and Chisnell's formula; for $A'(x)>0$, use Liu's scheme with Chisnell's formula

Chapter 1 Inhomogeneous Burgers' equation

1.1 Preliminaries

One of the most natural way to extend Glimm's scheme for solving the partial differential equations (1) is to follow closely his construction for a hyperbolic system of conservation laws

$$\bar{u}_t + \bar{f}_x(\bar{u}) = 0 \quad . \tag{1.1.1}$$

The only obstacle is that finding an exact solution to the Riemann problem corresponding to (1) proves much more difficult than to the Riemann problem coresponding to (1.1.1). This will be demonstrated vividly for the inhomogeneous Burgers' equation. Also, since Glimm's scheme for the hyperbolic system (1.1.1) is at best first order accurate, it is doubtful whether an exact solution to the Riemann problem is warranted. This leads us to Sod's operator splitting method which does <u>not</u> solve the Riemann problem corresponding to (1) exactly but has the advantage of fitting into the framework of Glimm's construction without requiring a lot more computational time. In section 1.6, test problems will indeed show that Glimm's scheme with operator splitting is superior than a straightforward generalization of Glimm's scheme for the inhomogeneous Burgers' equation.

1.2 Generalization of Glimm's scheme

Consider the nonlinear system of equations (1) with initial data (2). Divide time t into intervals of length k, and let h be the spatial increment. A discrete approximate to the solution $\bar{u}(x,t)$ is to be computed at the points (ih,nk) and $((i+1/2)h,(n+1/2)k)$ for $|i|$, $n=0,1,2,\ldots$. Denote the approximate values by $\bar{u}_i^n \simeq \bar{u}(ih,nk)$, $\bar{u}_{i+1/2}^{n+1/2} \simeq \bar{u}((i+1/2)h,(n+1/2)k)$, so that initially

$$\bar{u}_i^o = \frac{1}{h}\int_{ih}^{(i+1)h} \bar{u}_o(x)\,dx, \qquad |i|=0,1,2\ldots.$$

Suppose $\bar{u}_i^n$ has already been computed for all i, then $\bar{u}_{i+1/2}^{n+1/2}$ is computed from $\bar{u}_i^n$ and $\bar{u}_{i+1}^n$ by a random procedure described as follows.

Let $\bar{v}(x,t)$ be the solution to the Riemann problem of (1) defined by the initial data

$$\bar{u}(x,0) = \begin{cases} \bar{u}_i^n & \text{for } x<0 \\ \bar{u}_{i+1}^n & \text{for } x>0 \end{cases} \qquad (1.2.1)$$

Then $\bar{u}_{i+1/2}^{n+1/2} = \bar{v}(\theta_n h, k/2)$, where θ_n is a random variable equidistributed in the interval $[-1/2, 1/2]$. Similarly, $\bar{u}_i^{n+1}$ can be computed from $\bar{u}_{i+1/2}^{n+1/2}$ and $\bar{u}_{i-1/2}^{n+1/2}$ by this procedure via the use of another random variable $\theta_{n+1/2}$. This completes Glimm's construction.

As usual, the choice of h and k must satisfy the Courant-Fredrichs-Levy condition so that the correct problem is solved.

Finally, to ensure better results, the sequence of random variables is chosen by a procedure due to Colella[3].

When the source term is identically zero in (1), Glimm showed that the approximate solution tends to a weak solution of the corresponding conservation laws under some appropriate conditions. In order for this construction to be useful when the source term is present, a method of solving the Riemann problem is essential. Presumably, the solution of the Riemann problem for (1) is difficult, at least not much easier than the general initial value problem. This fact is in sharp contrast to the case when the source term $\overline{g}$ is zero. In next section, we will outline a method for solving Riemann problems.

1.3 The Riemann problem

We are concerned with solving (1) with the special initial data:

$$\bar{u}(x,0) = \begin{cases} \bar{u}_l^o & \text{for } x<0 \\ \bar{u}_r^o & \text{for } x<0 \end{cases} \qquad (1.3.1)$$

where $\bar{u}_l^o$ and $\bar{u}_r^o$ are two constant states. Intuitively, the initial discontinuity at the origin should be resolved immediately into various waves, then the source term comes into play to perturb the resolved waves. Thus, the procedure for solving the Riemann problem could be divided into two steps:

Step 1. Solve the Riemann problem by assuming that the source term is zero, hence resolving the initial discontinuity.

Step 2. Use the resolved waves as initial data to trace the change of characteristics under the perturbation due to the source term to obtain the final waves.

Note that here we have implicitly assumed that the perturbation due to the source term is not large enough to produce new waves.

This method of solving the Riemann problem is known as the method of characteristic tracing. Next, we shall illustrate the above idea by solving the Riemann problem for the inhomogeneous inviscid Burgers' equation (3). Solutions of the Riemann problems for radially symmetrical gas flow and for gas flow in a duct of variable cross-section are much more difficult to obtain and will be carried out in the next two chapters.

1.4 Solution of the Riemann problem for $u_t + (\frac{u^2}{2})_x = g(x,u)$ at a sample point $(\theta\Delta x, \Delta t)$

To begin, we shall put the partial differential equation into characteristic form which consists of two coupled ordinary differential equations:

$$\begin{cases} \frac{dx}{dt} = u \ , & (1.4.1) \\ \frac{du}{dt} = g(x,u) \ . & (1.4.2) \end{cases}$$

Here (1.4.1) describes the characteristic curve x(t) while (1.4.2) describes the solution u(t) along it. Equations (1.4.1&2) can thus be solved (at least numerically) whenever appropriate initial/boundary conditions are prescribed.

We now proceed to solve the Riemann problem using the two step as outlined in section 1.3.

Step 1: assume g(x,u)=0. Then the solution to the Riemann problem defined by equation (3) and initial data (1.3.1) is well-known. There are two possibilities:

(1) $u_l^o > u_r^o$. The solution in this case is given by a shock wave of speed $s^o = \frac{u_l^o + u_r^o}{2}$ joining the left and right state u_l^o and u_r^o respectively (see figure 1.1):

$$u(x,t) = \begin{cases} u_l^o & x < s^o t + x_o \\ u_r^o & x > s^o t + x_o \end{cases} \qquad (1.4.3)$$

(2) $u_l^o < u_r^o$. The solution is given by a rarefaction fan joining u_l^o and u_r^o (see figure 1.2):

$$u(x,t) = \begin{cases} u_l^o & x < u_l^o t + x_o \\ \dfrac{x}{t} & u_l^o < \dfrac{x - x_o}{t} < u_r^o \\ u_r^o & x > u_r^o t + x_o \end{cases} \qquad (1.4.4)$$

Step 2. From step 1 we know that the initial discontinuity can be resolved into either a shock wave or a rarefaction fan depending on whether $u_l^o > u_r^o$ or $< u_r^o$ respectively. We now proceed to solve the Riemann problem at the sample point $(\theta\Delta x, \Delta t)$ using these resolved waves as initial data. There are a total of five cases to consider.

Suppose $u_l^o > u_r^o$. Then because of the presence of the source term, the shock path will no longer be a straight line with initial speed s^o but rather a curve $x_s = x_s(t)$ to be determined later with initial conditions $x_s(0) = x_o$ and $x'_s(0) = s^o$. (See figure 1.3.)

Case 1. $\theta\Delta x < x_s(\Delta t) - x_o$: the sample point $\theta\Delta x$ lies to the left of the perturbed shock wave. The solution of the Riemann problem $u_l(\theta\Delta x, t)$ can be obtained by solving the characteristic equations (1.4.1 & 2) with the boundary conditions:

$$\begin{cases} x(\Delta t) = x_o + \theta\Delta x \ , & (1.4.5a) \\ u(0) = u_l^o \ . & (1.4.5b) \end{cases}$$

Case 2. $\theta\Delta x > x_s(\Delta t) - x_o$: the sample point $\theta\Delta x$ lies to the right of the perturbed shock wave. Similarly, the solution of the Riemann problem $u_r(\theta\Delta x, \Delta t)$ is obtained by solving the characteristic equations (1.4.1&2) of the partial differential equation with the boundary condition:

$$\begin{cases} x(\Delta t) = x_o + \theta\Delta x \ , & (1.4.6a) \\ u(0) = u_r^o \ . & (1.4.6b) \end{cases}$$

Suppose now that $u_l^o < u_r^o$, then the wave is a rarefaction fan with left boundary $x_l(t)$ and right boundary $x_r(t)$ whose initial speeds are u_l^o and u_r^o. (See figure 1.4.)

Case 3. $\theta\Delta x < x_l(\Delta t) - x_o$: the sample point lies to the left of the perturbed left boundary. As in case 1, the solution of the Riemann problem $u_l(\theta\Delta x, \Delta t)$ is obtained by solving the characteristic equations with the boundary conditions (1.4.5).

Case 4. $\theta\Delta x > x_r(\Delta t) - x_o$: the sample point $\theta\Delta x$ lies to the right of the perturbed right boundary. As in case 2, the solution of the Riemann problem $u_r(\theta\Delta x, \Delta t)$ is obtained by solving the characteristic equations with the boundary conditions (1.4.6).

Case 5. $x_l(\Delta t) - x_o < \theta\Delta x < x_r(\Delta t) - x_o$: the sample point $\theta\Delta x$ lies inside the perturbed rarefaction fan. The solution of the Riemann problem $u_c(\theta\Delta x, \Delta t)$ can be obtained by solving the characteristic equations with boundary conditions

$$\begin{cases} x(\Delta t) = \theta\Delta x + x_o \ , & (1.4.7a) \\ x(0) = x_o \ . & (1.4.7b) \end{cases}$$

To summarize, we have reduced the Riemann problem for the partial differential equation (3) at a given sample point $\theta\Delta x$ at time Δt to a pair of nonlinear ordinary differential equations with appropriate boundary conditions that depend on where the sample point lies with respect to the perturbed wave. Thus, the Riemann problem now becomes a two-point nonlinear boundary value problem. The numerical method in

solving boundary value problems commonly known in the literature are: simple shooting, multiple shooting, and finite differencing. A short but concise review can be found in Dahlquist and Bjork [7]. Since we do not know a priori how much accuracy will be adequate for the solution of the Riemann problem, it is natural to select a variable order method. A very efficient method for solving a two-point nonlinear boundary problem is readily available in the existing code of boundary value problem solvers. In fact, it is the only one available; it is known as PASVA3. For a detail description, see Lentini and Pereyra[12].

Now using PASVA3, the Riemann problem can be solved with arbitrary order of accuracy at a sample point $\theta\Delta x$ at time Δt.

Trajectory of a perturbed wave

In order to determine which one of the five cases a sample point $\theta\Delta x$ belongs to, it is imperative to determine a priori the locations of the perturbed left/right boundary of a rarefaction fan or the position of a shock wave at time Δt.

(1) Boundary of a perturbed rarefaction fan

Since the boundaries of a rarefaction fan are characteristics of the given partial differential equation, their trajectories are given by the characteristic equations with the appropriate initial conditions described below:

(a) for the left boundary

$$\begin{cases} x(0) = x_o \ , \\ u(0) = u_l^o \ , \end{cases} \tag{1.4.8}$$

(b) for the right boundary

$$\begin{cases} x(0) = x_o \ , \\ u(0) = u_r^o \ . \end{cases} \tag{1.4.9}$$

The locations of the left and right boundaries at time Δt can now be found by solving the initial value problems defined by the ordinary differential equations (1.4.1&2) with the initial conditions (1.4.8) and (1.4.9) respectively. In order to avoid the loss of information for taking unreasonable large time steps, we set $(\Delta t)_{max} = 10^{-1}$ in all test problems. The initial value problems are then solved by the

celebrated 4^{th}-order Runge-Kutta method in N steps. Since the global truncation error of this method is $O(h^4)$, our errors in solving the initial value problems will then be less than $(10N)^{-4}$. The desired accuracy can thus be attained by taking N sufficiently large.

(2) Trajectory of a perturbed shock

Denote the trajectory of the perturbed shock by $x_s(t)$. Then given fixed time Δt, we would like to determine the position of the shock. Now using the Rankine-Hugoniot condition, the path of the shock can be obtained by solving the initial value problem:

$$\begin{cases} \dfrac{dx_s}{dt} = \dfrac{u_l(t) + u_r(t)}{2} , & (1.4.10a) \\ x_s(0) = x_o , & (1.4.10b) \end{cases}$$

where $u_l(t)=u(t^-)$ and $u_r(t)=u(t^+)$. Obviously, in order to solve (1.4.10), we need to determine $u_l(t)$ and $u_r(t)$, this can be accomplished by tracing the left and right characteristics to the initial surface t=0. (See figure 1.5.)

Now the left and right characteristics are given by the following two systems of ordinary differential equations:

$$\begin{cases} \dfrac{dx_l}{dt} = u_l , & (1.4.11a) \\ \dfrac{du_l}{dt} = g(x_l,u_l) , & (1.4.11b) \end{cases}$$

with

$$u_l(0) = u_l^o ; \qquad (1.4.11c)$$

$$\begin{cases} \dfrac{dx_r}{dt} = u_r \quad , & (1.4.12a) \\ \dfrac{du_r}{dt} = g(x_r,u_r) \quad , & (1.4.12b) \end{cases}$$

with

$$u_r(0) = u_r^o \quad . \qquad (1.4.12c)$$

Equations (1.4.10-1.4.12) furnish us with five coupled ordinary differential equations and three initial conditions, thus we need two more pieces of information to solve for (x_s,x_l,u_l,x_r,u_r). These can be obtained by noting that at time Δt, the shock as well as both left and right characteristics collide together. Phrasing in terms of boundary conditions, we have:

$$\begin{cases} x_l(\Delta t) - x_s(\Delta t) = 0 \quad , & (1.4.13a) \\ x_r(\Delta t) - x_s(\Delta t) = 0 \quad . & (1.4.13b) \end{cases}$$

Now we have a well-posed boundary value problem and using the boundary value problem solver PASVA3 described previously, $x_s(\Delta t)$ can be determined with arbitrary accuracy.

The Courant-Fredrichs-Levy (C-F-L) condition

Recall that in Glimm's construction, we have to solve a sequence of Riemann problems for the given partial differential equation at each time level t. To ensure that waves generated by different Riemann problems will not interact at the next time level $t + \Delta t$, the C-F-L condition

$$\Delta t = \frac{\Delta x}{2|u(x,\vartheta)|} \tag{1.4.14}$$

must be satisfied. The initial data in our case are piecewise constant functions u_i^o. In the case of zero source (g=0), the C-F-L condition simply reduces to

$$\Delta t = \frac{\Delta x}{2\max_i |u_i^o|} \quad . \tag{1.4.15}$$

Geometrically, this amounts to requiring that the time increment Δt be chosen such that the characteristic curve ($\frac{dx}{dt} = u_i^o$) emanating from x_i must not penetrate the right side of the box $[x_i, x_i + \Delta x/2] \times [0, \Delta t]$. See figures 1.6 &1.7. In the case of nonzero source, the C-F-L condition will be satisfied by enforcing the same geometrical constraint described above. Of course, in this case the characteristics are curves described by the characteristic equations (1.4.1&2) with initial conditions

$$\begin{cases} x(0) = x_i \quad , \\ u(0) = u_i^o \quad . \end{cases} \tag{1.4.16}$$

Dividing the interval $[0, \Delta t]$ into N equal subintervals, we proceed to

solve the initial value problem numerically until we come to the first j ($0<j<N$) such that

$$x\left(\frac{j\Delta t}{N}\right) > x_i + \frac{\Delta x}{2}.$$

Letting $\Delta t_i = \frac{(j-1)\Delta t}{N}$ and $\Delta t_{min} = \min_i \Delta t_i$, then we can ensure that the waves generated by solving different Riemann problems at time t will not interact at the next time level $t+\Delta t_{min}$, that is , the C-F-L condition is satisfied.

We conclude by summarizing what we have done so far. By transforming the given partial differential equation, $u_t + uu_x = g(x,u)$, into its characteristic equations, the Riemann problem at a sample point $(\theta\Delta x, \Delta t)$ becomes a well-posed boundary value problem. Using the boundary value problem code PASVA3, we obtain a numerical scheme of variable order for solving the Riemann problem. Moreover, the position of a perturbed wave (a shock or a rarefaction fan) at a given time Δt can be computed using equations (1.4.1&2) with properly posed initial conditions (and boundary conditions in the case of a shock). Similarly, the position of a characteristic curve can be determined which enable us to ensure that the C-F-L condition is satisfied.

In the case when $g=0$, Lax[8] and Chorin[2] have shown that Glimm's scheme is at best a first order method, thus it is unclear whether it is worthwhile to solve Riemann problems with high accuracy even in the presence of a nonzero source. In fact, we will described a low order, but very efficient, scheme for solving Riemann problems next. Then by taking special source terms, we will see that such a

low order method sometimes gives better results.

1.5 The method of operator splitting

The idea behind operator splitting is similar to the method of characteristic tracing described in section 1.3. Again, we first resolve the initial discontinuity by solving the nonlinear system of partial differential equations (1) without the source term, that is, $\bar{u}_t + \bar{f}_x(\bar{u}) = 0$. Denote the solution at $(x_o + \theta\Delta x, \Delta t)$ by $\bar{v}_o$. Next, using $\bar{v}_o$ as initial data we obtain a new solution vector $\bar{v}(x_o + \theta\Delta x, \Delta t)$ by solving the ordinary differential equation

$$\frac{d\bar{v}}{dt} = \bar{g}(x_o + \theta\Delta x, \bar{v}) \tag{1.5.1a}$$

with initial condition

$$\bar{v}(0) = \bar{v}_o \quad . \tag{1.5.1b}$$

The influence of the source term $\bar{g}$ thus enters in this last step. The approximate solution of the Riemann problem is $\bar{v}(x_o + \theta\Delta x, \Delta t)$. Although the order of accuracy of this method is not known in general, the advantage of operator splitting is that it is simpler than the variable order method of characteristic tracing. Moreover, we have the following interesting lemma.

Lemma. The method of operator splitting gives an exact solution to the initial value problem

$$\bar{u}_t + \bar{f}_x(\bar{u}) = \bar{g}(\bar{u}) \quad , \tag{1.5.2a}$$

with initial data

$$\bar{u}(x,0) = \bar{u}_o \quad . \tag{1.5.2b}$$

Proof. The solution to (1.5.2) without the source term is simply $\bar{u}_o$. The approximate solution given by the method of operator splitting is then

$$\bar{v}(t) = \bar{u}_o + \int_0^t \bar{g}(v(\tau))d(\tau) \quad .$$

This solution is exact as

$$\frac{\partial \bar{v}}{\partial t} + \partial \frac{\bar{f}(\bar{v})}{\partial x} = \frac{\partial \bar{v}}{\partial t} + 0 \quad ,$$

and $\frac{\partial \bar{v}}{\partial t} = \bar{g}(\bar{v})$. Furthermore $\bar{v}(0) = \bar{u}_o$. Q.E.D.

In practice the ordinary differential equation (1.5.1a) is solved numerically by the simple Cauchy-Euler scheme

$$\bar{v}(x_o + \theta\Delta x, \Delta t) = \bar{v}_o + \bar{g}\,(x_o + \theta\Delta x, v_o)\,\Delta t \quad .$$

It is well-known that the Cauchy-Euler scheme is at most first order accurate; however, Glimm's scheme is itself at most first order accurate so there is no reason for using a higher order ordinary differential equation solver for (1.5.1a). In fact, from the first test problem it is interesting to see that the method of operator splitting gives more accurate results than that of characteristic tracing when used in the solution of Riemann problems in Glimm's scheme.

1.6 Test problems

In order to compare the performance of Glimm's construction using the two different numerical schemes characteristic tracing and operator splitting described in section 1.4 and 1.5 respectively, a suitable way of measuring their accuracies is essential. In the case of a smooth solution (e.g. a rarefaction fan), the l_1-norm is often used. In the presence of a shock, however one can measure the superiority of one scheme over the other by examining the shock-jump error at each time level defined by

$$\sum_{i=1}^{N} |u_{L,R}-v_{L,R}|\Delta t,$$

where

$u_{L,R}$=the difference between the exact values of the left and right state of the shock at time $N\Delta t$,

$v_{L,R}$=the difference between the estimated values of the left and right state at the shock.

Problem 1:

$$u_t + \left(\frac{u^2}{2}\right)_x = -x \qquad \text{on } [0,2] \tag{1.6.1}$$

with

$$u(x,0) = \begin{cases} 2 & \text{for } x<1 \\ 0 & \text{for } x>1 \end{cases} \tag{1.6.2}$$

The exact solution is

$$u(x,t) = \begin{cases} \dfrac{2-x\ \sin t}{\cos t} & \text{for } x<x_s(t) \\ -x\ \dfrac{\sin t}{\cos t} & \text{for } x>x_s(t) \end{cases} \qquad (1.6.3)$$

where $x_s(t) = \cos t + \sin t$ is the shock path.

The spatial grid size h used is 0.1. A comparison of the shock-jump errors of the two methods can be found in table 1.1. The logarithm of the shock-jump errors of each method is plotted against time t. See graph 1.1. At all five time levels 0.05 to 0.25, Glimm's construction using operator splitting gives better results than characteristic tracing. This is very surprising because characteristic tracing solves a Riemann problem with high order of accuracy (10^{-7}) while operator splitting is only first order accurate (recall that the Cauchy-Euler scheme is used as our ordinary differential equation solver). This paradox can be partially explained away as follows. Consider the Riemann problem

$$\begin{cases} u_t + \left(\dfrac{u^2}{2}\right)_x = -x\ , & (1.6.5a) \\ u(x,0) = u_o\ . & (1.6.5b) \end{cases}$$

Assume further that characteristic tracing solves this problem exactly,

$$u_{CT}(x,\Delta t) = \frac{u_o - x\sin(\Delta t)}{\cos(\Delta t)}\ . \qquad (1.6.6)$$

In Glimm's construction, however, the solution at $(x,\Delta t)$ is u_{CT} evaluated at the sample point $(x + \theta\Delta x, \Delta t)$ instead of $(x,\Delta t)$. Recall that θ is a random number between $[-\frac{1}{2}, \frac{1}{2}]$. Thus, the error committed by characteristic tracing is

$$\text{error}_{CT}\ (x,\Delta t) = u_{CT}\ (x+\theta\Delta x,\Delta t) - u_{CT}(x,\Delta t) \quad .$$

Expanding error_{CT} in powers of Δt, we get

$$\text{error}_{CT}\ (x,\Delta t) = \theta\Delta x\ \Delta t + \theta\Delta x\ \frac{\Delta t^3}{3} + 0(\Delta t^5) \quad . \qquad (1.6.7)$$

Similarly, the error committed by operator splitting is

$$\text{error}_{OS}\ (x,\Delta t) = \theta\Delta x\ \Delta t + u_o\ \frac{\Delta t^2}{2} - x\ \frac{\Delta t^3}{3} + 0(\Delta t^4) \quad . \qquad (1.6.8)$$

For simplicity, consider the special case when $x = 0$. Moreover in the case when $u_o = 2$, (1.6.8) reduces to

$$\text{error}_{OS}\ (x,\Delta t) = \theta\Delta x\ \Delta t + \Delta t^2 + 0(\Delta t^4) \quad . \qquad (1.6.8')$$

When $\theta < 0$, $|\theta\Delta x\Delta t + \theta\Delta x\frac{\Delta t^3}{3}| > |\theta\Delta x\Delta t + \Delta t^2|$ so

$$|\text{error}_{CT}(x,\Delta t)| \gtrsim |\text{error}_{OS}(x,\Delta t)| \quad ! \qquad (1.6.9)$$

Thus the high order of accuracy of characteristic tracing in solving Riemann problems can be lost in the process of random sampling. It is wrong to conclude, however, that the method of operator splitting should be preferred over that of characteristic tracing in the solution of Riemann problems. The reason is very simple, when $\theta > 0$ the inequality in (1.6.9) reverses. Thus the performance of operator splitting is not always better than characteristic tracing. But from this test problem, we see that high order of accuracy in solving Riemann problems does not necessarily guarantee a better solution. In order to decide which methods should be used in solving Riemann problems, one has to do a detail error analysis for the general equation (3). It should be noted, however, that rigorous error analysis of Glimm's scheme even for the the inviscid Burgers' equation

$$u_t + \left(\frac{u^2}{2}\right)_x = 0$$

is extremely difficult (for details see Colella[3]); thus, we shall resort to numerical experiment instead.

In the following test problems, we have chosen the source term g to be of the form $-\frac{u^2}{x}$ and $+\frac{u^2}{x}$, $x > 0$. Moreover, the initial data is piecewise constant and will initially result in a shock wave. There are two reasons for restricting our attention to such special cases:

(1) Exact solutions can be obtained rather easily so that a comparison of the accuracies when using characteristic tracing and operator splitting can be carried out explicitly.

(2) Our main concern for the next chapter will be the propagation of shock waves in a duct of x-sectional area A(x). In particular, $A(x) = \pm\frac{1}{x+x_o}$ for some constant x_o, hence the spatial part of the source term has the form

$$\frac{A'(x)}{A(x)} = \mp\frac{1}{x+x_o} \quad . \tag{1.6.10}$$

Thus, the source terms we have chosen closely mimic (1.6.10), hence the results we obtain in the following test problems should help us decide which of the two numerical schemes we should use in solving Riemann problems in the more complicated cases.

Finally, we say a numerical scheme is more efficient than another if it requires less computational (or execution) time to attain a given level of accuracy.

Problem 2:

$$u_t + \left(\frac{u^2}{2}\right)_x = \frac{u^2}{x} \qquad \text{on} \quad [1,5] \tag{1.6.11}$$

with

$$u(x,0) = \begin{cases} u_1^o & \text{for } x<3 \\ u_r^o & \text{for } x>3. \end{cases} \tag{1.6.12}$$

The exact solution is

$$u(x,t) = \begin{cases} u_1^o \left(1+u_1^o \frac{t}{x}\right)^{1/2} - u_1^o \frac{t}{x} & \text{for } x<x_s(t) \\ u_r^o \left(1+u_r^o \frac{t}{x}\right)^{1/2} - u_r^o \frac{t}{x} & \text{for } x>x_s(t) \end{cases} \tag{1.6.13}$$

where $x_s(t)$ is the shock path given implicitly by the nonlinear equation

$$\left[1 + \left(\frac{x_s}{u_1^o}\right)^2\right]^{3/2} - 1.5\left(1 + \left(\frac{x_s}{u_r^o}\right)^2\right) - \left(\left(\frac{x_o}{u_1^o}\right)^3 - 0.5\right) = 0.$$

In this test problem, we will use $u_1^o = 2$, $u_r^o = 0$, and $s^o = 3$. The shock-jump errors from time levels 0.1 to 0.5 and the execution time of the two methods can be found in tables 1.2 and 1.3 respectively. Finally, the logarithms of the shock-jump errors of operator splitting and characteristic tracing versus time t are plotted in graph 1.2. The spatial step sizes used are $\frac{h}{2^n}$, where h = 0.2 and n=0,1,2,3.

Observations: for all spatial step sizes used, the shock-jump errors committed by operator splitting is less than characteristic tracing. However, it is interesting to observe that the high accuracy of characteristic tracing in all cases can be obtained by operator splitting by simply halving the spatial grid size h. (See graph 1.2.)

Moreover, the execution time required by operator splitting is dramatically less than characteristic tracing. In fact, the amount of time required by operator splitting with $\frac{h}{8}$ is still less than that required by characteristic tracing with h !

Problem 3:

$$u_t + \left(\frac{u^2}{2}\right)_x = \frac{u^2}{x} \qquad \text{on} \quad [1,5] \tag{1.6.14}$$

with

$$u(x,0) = \begin{cases} u_l^o & \text{for } x<3 \\ u_r^o & \text{for } x>0 \end{cases} \tag{1.6.15}$$

The exact solution is

$$u(x,t) = \begin{cases} u_l(x,t) & \text{for } x<x_s(t) \\ u_r(x,t) & \text{for } x>x_s(t) \end{cases} \tag{1.6.16}$$

where $u_l(x,t)$ and $u_r(x,t)$ are given implicitly by the following non-linear equation

$$u_{l,r} = u_{l,r}^o \; e^{u_{l,r}\frac{t}{x}} \tag{1.6.17}$$

and the shock path $x_s(t)$ is given by the initial value problem

$$\frac{dx_s}{dt} = \frac{u_l + u_r}{2}, \tag{1.6.18a}$$

$$x_s(0) = 3, \tag{1.6.18b}$$

where $u_{l,r}$ are given implicitly by (1.6.17). As in test problem 2, we use $u_l^o = 2$, and $u_l^o = 0$. The shock-jump errors from time levels 0.05 to 0.25 and the execution time of the two methods can be found in tables 1.4 and 1.5 respectively. The spatial grid size used are $\frac{h}{2^n}$, where $h = 0.2$ and $n=0,2$.

Observations: solving Riemann problems with characteristic tracing

give more accurate results than operator splitting in Glimm's construction. However, operator splitting can attain the same accuracy as characteristic tracing with step size h by using $\frac{h}{4}$. As in the previous test problem, the execution time by operator splitting is much less than characteristic tracing. Thus the lower of accuracy operator splitting is being compensated by its efficiency.

1.7 Conclusions

On the whole, the higher order of accuracy of characteristic tracing do sometimes provide us with better Glimm solutions than operator splitting. However, the execution time required is astoundingly larger than with operator splitting so that it is more efficient to use operator splitting with half (or quarter) the spatial grid size in order to achieve the same accuracy. Furthermore, using characteristic tracing does not necessarily guarantee better solutions than operator splitting. (See graphs 1.1 and 1.2.) Roughly speaking, the random sampling kills off a substantial amount of the accuracy of characteristic tracing in the solution of Riemann problem. In conclusion, if one measures the superiority of one scheme over the other by comparing their efficiencies, operator splitting should be preferred over characteristic tracing in solution of Riemann problems for Glimm scheme for the special source terms $\pm \frac{u^2}{x}$.

Chapter 2 Radially Symmetric Gas Flows

2.1 Preliminaries

In the next two chapters, we wish to study the equations of an inviscid non-heat conducting, radially symmetric gas flow and gas flow in a duct of variable cross-section. The equations are given respectively by (4) and (6) which we can replace for simplicity by

$$\frac{\partial}{\partial t}\begin{bmatrix}\rho\\ m\\ e\end{bmatrix}+\frac{\partial}{\partial x}\begin{bmatrix}m\\ \frac{m^2}{\rho}+p\\ \frac{m(e+p)}{\rho}\end{bmatrix}=-G(x)\begin{bmatrix}m\\ \frac{m^2}{\rho}\\ \frac{m(e+p)}{\rho}\end{bmatrix} \tag{2.1.1}$$

Our numerical method has been a generalization of Glimm's scheme (see Section 1.2). Recall from Chapter 1 that the successful implementation of such a scheme hinges on solving the Riemann problem for the corresponding set of partial differential equations. In other words, in this case we need to solve (2.1.1) with piecewise constant initial data

$$(\rho,m,e)^T(x,0)=\begin{cases}(\rho_l^o,m_l^o,e_l^o)^T & \text{for } x<x_o,\\ (\rho_r^o,m_r^o,e_r^o)^T & \text{for } x>x_o\end{cases} \tag{2.1.2}$$

In the last chapter, we presented two methods for solving the Riemann problem, they are

(1) the method of characteristic tracing,

(2) the method of operator splitting.

Although the first method is supposed to be exact, it has two important disadvantages as compared with the second method:

(1) tracing characterisitcs is not feasible in general for the hyperbolic system of partial differential equations (1) for $n > 1$.

(2) it is a very inefficient method even in the simple case of the inviscid inhomogeneous Burgers' equation (see Section 1.6).

Of course, we may be able to off-set these two disadvantages by devising some (ad-hoc) high order approximate schemes for solving the Riemann problem. But how much accuracy is enough?? In the last chapter, we have discovered that the first order method of operator splitting can sometimes beat the 'exact' method of characteristic tracing in the construction of a global solution, not to mention that it is more efficient. Thus any arbitrary approximate schemes for solving the Riemann problem will <u>not</u> do in general. However, the numerical scheme to be described next, due to T. P. Liu, is quite different; it has something that cannot be matched by operator splitting. Liu's scheme converges under the same assumptions made by Glimm in his scheme and with the added assumption that the characteristic speeds are nonzero. For details of the assumptions made and proof of convergence, see Liu [9]&[10]. In the next section, Liu's scheme will be described with emphasis on constructing a solution to (2.1.1).

2.2 Liu's construction

Basically, Liu's construction is similar to the generalization of Glimm's construction as described in Section 1.2. Again, we consider the nonlinear system of equations (1) with initial data (2). Let k and h be the time and spatial increments respectively. A discrete approximation to the solution $\bar{u}(x,t)$ is to be computed at the points (ih,nk) and $((i+\frac{1}{2})h,(n+\frac{1}{2})k)$ for $|i|$, $n = 0,1,2,\ldots$. Denote the approximate values by $\bar{u}_i^n \simeq \bar{u}(ih,nk)$, $\bar{u}_{i+1/2}^{n+1/2} \simeq \bar{u}((i+1/2)h,(n+1/2)k)$, and suppose that $\bar{u}_i^n$ has already been computed for all i. Then $\bar{u}_{i+1/2}^{n+1/2}$ is computed from $\bar{u}_i^n$ and $\bar{u}_{i+1}^n$ by a procedure described as follows.

Step 1. We solve the ordinary differential equation

$$\frac{df(\bar{w})}{dx} = g(x,\bar{w}) \tag{2.2.1}$$

assuming that the initial condition $\bar{u}(x_o)$ is given. Denote the solution by $\bar{w}(x;\bar{u}(x_o))$. This (unique) solution is called the standing wave solution because it has no time dependence. Also, (2.2.1) is called the steady-state equation for the general hyperbolic system (1).

Step 2. Using the solution to the steady-state equations, we solve the Riemann problem without the source term using the following initial data

$$\bar{u}(x,0) = \begin{cases} \bar{w}(h;\bar{u}_i^n) & , x<0 \\ \bar{w}(-h;\bar{u}_{i+1}^n) & , x>0 \end{cases} \qquad (2.2.2)$$

and denote the solution by $\bar{v}(x,t)$. Then $\bar{u}_{i+1/2}^{n+1/2} = \bar{v}(\theta_n h, \frac{k}{2})$, where θ_n is a random variable equidistributed in the interval $[-\frac{1}{2},\frac{1}{2}]$. Similarly, $\bar{u}_i^{n+1}$ can be computed from $\bar{u}_{i-1/2}^{n+1/2}$ and $\bar{u}_{i+1/2}^{n+1/2}$ by this procedure via the use of another random variable $\theta_{n+\frac{1}{2}}$. This completes the construction.

Thus, given initial data at any time level, Liu's scheme carries out the same construction devised by Glimm for the case of zero source ($g \equiv 0$) except that initial data has to be <u>first</u> recomputed using the steady-state equations. Since the source term g enters into the whole picture solely via the steady-state equations (2.2.1), the effect of the source term in Liu's construction is thus introduced <u>only</u> in the process of setting up initial data at each time level. Finally, if a global solution consists in part of steady-states, then Liu's scheme will reproduce these steady-states without any difficulty because they are used explicitly in the construction process. This is a major advantage over Glimm's scheme with operator splitting and will be illustrated clearly in test problem 3 of the next chapter.

<u>Example 2.2</u> The steady-state equations of (2.1.1) are

$$\frac{dm}{dx} = -G(x)m \quad , \qquad (2.2.3a)$$

$$\frac{d}{dx}\left(\frac{m^2}{\rho} + p\right) = -G(x)\frac{m^2}{\rho} \quad , \qquad (2.2.3b)$$

$$\frac{d}{dx}\left(\frac{m(e+p)}{\rho}\right) = -G(x)\frac{m(e+p)}{\rho} \quad , \tag{2.2.3c}$$

or expressing in terms of the dependent variables ρ,u,p alone, (2.2.3) can be rewritten as

$$\frac{d\rho}{dx} = G(x)\cdot\frac{\rho u^2}{c^2-u^2} \quad , \tag{2.2.4a}$$

$$\frac{du}{dx} = -G(x)\frac{c^2 u}{c^2-u^2} \quad , \tag{2.2.4b}$$

$$\frac{dp}{dx} = G(x)\frac{\rho u^2 c^2}{c^2-u^2} \quad . \tag{2.2.4c}$$

Recall that $c = \sqrt{\gamma\frac{p}{\rho}}$ is the sound speed in the gas. Notice also the assumption that the characteristic speeds u, $u \pm c \neq 0$, is used explicitly here. Given the initial conditions

$$(\rho,u,p)^T(x_o \pm \Delta x) = (\rho_{\pm}^o, u_{\pm}^o, p_{\pm}^o)^T \quad ,$$

(2.2.3a) can be integrated to give

(2.2.5)

$$\rho_{\pm} u_{\pm} = \rho_{\pm}^o u_{\pm}^o \exp\left(-\int_{x_o \pm \Delta x}^{x} G(\xi)\,d\xi\right) \quad .$$

Next, by introducing the variable $\eta_{\pm}(x) = \frac{u_{\pm}(x)}{c_{\pm}(x)}$ and using (2.2.4) we get after some simplifications

$$\frac{d\eta_{\pm}}{dx} = 2G(x)\frac{\eta_{\pm}\left(1 + \frac{\gamma-1}{2}\eta_{\pm}\right)}{1-\eta_{\pm}}$$

that can be integrated again to give

(2.2.6)

$$\frac{(1+\frac{\gamma-1}{2}\eta_{\pm})^{\frac{\gamma+1}{\gamma-1}}}{\eta_{\pm}} = \frac{(1+\frac{\gamma-1}{2}\eta_{\pm}^{o})^{\frac{\gamma+1}{\gamma-1}}}{\eta_{\pm}^{o}} \exp\left(2\int_{x_o \mp \Delta x}^{x} G(\xi)\,d\xi\right),$$

where $\eta_{\pm}^{o} = \left(\frac{u_{\pm}^{o}}{c_{\pm}^{o}}\right)^2$. Suppose a solution to the nonlinear algebraic equation (2.2.6) exists, then using (2.2.5) $(\rho_{\pm},u_{\pm},p_{\pm})^T(x)$ can easily be recovered from $p_{\pm}u_{\pm}$ and $\left(\frac{u_{\pm}}{c_{\pm}}\right)^2$ once these two values at a given x are found. In particular, $p_{\pm}(x_o)$, $u_{\pm}(x_o)$, $p_{\pm}(x_o)$ can be computed. The key step in Liu's construction will then be complete if we can solve the source-free Riemann problem of (2.1.1), i.e.,

$$\frac{\partial}{\partial t}\begin{bmatrix}\rho\\ m\\ e\end{bmatrix} + \frac{\partial}{\partial x}\begin{bmatrix} m\\ \frac{m^2}{\rho}+p\\ \frac{m(e+p)}{\rho}\end{bmatrix} = 0 \qquad (2.2.7a)$$

with the piecewise constant initial data

$$(\rho,m,e)^T(x,0) = \begin{cases}(\rho_+,m_+,e_+)^T(x_o) & , x<x_o\\ (\rho_-,m_-,e_-)^T(x_o) & , x>x_o.\end{cases} \qquad (2.2.7b)$$

But (2.2.7a) is just the one-dimensional equations of gas dynamics whose Riemann problem can be solved easily. A detailed description can be found in Chorin [2], or Sod [13]. Qualitatively, the solution consists of two waves (either rarefaction fans or shock waves), w_1 and w_2, separated by a slip line defined by the ordinary differential equation

$\frac{dx}{dt} = u_*$ with initial condition $x(0) = x_o$. Here u_* is the speed of the gas at the center state. (See figure 2.1.) Furthermore, this slip line subdivides the center region into two parts with possibly different values of density but equal values of u_* and p_* (pressure of the center state).

Remark

It is important to note that Liu's scheme cannot be carried out for transonic flows. The reason is as follows. Suppose a standing wave solution exists between two points x_1 and x_2 at which the flows are subsonic and supersonic respectively, then a standing wave solution must automatically exist connecting x_2 and $x_o \in (x_1, x_2)$ where the flow is sonic. However, that is impossible because the steady-state equations fail to hold at x_o as one of the characteristic speeds $u \pm c$ is zero at x_o. This is the major drawback of Liu's construction, and no progress has yet been made towards resolving it. (See, however, Liu[11] for the most recent development.) In the next section, we will look at operator splitting, which appears to handle transonic flow problems with relative ease.

2.3 Operator splitting

The method of operator splitting for solving the Riemann problem for the general equation (1) has already been outlined in Section 1.5. In the present section, we want to apply the method explicity to (2.1.1). Recall that the first step involves solving the source-free Riemann problem corresponding to (2.1.1); this has already been discussed in Section 2.2. Let the solution thus obtained at a given sample point $x_o + \theta\Delta x$ at time Δt be denoted by (ρ_o, u_o, p_o). Then the solution to the original Riemann problem with nonzero source at $(x_o + \theta\Delta x, \Delta t)$ is obtained by solving the set of ordinary differential equations

$$\begin{cases} \frac{d\rho}{dt} = -G(x_o + \theta\Delta x)\rho u & (2.3.1a) \\ \frac{du}{dt} = 0 & (2.3.1b) \\ \frac{dp}{dt} = -\gamma G(x_o + \theta\Delta x)pu & (2.3.1c) \end{cases}$$

with initial data

$$(\rho, u, p)(0) = (\rho_o, u_o, p_o) \quad .$$

Since (2.3.1b) has a trivial solution

$$u(x_o + \theta\Delta x, t) = u_o \quad , \qquad (2.3.2a)$$

(2.3.1a) and (2.3.1c) thus uncouple conveniently and can be integrated exactly to give at time Δt

$$\rho(x_o + \theta\Delta x, \Delta t) = \rho_o \exp(-u_o G(x_o + \theta\Delta x)\Delta t) \qquad (2.3.2b)$$

and

$$p(x_o + \theta\Delta x,\Delta t) = p_o \exp(-\gamma u_o G(x_o + \theta\Delta x)\Delta t) \quad . \qquad (2.3.2c)$$

The solution to the Riemann problem for (2.1.1) as obtained by operator splitting at $(x_o + \theta\Delta x,\Delta t)$ is now given by (2.3.2a-c).

Next, we shall study the problem of a point blast explosion and use this as a test problem for determining whether Liu's scheme or Glimm's scheme does a better job in treating spherical shock wave problems.

2.4 Point blast explosion

The formation of a blast wave by a very intense explosion was studied very closely by Taylor[14] in connection with atomic bomb research. The explosion can be idealized as a sudden release of an amount of energy E concentrated at a point. Furthermore, we assume that the resulting disturbance will be so strong that the atmospheric pressure p_o and sound speed a_o are negligible compared with post-shock pressure and velocity. Also, the velocity of the undisturbed region is assumed to be zero. Then it can be argued on dimensional grounds (see Whitham[16]) that the spherical shock wave propagating outwards, whose radius R, is related to time t by

$$R = S(\gamma) \left(\frac{E}{\rho_o} \right)^{1/5} t^{2/5} , \qquad (2.4.1)$$

where ρ_o is the atmospheric density, $S(\gamma)$ is some calculated function of γ determined by the problem.

Now the equations of spherical wave motion are simply (2.1.1) with $G(x) = \frac{2}{r}$ (where r is the radial co-ordinate) which we can rewrite as

$$\frac{\partial u}{\partial t} + u \frac{\partial u}{\partial r} = \frac{1}{\rho} \frac{\partial p}{\partial r} , \qquad (2.4.2a)$$

$$\frac{\partial p}{\partial t} + u \frac{\partial p}{\partial r} + \rho \left(\frac{\partial u}{\partial r} + \frac{2u}{r} \right) = 0 , \qquad (2.4.2b)$$

$$\left(\frac{\partial}{\partial t} + u \frac{\partial}{\partial r} \right) \left(p \rho^{-\gamma} \right) = 0 . \qquad (2.4.2c)$$

Following Taylor, we introduce the similarity variable $\eta = \frac{r}{R}$ and take

$$\text{pressure,} \quad p = \frac{p_o}{a_o^2} \left(R^{-3/2} A \right)^2 f(\eta) , \qquad (2.4.3a)$$

$$\text{density,} \quad p = p_o \Psi(\eta) \quad , \tag{2.4.3b}$$

$$\text{radial velocity,} \quad u = R^{-3/2} A \phi(\eta) \quad , \tag{2.4.3c}$$

where again p_o and a_o are respectively the atmospheric pressure and sound speed and A is a constant equal to $\frac{2}{5}\left[S(\gamma)^5 \frac{E}{p_o} \right]^{1/2}$. Substituting (2.4.3a-c) into (2.4.2a-c), this set of partial differential equations reduces to a set of first order ordinary differential equations:

$$\phi' (\eta - \phi) = \frac{1}{\gamma} \frac{f'}{\Psi} - \frac{3}{2}\phi \quad , \tag{2.4.4a}$$

$$\frac{\Psi'}{\Psi} = \frac{\phi' + 2\frac{\phi}{\eta}}{\eta - \phi} \quad , \tag{2.4.4b}$$

$$3f + \eta f' + \gamma \frac{\Psi'}{\Psi} f(\phi - \eta) - \phi f' = 0 \quad , \tag{2.4.4c}$$

or after some simplifications,

$$\begin{cases} \dfrac{df}{d\eta} = \dfrac{f\psi(3(\eta - \phi) + \gamma\phi(\frac{2}{\eta} - \frac{1}{2})}{f - \psi(\phi - \eta)^2} \quad , \\[2ex] \dfrac{d\phi}{d\eta} = \dfrac{f(\frac{3}{\gamma} - \frac{2}{\eta}\phi) - \frac{3}{2}(\phi - \eta)\phi\psi)}{f - \psi(\phi - \eta)^2} \quad , \\[2ex] \dfrac{d\psi}{d\eta} = \dfrac{\psi(\psi\phi(\phi - \eta)(\frac{2}{\eta} - \frac{1}{2}) - \frac{3f}{\gamma}}{(\phi - \eta)(f - \psi(\phi - \eta)^2)} \quad . \end{cases} \tag{2.4.5}$$

Shock-wave conditions

By assumptions, the post-shock pressure is much larger than the atmospheric pressure, the Rankine-Hugoniot conditions then become

$$\frac{p_1}{p_o} = \frac{2\gamma}{\gamma+1}\frac{U^2}{a_o^2} \quad , \tag{2.4.6a}$$

$$\frac{\rho_1}{\rho_o} = \frac{\gamma+1}{\gamma-1} \quad , \tag{2.4.6b}$$

$$\frac{u_1}{U} = \frac{2}{\gamma+1} \quad , \tag{2.4.6c}$$

where U is the shock speed. Differentiating (2.4.1), we get $U=A\,R^{-3/2}$. Furthermore, evaluating (2.4.3a-c) at $\eta=1$, we get on comparison with (2.4.6)

$$f(1) = \frac{2\gamma}{\gamma+1} \quad , \tag{2.4.7a}$$

$$\phi(1) = \frac{2}{\gamma+1} \quad , \tag{2.4.7b}$$

$$\Psi(1) = \frac{\gamma+1}{\gamma-1} \quad . \tag{2.4.7c}$$

Now (2.4.5) together with (2.4.7) constitute a well-posed initial value problem at $\eta=1$ which can be solved numerically backwards to $\eta=0$ so that f, ϕ, Ψ for $\eta \in [0,1)$ can be found. Unfortuately Taylor did not realize that (2.4.5) was mildly stiff, hence his results could be improved. Table 2.1 contains values of $f(\eta), \phi(\eta), \Psi(\eta)$ obtained by a standard stiff ordinary equation package by Gear[5]. Curves of f, ϕ, Ψ can also be found in figure 2.2.

Now with the values of f, ϕ, Ψ known for any $\eta \in [0,1]$, the following example illustrates how to find the state of the gas (ρ,u,p) in the region behind the shock for a given problem.

Example 2.4 In a atomic explosion in New Mexico in 1947, the amount of energy E released was measured to be 7.14×10^{20} ergs. Taking $\rho_o = 1.25$ kg/m^3 and $\gamma = 1.4$, (2.4.1) becomes

$$\frac{5}{2} \log_{10} R = \log_{10} t + 11.915 \quad , \tag{2.4.8}$$

or

$$R(t) = (t \times 10^{11.915})^{2/5} \quad . \tag{2.4.9}$$

Using the defintion of A,

$$R^{-3/2} A = \frac{2}{5} \frac{R}{t} \quad . \tag{2.4.10}$$

Substituting (2.4.10) into (2.4.3a-c), we get

$$p = \frac{\rho_o}{a_o^2} \left(\frac{2}{5} \frac{R}{t} \right)^2 f(\eta) \quad , \tag{2.4.11a}$$

$$\rho = \rho_o \Psi(\eta) \quad , \tag{2.4.11b}$$

$$u = \frac{2}{5} \frac{R}{t} \phi(\eta) \quad . \tag{2.4.11c}$$

For any given time t, we first determine the position R(t) of the spherical shock wave by (2.4.8). Then using (2.4.11) the state of the gas at any distance R-r behind the shock at time t can be computed.

In the next section, we proceed to solve this spherical shock wave problem with Liu's and Glimm's scheme with operator splitting and then compare both solutions with the exact solution.

2.5 Test problem

We consider the partial differential equations (2.4.2a-c) which we write compactly as

$$\begin{bmatrix} \rho \\ u \\ p \end{bmatrix}_t + \begin{pmatrix} u & \rho & 0 \\ 0 & u & \frac{1}{\rho} \\ 0 & \rho c^2 & u \end{pmatrix} \begin{bmatrix} \rho \\ u \\ p \end{bmatrix}_x = -\frac{2}{r} \begin{bmatrix} \rho u \\ 0 \\ -\gamma p u \end{bmatrix} \tag{2.5.1}$$

with initial conditions

$$(\rho,u,p)^T = \begin{cases} (\rho_o,u_o,p_o)^T & \text{for } r=R_o \\ (1.25,0,0.098)^T & \text{for } r>R_o \end{cases} \tag{2.5.2}$$

where t_o = 0.217558 milliseconds and R_o,ρ_o,u_o,p_o are defind by (2.4.9) and (2.4.11) respectively at $t = t_o$ and $\eta = 1$. Also, mass, length and time are measured in kilograms, meters, and milliseconds. The initial value problem as defined by (2.5.1) and (2.5.2) is then solved by both Liu's scheme (see section 2.3) and Glimm's scheme with operator splitting (see section 2.4). The spatial grid size used is $\frac{h}{2^n}$, where h = 0.2 and n=0,1,2. Finally, as in the last chapter, we measure the superiority of one scheme over the other by examining the shock-jump errors at each time level N defined by

$$\sum_{i=1}^{N} |p_{l,r} - \hat{p}_{l,r}|\Delta t, \quad \text{where} \tag{2.5.3}$$

$p_{l,r}$ = exact pressure difference between the left and right

states of the shock at time $N\Delta t$,

$\hat{p}_{l,r}$ = estimated pressure difference between the left and right states of the shock.

The shock-jump errors from time levels 18-48 μseconds are displayed in table 2.2 and graphed in graph 2.1 while the execution times for both schemes are tabulated in table 2.3.

Observations and comments

The shock-jump errors resulted when using Liu's scheme and Glimm's scheme with operator splitting are close for for h=0.05 and h=0.2. However, for h=0.1, the results obtained by Glimm's scheme with operator splitting is definitely better than Liu's scheme, see table 2.2 and graph 2.1. Moreover, the execution time is less for Glimm's scheme in all cases. Hence if we judge the superiority of one scheme by its efficiency, that is, the amount of labor required to achieve a certain level of accuracy, Glimm's construction with operator splitting is definitely superior to Liu's.

Moreover, there is one major difference between Liu's scheme and Glimm's scheme. When transonic flow takes place, Liu's construction fails (see section 2.2), but Glimm's scheme with operator splitting has no difficulties in continuing the construction of a global solution. For example in this case when $t-t_o>50$ μseconds, transonic flow develops and Liu's scheme cannot be carried out any further, but this has no effect on operator splitting; in fact, even for time up to 859 μseconds and using only spatial grid size 0.2, the shock locations are determined with great accuracy (see graph 2.2). The density, velocity, and pressure profiles at time 859 μseconds are also displayed in graphs 2.3-2.5 for comparisons with exact solutions.

2.6 Conclusion

For the treatment of spherical shock wave problems (typically blast wave problems), Glimm's scheme with operator splitting should be preferred over Liu's scheme.

Finally, the method of characteristic tracing which solves the Riemann problem (exactly) as defined by the partial differential equation (2.1.1) and initial data (2.1.2) with $G(x) = + \frac{2}{x}$ cannot be carried out. Thus the straightforward generalization of Glimm's scheme as described in the last chapter is not feasible for spherical shock wave problems.

Chapter 3 Shock propagation down a duct of variable cross-section

3.1 The Classical and Generalized Chisnell formula

If the cross-sectional area A(x) does not vary too rapidly, gas flow in the variable area duct is given by (2.1.1) with $G(x)=A'(x)/A(x)$. Using this set of equations, Chisnell [1] studied the problem of shock propagation down a duct of variable cross-section where the gas ahead of the shock was at rest. Under the assumptions that the flow behind the shock is nearly steady, and that wave generated behind the shock do not interact strongly with it, he was able to derive the following ordinary differential equation for the mach number M(x) of the shock:

$$\frac{M}{M^2-1}\lambda(M)\frac{dM}{dx}+\frac{1}{A}\frac{dA}{dx}=0, \tag{3.1.1a}$$

where

$$\lambda(M)=\left(1+\frac{2}{\gamma+1}\frac{1-\mu^2}{\mu}\right)\left(1+2\mu+\frac{1}{M^2}\right) \tag{3.1.1b}$$

$$\mu^2=\frac{(\gamma-1)M^2+2}{2\gamma M^2-(\gamma-1)}. \tag{3.1.1c}$$

Recall that the mach number of the shock is related to the shock speed U by

$$M=\frac{U-u_r}{c_r}, \tag{3.1.2}$$

where u_r and c_r are respectively the speed of the gas and the sound speed of the flow ahead of the shock. A very neat derivation (but less general than the one described next) of (3.1.1) can be found in Whitham [16]. We shall derive this formula via a more general setting.

Generalization of Chisnell's formula

We return again to the general hyperbolic system (1), which we rewrite as

$$\bar{u}_t + A\,\bar{u}_x = \bar{g}\,(\bar{x},u) \quad . \tag{3.1.3}$$

Consider a shock moving at constant speed from a region where g=0 into a region where g≠0. See figure 3.1. Futhermore, assume that the shock arrives at the position x_{n-1} at time t=0 with speed U_{n-1}. (See figure 3.2) Denote the post-shock state by $\bar{u}_{n-1}$ and the pre-shock state by $\bar{u}_r$. First let $\bar{v}$ be the solution to the steady- state equation

$$A\,\bar{u}_x = \bar{g}\,(x_{n-1},\bar{u}) \tag{3.1.4a}$$

with

$$\bar{u}\,(x_{n-1}) = \bar{u}_{n-1} \tag{3.1.4b}$$

evaluated at $x_n = x_{n-1} + \Delta x$. Next, we solve the Riemann problem with g=0 and initial data

$$\bar{u}(x,0) = \begin{cases} \bar{v} & x<x_n, \\ \bar{u}_r & x>x_n. \end{cases} \tag{3.1.5}$$

Assume that a leading shock is produced with a new post-shock state $\bar{u}_n$ and shock speed U_n. Our objective now is to compute the change in shock speed, that is, $\frac{U_n - U_{n-1}}{\Delta x}$.

Using the Rankine-Hugoniot condition, the post-shock state can be parameterized by its speed, so we can write $\bar{u}=H(U)$. In particular, $\bar{u}_{n-1}=H(U_{n-1})$. Also if $S(x,\bar{u}_{n-1},x_{n-1})$ is the solution operator to (3.1.4), we get

$$\bar{v} = S(\Delta x, \bar{u}_{n-1}, x_{n-1}). \tag{3.1.6}$$

Finally if $R(\bar{u})$ denotes the speed of the leading shock resulting from the Riemann problem with left state $\bar{u}$, right state $\bar{u}_r$, then

$$U_n = R(\bar{v}) = R \cdot S(\Delta x, \bar{u}_{n-1}, x_{n-1}) \quad .$$

Then using Taylor's expansion, we find,

$$U_n = R \cdot S(0, \bar{u}_{n-1}, x_{n-1}) + \frac{\partial}{\partial x} R \cdot S(0, \bar{u}_{n-1}, x_{n-1}) \, \Delta x + O(\Delta x^2).$$

But $S(0, \bar{u}_{n-1}, x_{n-1}) = \bar{u}_{n-1}$ and $R(\bar{u}_{n-1}) = U_{n-1}$, so

$$\frac{U_n - U_{n-1}}{\Delta x} = \frac{\partial}{\partial x} R \cdot S(0, \bar{u}_{n-1}, x_{n-1}) + O(\Delta x) \quad . \tag{3.1.7}$$

Since $\frac{\partial}{\partial x} R \cdot S(x, \bar{u}_{n-1}, x_{n-1}) = R' \cdot S(x, \bar{u}_{n-1}, x_{n-1}) S_x$ and by definition

$S_x = A^{-1} g(x_{n-1}, \bar{u})$, then

$$\frac{U_{n-1} - U_n}{\Delta x} = R \cdot S(0, \bar{u}_{n-1}, x_{n-1}) A^{-1} g(x_{n-1}, \bar{u}_{n-1}). \tag{3.1.8}$$

Formally passing to the limit, we get

$$\frac{dU}{dx} = R'(H(\sigma)) A^{-1} g(x, H(\sigma)). \tag{3.1.9}$$

This is the generalized Chisnell shock propagation equation.

The above derivation was due to Wendroff[15]where he also applied (3.1.8) to shock propagation problems in variable area ducts with phase changes.

Suppose now that the speed of the shock at the position x_o is U_o, then the generalized Chisnell shock propagation equation (3.1.9) is an ordinary differential equation that informs us what the shock speed is at a latter position x due to the influence of the source term. We illustrate this more concretely by looking at the following example.

Example 3.1

Consider now the problem of a shock moving into a duct of variable cross-section A(x). Using the steady equations (2.2.4),

$$A^{-1}g(x,H(\sigma)) = \frac{A'(x)}{A(x)} \frac{1}{c^2 - u^2} \begin{pmatrix} \rho u^2 \\ -c^2 u \\ \rho u^2 c^2 \end{pmatrix} \tag{3.1.10}$$

Hence (3.1.9) reduces to

$$\frac{dU}{dx} = \frac{A'(x)}{(c^2 - u^2)A(x)} \rho c^2 \frac{\partial R}{\partial \rho} - c^2 \frac{\partial R}{\partial u} + c^2 \rho u \frac{\partial R}{\partial p} . \tag{3.1.11}$$

Using the assumptions made by Chisnell and using the Rankine-Hugoniot conditions (see Whitham[16]):

$$\begin{cases} u = c_r \frac{2}{\lambda + 1}\left(M + \frac{1}{M} \right) \\ p = p_r c_r^2 \left(\frac{2}{\lambda - 1} M^2 - \frac{\lambda - 1}{\lambda(\lambda + 1)} \right) \\ \rho = \rho_r \frac{(\lambda + 1)M^2}{(\lambda - 1)M^2 + 2} \end{cases} \tag{3.1.12}$$

$\frac{\partial U}{\partial \rho}$, $\frac{\partial U}{\partial u}$, $\frac{\partial U}{\partial p}$ can be computed in terms of M. Moreover, using (3.1.12) ρ, p, u and c can be expressed in terms of M. Substituting all these into (3.1.11), the originalChisnell formula (3.1.1) will be recovered after some simplications.

Note that according to this classical Chisnell formula (3.1.1), the factor that determines the mach number of a given shock at a latter location of the duct is simply the relative rate of change of the duct area, that is, $A'(x)/A(x)$ and nothing else. This fact is crucial as we shall see in case 1 and 2 of the test problem to be described in section 3.3.

Remarks

(1) It is interesting to note that the similarity between the procedure used in obtaining Wendroff's generalized Chisnell formula and the solution of a Riemann problem used in Liu's scheme (see section 2.2). Given the Riemann problem with initial data

$$\bar{u}(x,0) = \begin{cases} \bar{u}_{n-1} & \text{for } x<x_n \\ \bar{u}_r & \text{for } x>x_n \end{cases},$$

step 1 of both Liu's scheme and Wendroff's procedure is the recomputation of the given data by the steady state equation (3.1.4a). Then step 2 of both procedures is the solution of the Riemann problem with the new initial data assuming that $\bar{g} = 0$. The major difference, however, is that in Liu's scheme this procedure is only a key step in a more elaborate global construction scheme for the general hyperbolic system (3.1.3) with arbitrary initial data. In Wendroff's scheme this procedure is a means of obtaining a finite difference approximation to the local change in shock speed due to the influence of the source term assuming implicitly that the given initial data in all cases resulted into shock waves.

(2) For a shock that slows down due to the expanding geometry of the duct, continuing interactions with the flow behind are expected, and Chisnell's formula is not appropriate. In a converging duct, however, a shock wave typically speeds up and thus Chisnell's formula is good, see Whitham[16]. In section 3.3, we shall study shocks propagating in various converging ducts, moreover, we shall compare the results obtained by Glimm's scheme with operator splitting and Liu's scheme with that

obtained by Chisnell's formula. But first, we shall examine the possibility of incorporating Chisnell's formula into Glimm's scheme and Liu's scheme.

3.2 The Chisnell formula and the numerical schemes of Glimm and Liu

One of the most crucial assumption in the derivation of Chisnell's formula is that waves generated behind the shock do not interact strongly with it (see 3.1). Therefore quite naturally in order to improve Chisnell's formula one must be able to take care of all the wave interactions behind the leading shock. At first glance this seems to be a formidable task but this is precisely what both the Glimm and Liu schemes are geared towards -- construction of a global solution without going through the painful process of characteristic tracing. More precisely, we improve Glimm's and Liu's scheme (or Chisnell's formula depending on how one looks at it) in the following way.

Let the approximate values of the solution at time nk obtained by either Liu's scheme or Glimm's scheme (with operator splitting) be denoted by (ρ_i^n, u_i^n, p_i^n), $|i|=0,1,2,\ldots$. Then we compute $(\rho_{i+1/2}^{n+1/2}, u_{i+1/2}^{n+1/2}, p_{i+1/2}^{n+1/2})$ from (ρ_i^n, u_i^n, p_i^n) and $(\rho_{i+1/2}^n, u_{i+1/2}^n, p_{i+1/2}^n)$ by Glimm's or Liu's construction exactly as described in 2.2 except when we come to the position of the leading shock, say, at (l+1/2)h. Thus, $(\rho_{l+1/2}^n, u_{l+1/2}^n, p_{l+1/2}^n) = (\rho_r, u_r, p_r)$ which is the state of the gas ahead of the leading shock and is given initially. Then given the initial left state (ρ_l^n, u_l^n, p_l^n) and the right state (ρ_r, u_r, p_r), the Riemann problem without the source term can be solved readily and there are two possibilities:

(1) the right wave is not a shock: we simply compute $(\rho_{l+1/2}^{n+1/2}, u_{l+1/2}^{n+1/2}, p_{l+1/2}^{n+1/2})$ from (ρ_l^n, u_l^n, p_l^n) and $(\rho_{l+1}^n, u_{l+1}^n, p_{l+1}^n)$ as before by our numerical schemes.

(2) the right wave is a shock: let the initial mach number of the shock

be M_o. Then the mach number of the shock at time $(n+1/2)k$ can be obtained by computing the solution at $k/2$ of the initial value problem defined by the Chisnell formula :

$$\frac{dx}{dt} = c_r M \quad , \tag{3.2.1a}$$

$$\frac{dM}{dt} = -c_r \frac{M^2-1}{\lambda(M)} \frac{A'(x)}{A(x)} \quad , \tag{3.2.1b}$$

with initial data

$$x(nk)=(1+1/2)k, \qquad M(nk)=M_o \quad . \tag{3.2.1c}$$

The post-shock state (ρ^*,u^*,p^*) at time $(n+1/2)k$ is then obtained by the Rankine-Hugoniot conditions. Thus

$$(\rho^{n+1/2}_{1+1/2},u^{n+1/2}_{1+1/2},p^{n+1/2}_{1+1/2}) = \begin{cases} (\rho_r,u_r,p_r) & x(n+1/2k)>(1+1/2+\theta_n)h \\ (\rho^*,u^*,p^*) & x(n+1/2k)<(1+1/2+\theta_n)h \end{cases}$$

The superiority of using Chisnell's formula with Glimm's scheme and Liu's scheme in this way is demonstrated in the test problems described in the next section.

3.3 Test problems

In this section we consider a shock propagating into monotonically converging and diverging ducts defined respectively by $A'(x)/A(x)=-1/(x_0-x)$ and $1/(x_0+x)$ where x_0 is known as the apex of the ducts and $x_0 \notin [x_l, x_r]$. In the case of a converging duct, we differentiate between two cases, namely $|A'(x)/A(x)|<1$ and $|A'(x)/A(x)|>1$ with $x_0=x_r$. While for a diverging duct, we look at the case where $A'(x_l)/A(x_l)=1$ and $A'(x_r)/A(x_r)<<1$. We shall see that the results obtained are drastically different form each other.

For definiteness, the test problems to be described are concerned with the solution of the initial problem defined by the partial differential equations

$$\begin{bmatrix} \rho \\ u \\ p \end{bmatrix}_t + \begin{pmatrix} u & \rho & 0 \\ 0 & u & \frac{1}{\rho} \\ 0 & \rho c^2 & u \end{pmatrix} \begin{bmatrix} \rho \\ u \\ p \end{bmatrix}_x = -\frac{A'(x)}{A(x)} \begin{bmatrix} \rho u \\ 0 \\ \gamma p u \end{bmatrix}$$

with initial conditions

$$(\rho,u,p)\ (0) = \begin{cases} (1.0, 0.0, 1.4) & \text{for } x>x_1 \\ (5.5, 11.6, 152.9) & \text{for } x<x_1 \end{cases}$$

The initial discontinuity is immediately resolved into a shock of mach number $M(x_l)=10$. Using this as initial conditions for the Chisnell formula (3.1.1), the shock speed as well as the post-shock state can theoretically be computed for $x \notin (x_l, x_r]$. As mentioned before,

Chisnell's formula provides us with accurate predictions for converging ducts. Thus, in cases 1 and 2 below we wish to solve the initial value problem (3.2.1) by Glimm's scheme (with operator splitting), Liu's scheme, Glimm's scheme (with operator splitting) with Chisnell's formula and compare their errors of the post-shock states with respect to Chisnell's results.

Case 1:

$$A'(x)/A(x) = \begin{cases} -1/(7-x), & x \in (5,6] \\ 0, & x<5. \end{cases}$$

In this case, two different spatial grid sizes h=0.04, and h= 0.02 are used. The computed post-shock states form x=5.1 to 5.9 of the three numerical schemes are shown in tables 3.1 and 3.2 while their errors relative to Chisnell's formula can be found in tables 3.3 and 3.4. For convenience, the averaged errors are also computed and displayed in table 3.9. Finally, the computational time is displayed in table 3.10 for comparison purposes.

Observations:

(1) The post-shock density of both the Liu and Glimm schemes oscillates, see tables 3.1 and 3.2. This is not physically realistic because the shock accelerates as the duct narrows hence the post-shock density should increase in the positive x-direction. However, this phenomenon does not exist for Glimm's scheme with Chisnell's formula; in fact, the post-shock density increases as desired.

(2) From table 3.9, we see that Glimm's scheme with Chisnell's formula is definitely superior to the other two numerical schemes. Moreover,

Glimm's scheme is better than Liu's scheme and the computational time is less.

Case 2:

$$A'(x)/A(x)= \begin{cases} -1/(7-x), & x\in(6,7], \\ \\ 0, & x<6. \end{cases}$$

The two spatial grid sizes used are h=0.02, and h=0.01. Tables 3.5 and 3.6 contain the computed post-shock states form x=6.1 to 6.9 of the three numerical schemes while tables 3.7 and 3.8 contain their relative errors.

Observations:

(1) Again form tables 3.5 and 3.6 we see that the post-shock density of both Liu's and Glimm's scheme oscillates while that of Glimm's scheme with Chisnell's formula increases. (2) As in case 1, we see from table 3.9 that Glimm's scheme with Chisnell's formula on the average is the superior one of the three schemes. Liu's scheme, however, is better than Glimm's scheme in this case. In fact, as the shock approaches the apex x_0=7 (where $|A'(x)/A(x)|=\infty$), Liu's scheme is surprisingly good.

In conclusion for the cases of converging ducts, Glimm's scheme with operator splitting and Chisnell formula's is the best scheme among the three not only because the errors relative to Chisnell's formula is less, but most important of all it gives physically realistic post-shock densities as the shock accelerates down the ducts. Between Glimm's scheme and Liu's scheme, one has to look at the relative change in x-sectional area $A'(x)/A(x)$. $|A'(x)/A(x)|=1$ is approximately the dividing

line. If $|A'(x)/A(x)|<1$, then Glimm's scheme is more accurate and takes less time. If $|A'(x)/A(x)| >> 1$, then Liu's scheme is very good and should be used even though it takes more time.

Before considering the case of a diverging duct, it is instructive to look at the pressure, velocity, and density profiles: they are plotted respectively in graphs 3.1a-c for case 1 using h=0.02 and in graphs 3.2a-c for case 2 using h=0.01. Immediately, one will notice the difference in their post-shock wave structures as described below.

Profile 3.1: the post-shock wave structure is the simpler of the two cases. It consists of a steady-state compression wave of the C- family follow by a rarefaction fan again of the C- family before ending in a shock of incresing strength. Both the compression wave and rarefaction fan are propagating in the positive x-direction.

Profile 3.2: in the begining (for $x<6.5$), the wave structure still consists mainly of a steady-state compression wave and a rarefaction fan (both of the C- family), however, as the relative rate of narrowing of the duct increases, the two waves interact producing a C+ rarefaction fan in between. While the compression wave and the C+ rarefaction fan are expanding to the right, the C- rarefaction fan is slowly being 'eaten up'. The post-shock wave structure becomes more complicated as the shock approaches the apex. As for the shock, it is accelerating faster and faster with $M(x)\rightarrow\infty$ as $x\rightarrow x_0$.

It is important to note that the difference in wave structures in both cases are not determined by the rate at which the ducts are converging because for both ducts, $A'(x)=-1$. Furthermore, it is not the

difference in x-sectional area change which is the key factor because $A(x_l)-A(x_r)=1$. The determining factor is $|A'(x)/A(x)|$ -- the relative rate of change of the duct, and this can be seen plainly from the Chisnell formula (3.1.1). For $|A'(x)/A(x)|<1$, the post-shock wave structure is simple, consisting of a compression wave followed by a rarefaction fan. For $|A'(x)/A(x)|>>1$, one should expect the post-shock waves to interact hence producing new waves and thus a more complicated picture.

Case 3:

We now concentrate on the problem of sending a shock down a linearly diverging duct. As explained in section 3.1, the Chisnell formula no longer can give us good predictions on the mach number M(x) of the shock as well as the post-shock states (ρ,u,p)(x). However, by examining carefully the density, velocity, pressure profiles of the three numerical schemes (namely Liu's, Glimm's, and Glimm's scheme with Chisnell's formula), we can still recognize each one's better quality (if any) over the others.

$$A'(x)/A(x) = \begin{cases} 1/(1+x), & x \in (0,16] \\ 0, & x<0. \end{cases}$$

The spatial grid size used for all numerical schemes will be h=0.2. The density, velocity, and pressure profiles for Glimm's scheme are displayed in graphs 3.3a-c and that for Glimm's scheme with Chisnell's formula in graphs 3.4a-c. Also, the computational time of different numerical schemes used can be found in table 3.11. The detailed post-shock wave structure will be discussed later. Except for minor differences, the wave structures for all numerical schemes are almost identical. However, the major advantage of Glimm's scheme with Chisnell's formula is that it gives physically realistic post-shock states. The reason being that as the shock slows due to the expanding geometry of the duct, the post- shock pressure, density, and velocity should decrease. While both schemes predict that the post-shock pressure and

velocity will decrease only Glimm's scheme with Chisnell's formula gives a monotonic decreasing sequence of post-shock densities.

One of the most prominent and undesirable feature for both schemes is the presence of heavy oscillations coalescing together in the beginning of each velocity profile. Such violent oscillations are clearly absent in the pressure and density profiles suggesting that we might have a steady-state rarefaction fan of the C- family. This brings out one advantage of Liu's scheme which uses steady states in his construction, see secion 2.2. If indeed a steady- state rarefaction fan exists, then Liu's scheme shall produce one without any undesirable oscillations whatsoever. This is clearly illustrated in the profiles produced by Liu's scheme (graphs 3.4a-c). Unfortuately Liu's scheme still has the problem of not producing a monotonic decreasing sequence of post-shock densities. This can be remedied easily.

Liu's scheme with Chisnell's formula

As described in section 3.2, Chisnell's formula can be easily incorporated in Liu's scheme. The results are illustrated in graphs 3.5a-c, where the advantage of using Liu's scheme to produce steady-state waves and the advantage of Chisnell's formula to produce the physically realistic post-shock state are combined. These two major advantages of Liu's scheme with Chisnell'sformula prove itself to be the best scheme among the four numerical schemes we have discussed so far. Before concluding this section, we now turn to examine the post-shock wave structure. Profile 3.5: the wave structure is more complicated than the ones we have seen for converging ducts. At first we have a steady-state rarefaction fan (C- family), then a shock and compression

waves (C+ family) before ending into the leading shock which decreases in strength as the duct widens. The steady-state rarefaction is very strong and it moves in the positive x-direction. The compression wave is very small at first but gradually widens and decreases in strength as it travels down the duct.

3.4 Conclusions

(1) The Chisnell formula in general is very good only as a local result because new waves typically develope behind the shock and interact with it. The wave structure can be rather complicated as seen in case 1 and 2 in the last section. Thus, it is imperative to be able to track all the new waves generated behind the shock. This, however, can be accomplished readily by resorting to Glimm's scheme and Liu's scheme and then using Chisnell's formula as a way of obtaining the appropriate boundary conditions at the leading shock. The result is a scheme which gives physically realistic post-shock states as well as one which takes care of all the wave interactions due to the geometry of the duct with relative ease.

(2) Of the four numerical schemes developed so far, Glimm's scheme with Chisnell's formula is the best for a converging duct. However, for a diverging duct, heavy oscillations typically set in and mask up the presence of a steady-state rarefaction fan and thus Liu's scheme with Chisnell's formula is superior in this case.

(3) Finally because of the generalized Chisnell formula derived by Wendroff in section 3.1, the coupling of Chisnell's formula with Glimm's scheme and Liu's scheme can be theoretically extended from the case of a variable x-sectional duct to the case of a general hyperbolic system (1).

Chapter 4 Conclusions and Discussions

In the last chapter, we have developed two new schemes, namely

(1) Glimm's scheme with operator splitting and Chisnell's formula, and

(2) Liu's scheme with Chisnell's formula.

While (1) is best in treating the problem of a shock propagating down a duct of monotonic decreasing area, (2) is best for a duct of monotonic increasing area. Both scheme 1 and 2 have been coded in FORTRAN; they are known as subroutines GLIMM and LIU respectively and are available from the author. Given arbitrary initial data and cross-sectional area (either monotonic decreasing or increasing), one can advance from one time-level to the next by making calls to either GLIMM or LIU.

Now using these two subroutines, the case of a arbitrary cross-sectional area duct can be handled easily as illustrated by the following example. Consider a duct known as the de Laval nozzle depicted in the diagram below:

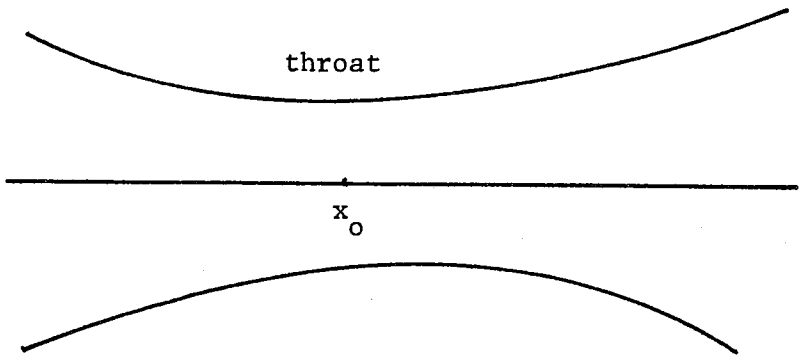

De Laval nozzle

The section at $x = x_o$ is known as the throat of the nozzle. For $x < x_o$, the duct area is monotonic decreasing, while for $x > x_o$, the duct area is monotonic increasing. Hence to obtain the best results at each time level, one simply utilizes subroutines GLIMM and LIU at different section of the nozzle. In other words, for the section that is decreasing in area ($x < x_o$), call subroutine GLIMM, while for the section that is increasing in area ($x > x_o$), call subroutine LIU. The extension to the general case of arbitrary cross-sectional area is clear.

At this point, a word of caution is in order. For a de Laval nozzle, transition from subsonic to supersonic flow is possible, see for example Courant and Fredrichs[4]. In this situation, Liu's scheme by itself is not applicable as explained at the end of section 2.2. In fact, as noted by Liu[11] in his recent paper on transonic gas flow for a variable area duct, in the event of such a transition, the flow is sonic at $x = x_o$ where the duct is narrowest. But on the other hand, it is also observed that a stable standing shock wave may occur in the expanding portion of the duct which indicates that Liu's scheme is better suited than Glimm's scheme for that section of the duct. Thus hybridizing subroutine GLIMM and LIU for different section of the duct at each time level is indeed sensible.

Finally, it would be a substantial improvement if one could extend Liu's scheme to handle transonic flow as well. Moreover, more need to be known about the phenomenon of transonic flow itself as modeled by the one-dimensional equations (3.3.1a). As Liu[11] has pointed out: if one uses (3.3.1a), then for a de Laval nozzle, bifuracating phenomena may occur and a flow may not depend on its values at $x = \pm\infty$ uniquely and

smoothly. This raises an important question: is it even correct to use these one-dimensional equations to model a phenomena which is inherently two- or three-dimensional ?? To this date, this question is far from being satisfactorily answered.

Figure 1.1

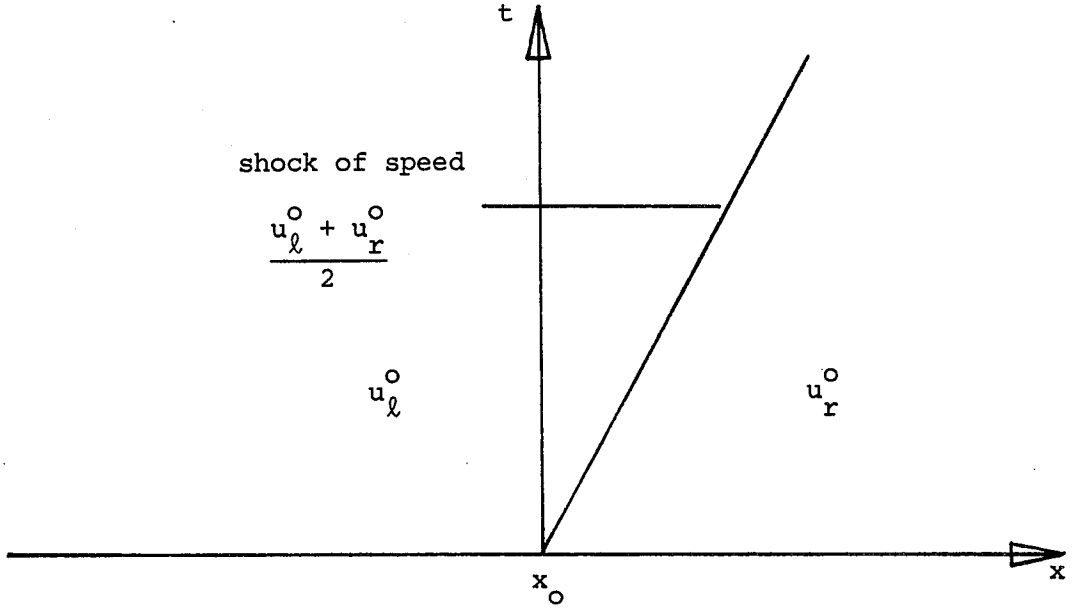

Figure 1.2

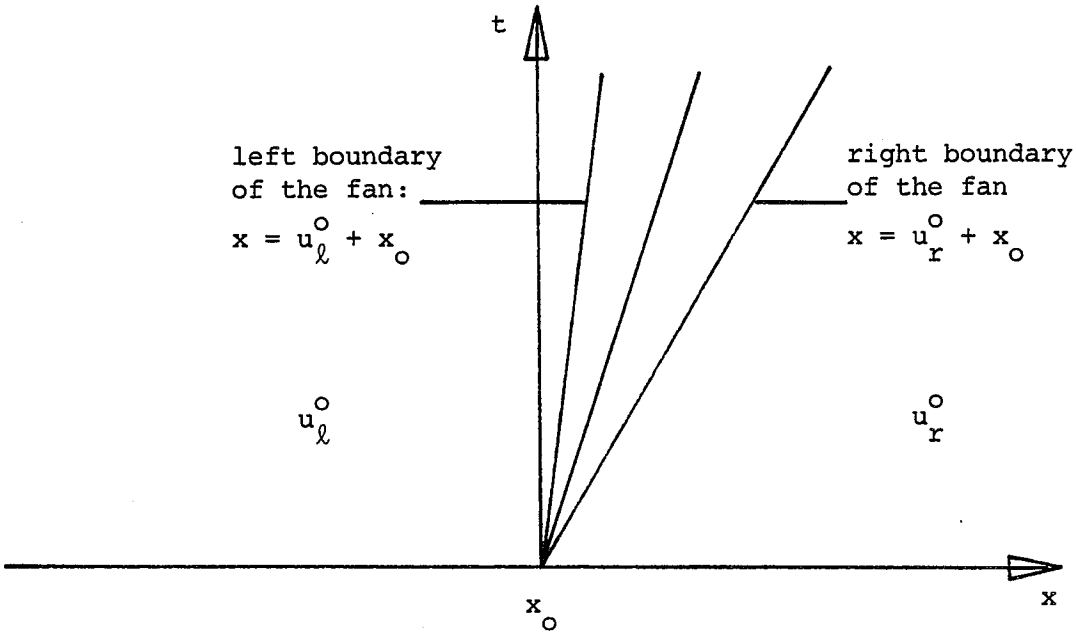

Figure 1.3

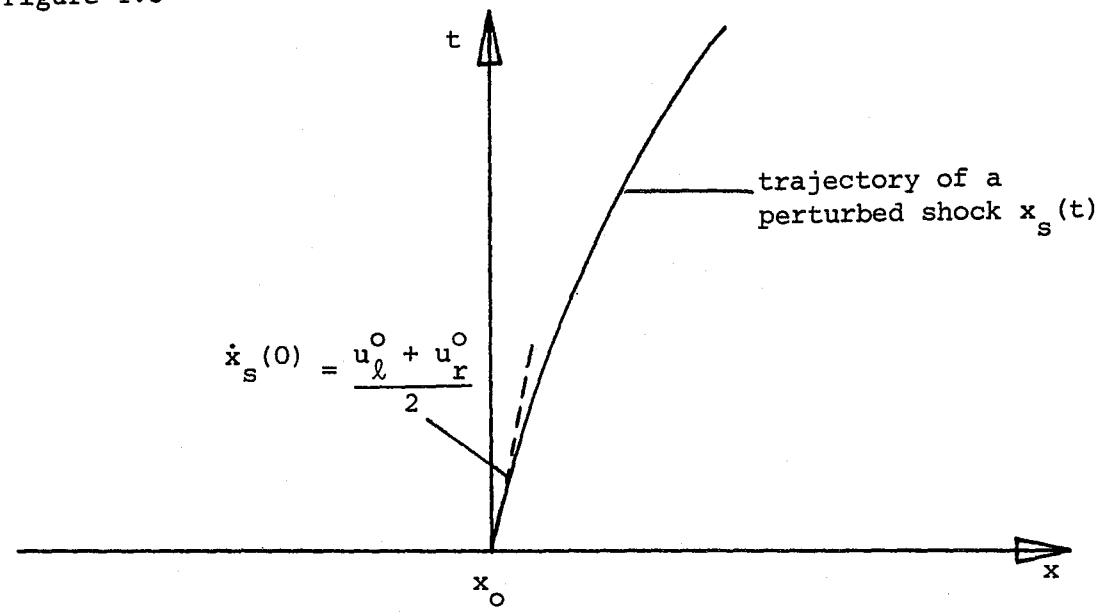

Figure 1.4

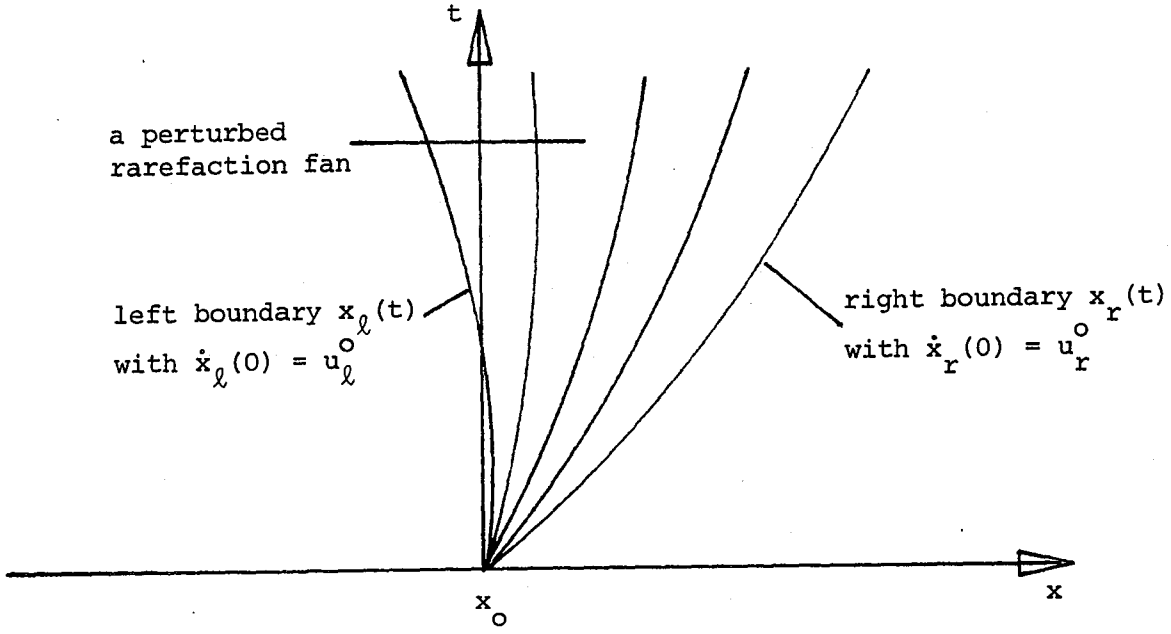

Figure 1.5

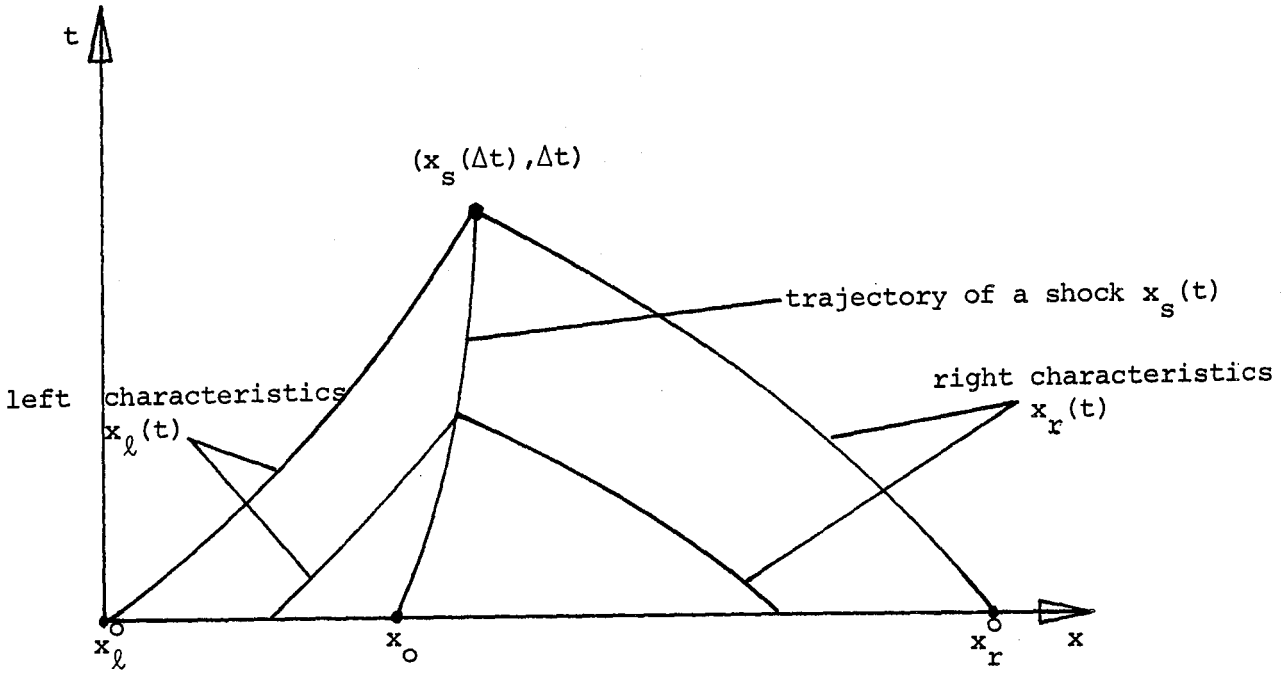

Figure 1.6

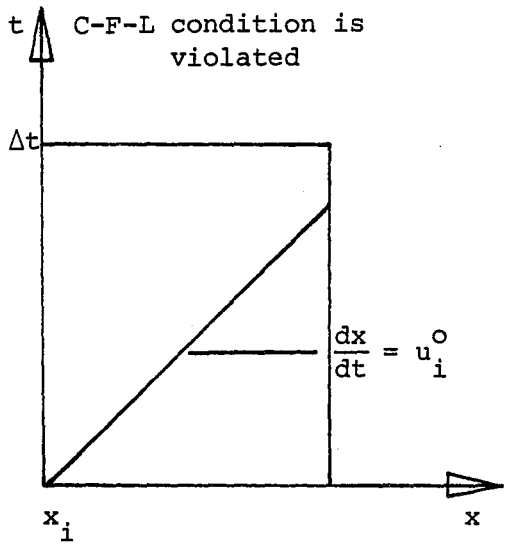

Figure 1.7

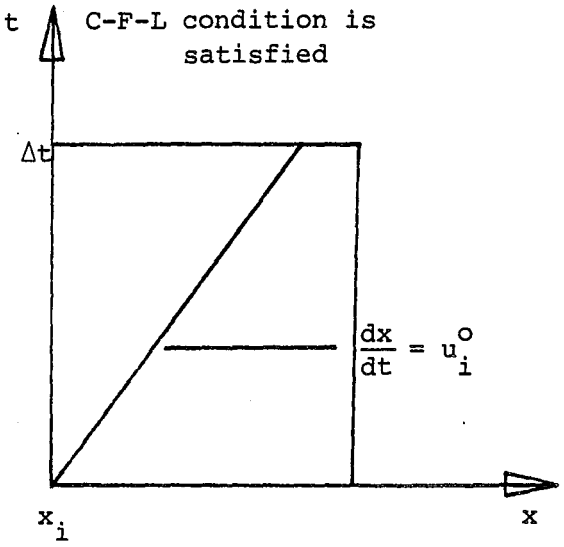

Table 1.1

t	shock-jump errors of characteristic tracing	shock-jump errors of operator splitting
0.05	0.219×10^{-3}	0.172×10^{-3}
0.10	0.687×10^{-3}	0.530×10^{-3}
0.15	0.140×10^{-2}	0.107×10^{-2}
0.20	0.235×10^{-2}	0.178×10^{-2}
0.35	0.350×10^{-2}	0.263×10^{-2}

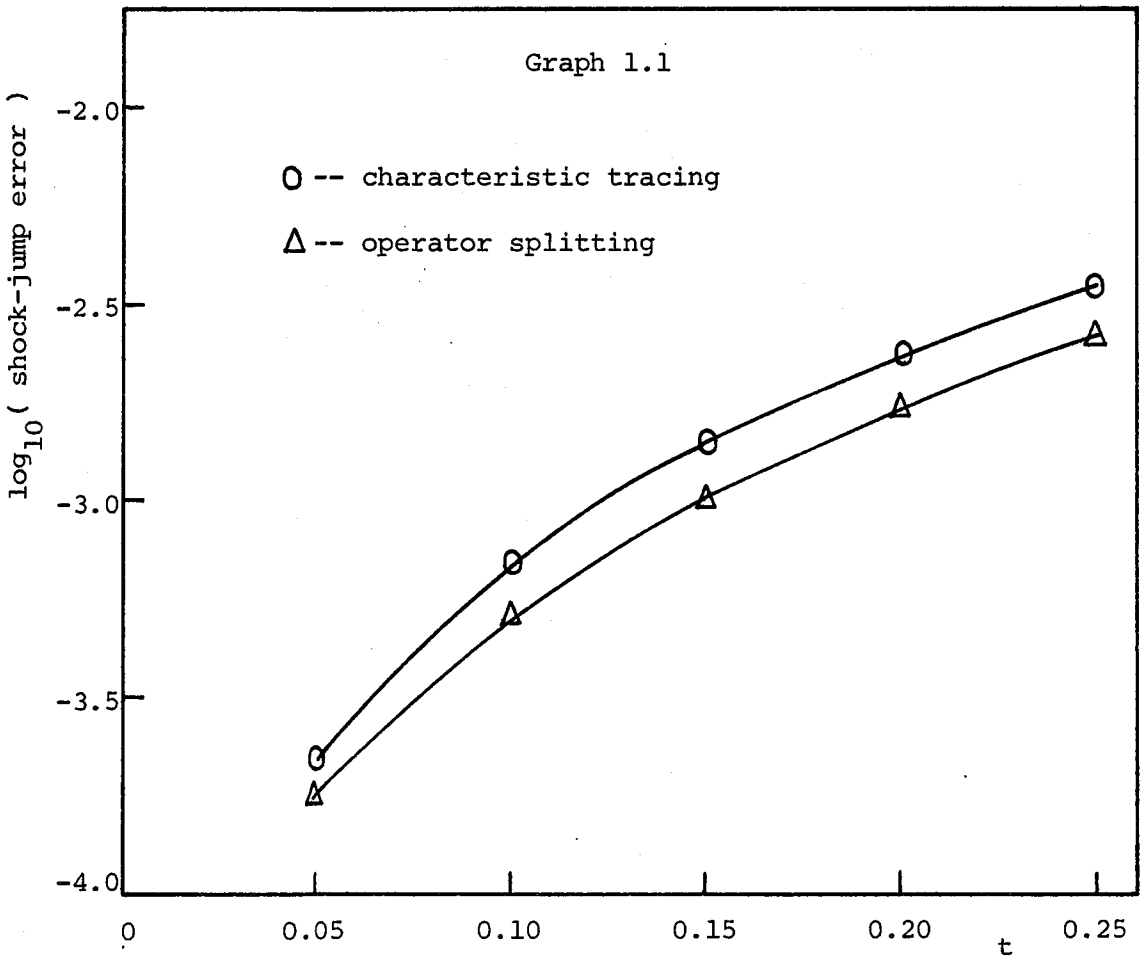

Table 1.3

h	execution time required by characteristic tracing	execution time required by operator splitting
0.2	1.00	0.01
0.1	3.05	0.04
0.0	10.67	0.16
0.025	38.70	0.64

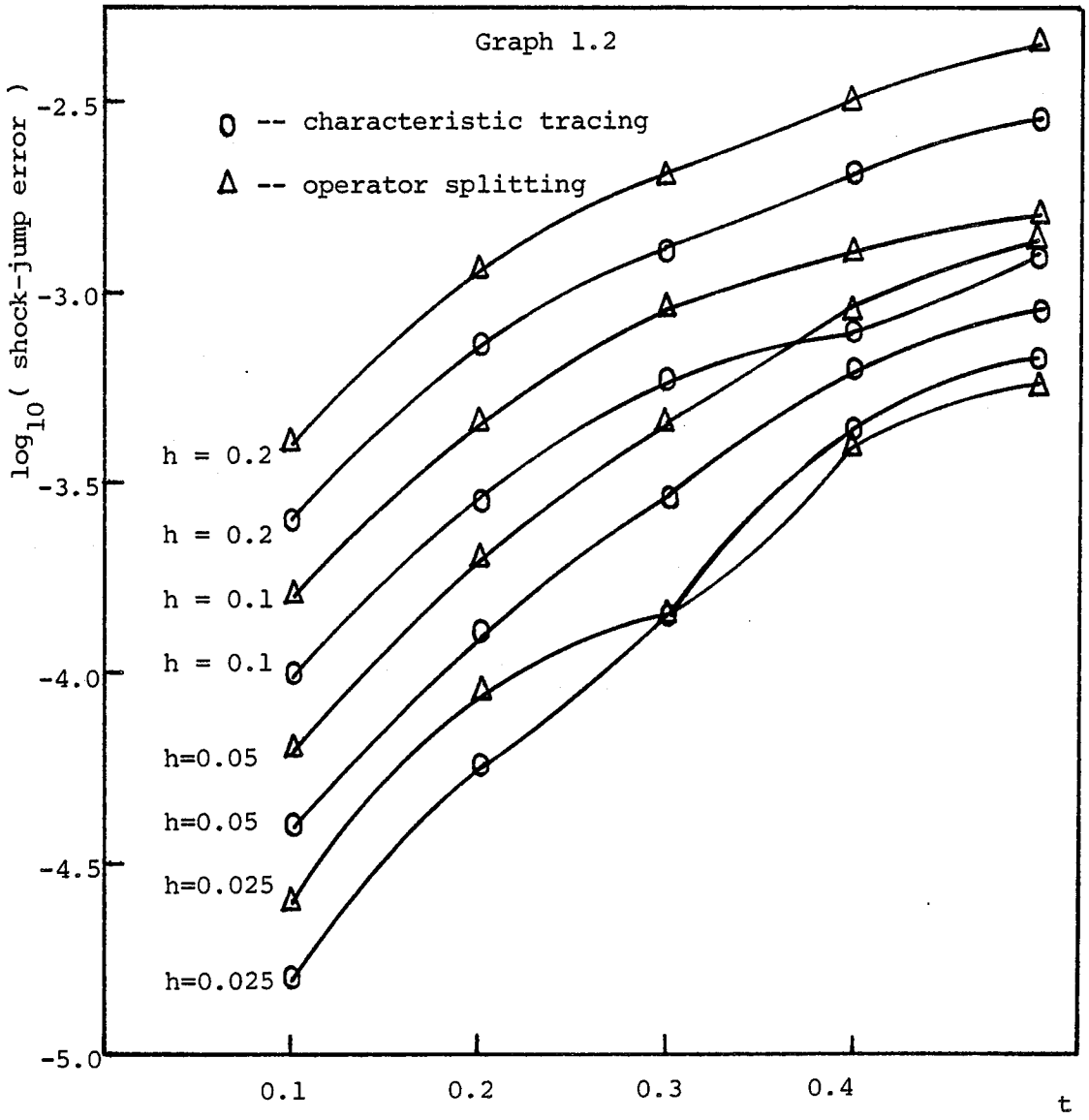

Table 1.2

	t	shock-jump errors of characteristic tracing	shock-jump errors of operator splitting
h = 0.2	0.1	0.249×10^{-3}	0.401×10^{-3}
	0.2	0.696×10^{-3}	0.115×10^{-2}
	0.3	0.121×10^{-2}	0.207×10^{-2}
	0.4	0.199×10^{-2}	0.322×10^{-2}
	0.5	0.279×10^{-2}	0.458×10^{-2}
h = 0.1	0.1	0.946×10^{-4}	0.157×10^{-3}
	0.2	0.284×10^{-3}	0.458×10^{-3}
	0.3	0.557×10^{-3}	0.895×10^{-3}
	0.4	0.786×10^{-3}	0.121×10^{-2}
	0.5	0.130×10^{-2}	0.161×10^{-2}
h = 0.05	0.1	0.382×10^{-4}	0.615×10^{-4}
	0.2	0.126×10^{-3}	0.201×10^{-3}
	0.3	0.268×10^{-3}	0.430×10^{-3}
	0.4	0.638×10^{-3}	0.919×10^{-3}
	0.5	0.922×10^{-3}	0.143×10^{-2}
h = 0.025	0.1	0.167×10^{-4}	0.263×10^{-4}
	0.2	0.572×10^{-4}	0.886×10^{-4}
	0.3	0.145×10^{-3}	0.148×10^{-3}
	0.4	0.436×10^{-3}	0.382×10^{-3}
	0.5	0.654×10^{-3}	0.560×10^{-3}

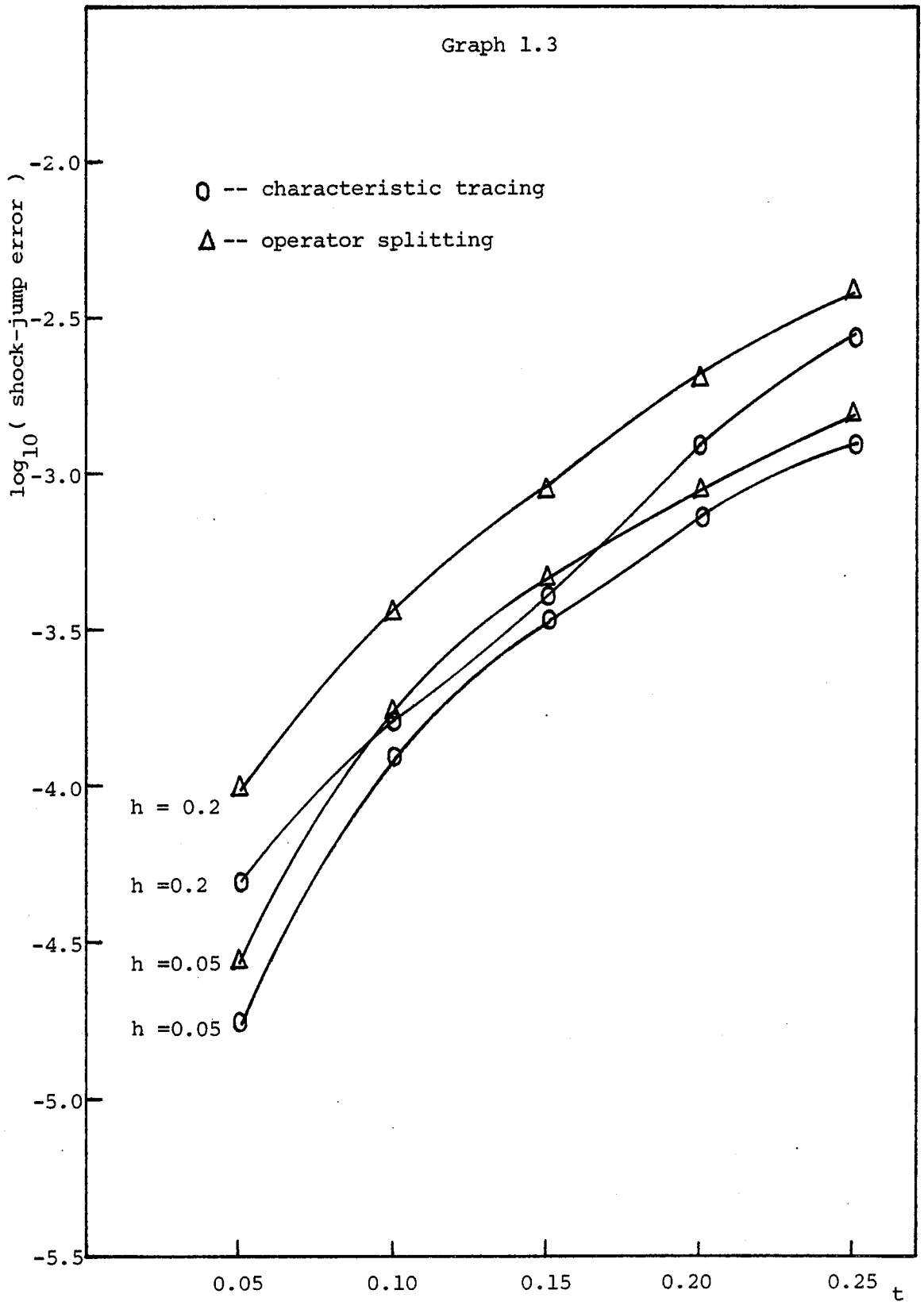
Graph 1.3
O -- characteristic tracing
Δ -- operator splitting
log10 (shock-jump error)
-2.0
-2.5
-3.0
-3.5
-4.0
-4.5
-5.0
-5.5
h = 0.2
h =0.2
h =0.05
h =0.05
0.05
0.10
0.15
0.20
0.25
t

Table 1.4

	t	shock-jump errors of characteristic tracing	shock-jump errors of operator splitting
h = 0.2	0.05	0.490×10^{-4}	0.980×10^{-4}
	0.10	0.166×10^{-3}	0.357×10^{-3}
	0.15	0.404×10^{-3}	0.866×10^{-3}
	0.20	0.124×10^{-2}	0.208×10^{-2}
	0.25	0.280×10^{-2}	0.414×10^{-2}
h = 0.05	0.05	0.174×10^{-4}	0.293×10^{-4}
	0.10	0.134×10^{-3}	0.181×10^{-3}
	0.15	0.365×10^{-3}	0.475×10^{-3}
	0.20	0.736×10^{-3}	0.943×10^{-3}
	0.25	0.127×10^{-2}	0.156×10^{-2}

Table 1.5

h	computational time of characteristic tracing	computational time of operator splitting
0.2	2.38	0.01
0.05	35.40	0.16

Figure 2.1

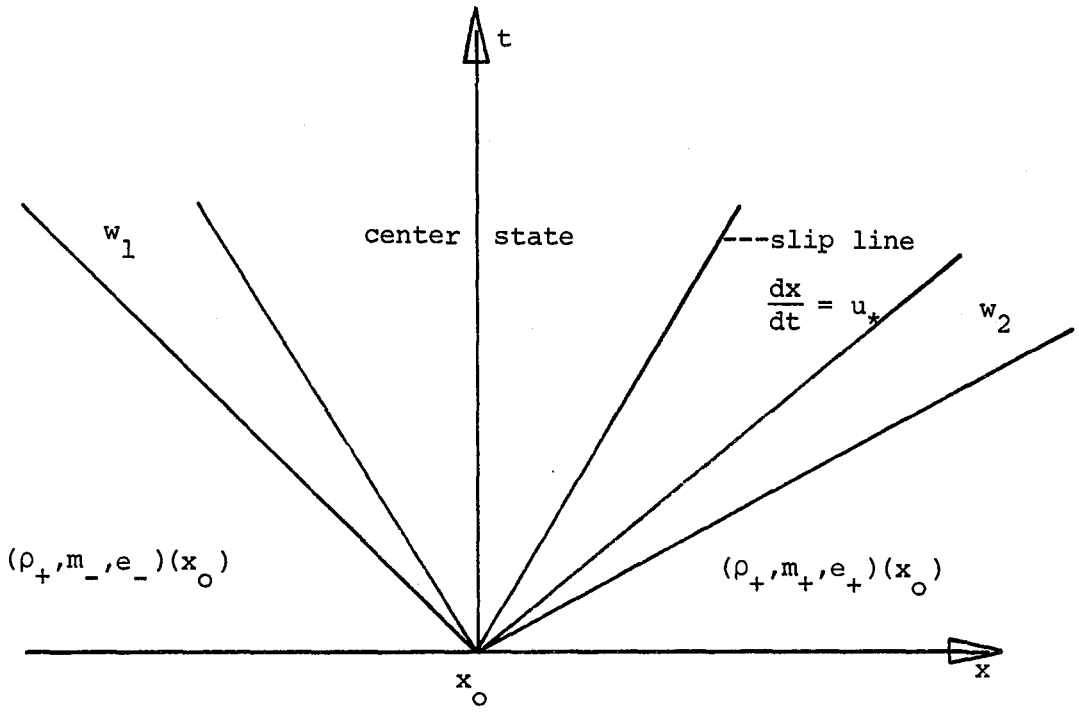
t
w_1
center state
---slip line
$\frac{dx}{dt} = u_*$
w_2
$(\rho_+, m_-, e_-)(x_o)$
$(\rho_+, m_+, e_+)(x_o)$
x_o
x

Table 2.1

η	f	ϕ	ψ
0.	0.426	0.	0.
0.1	0.426	0.072	0.560×10^{-7}
0.2	0.426	0.143	0.107×10^{-4}
0.3	0.426	0.214	0.223×10^{-3}
0.4	0.426	0.286	0.193×10^{-2}
0.5	0.427	0.357	0.103×10^{-1}
0.6	0.429	0.429	0.407×10^{-1}
0.7	0.439	0.503	0.133
0.8	0.472	0.584	0.393
0.9	0.592	0.685	1.232
1.0	1.167	0.833	6.000

Figure 2.2

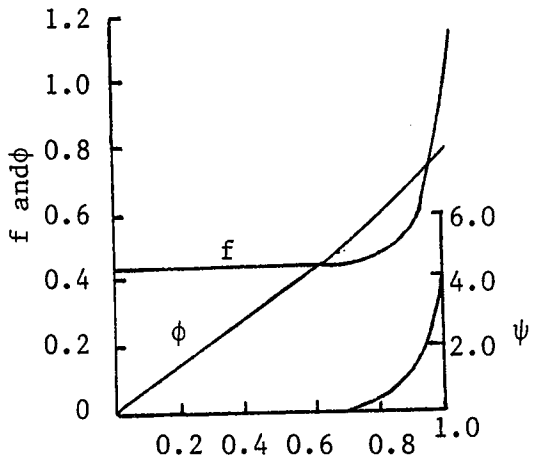

Table 2.2

	$t-t_o$ (μsec)	shock-jump errors of Liu's scheme	Glimm's scheme
h = 0.2	18	0.517	0.533
	24	0.696	0.689
	30	0.820	0.881
	36	0.964	0.980
	42	1.135	1.180
	48	1.445	1.492
h = 0.1	18	0.380	0.329
	24	0.464	0.412
	30	0.763	0.660
	36	0.939	0.812
	42	1.087	0.936
	48	1.417	1.222
h = 0.05	18	0.175	0.156
	24	0.245	0.225
	30	0.354	0.342
	36	0.436	0.423
	42	0.531	0.526
	48	0.631	0.627

Table 2.3

h	execution time required by Liu' scheme	Glimm's scheme
0.2	0.28	0.24
0.1	0.63	0.51
0.05	2.24	1.77

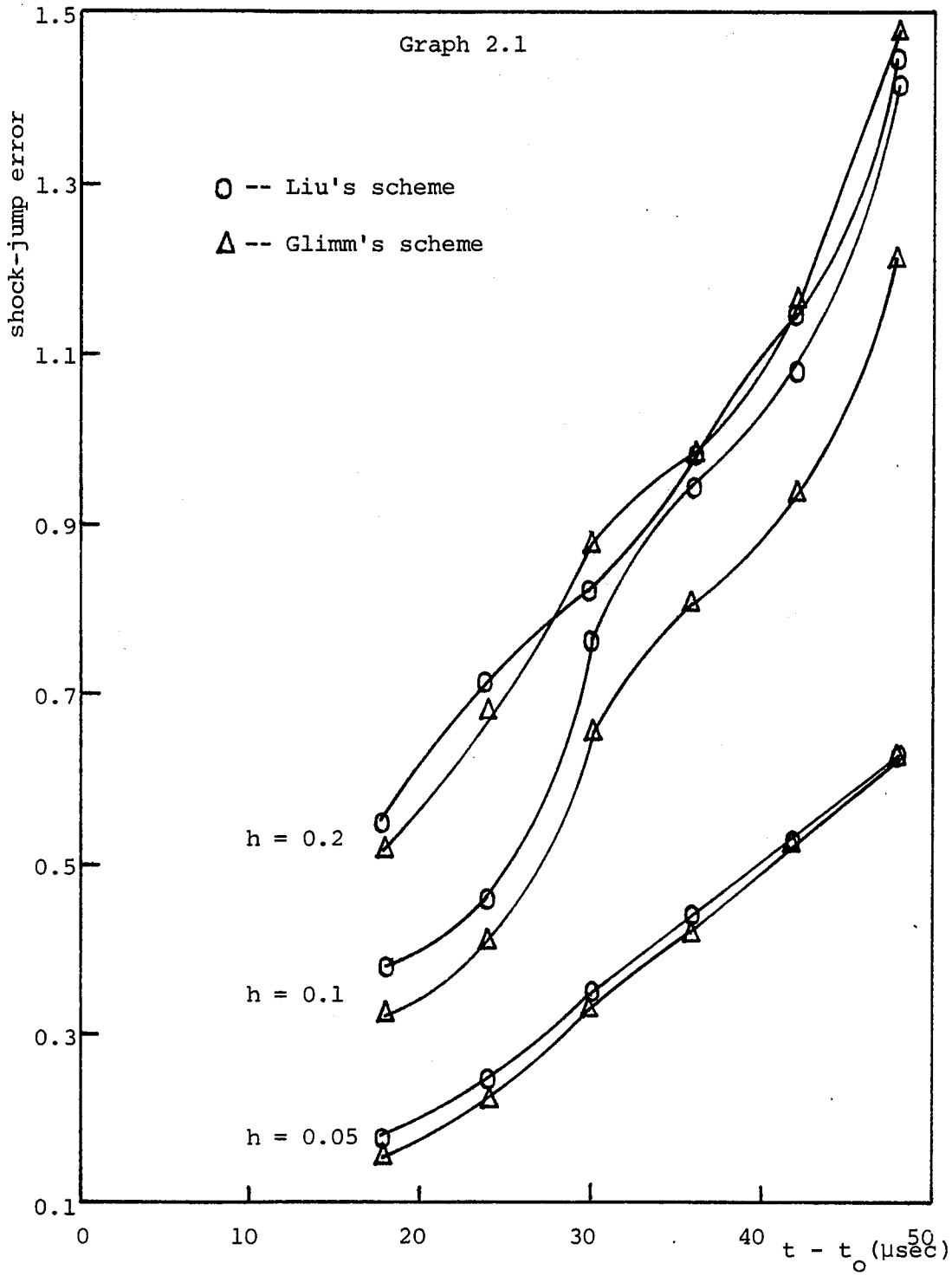

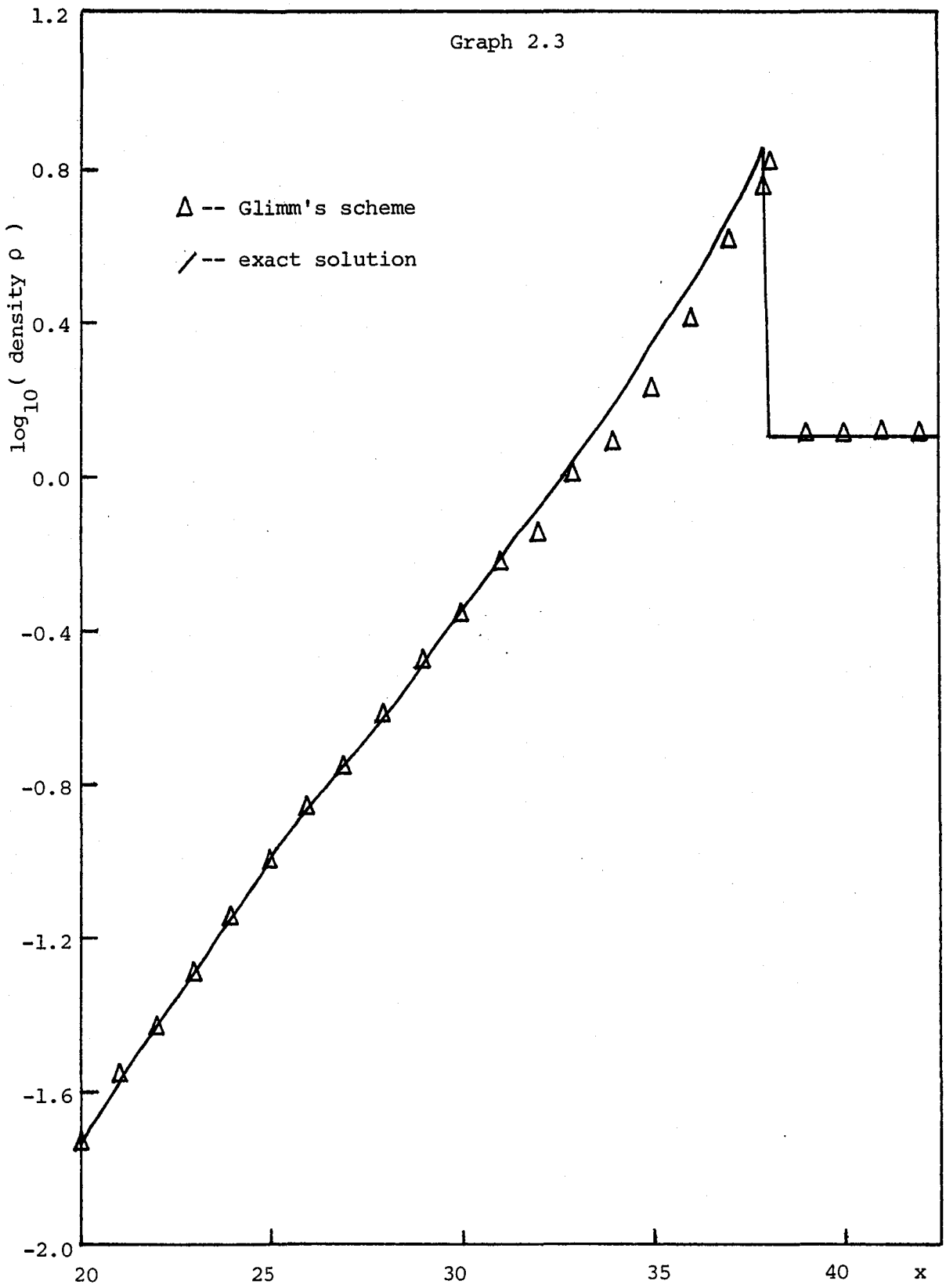
Graph 2.3
Δ -- Glimm's scheme
/ -- exact solution
log10(density ρ)
1.2
0.8
0.4
0.0
-0.4
-0.8
-1.2
-1.6
-2.0
20
25
30
35
40
x

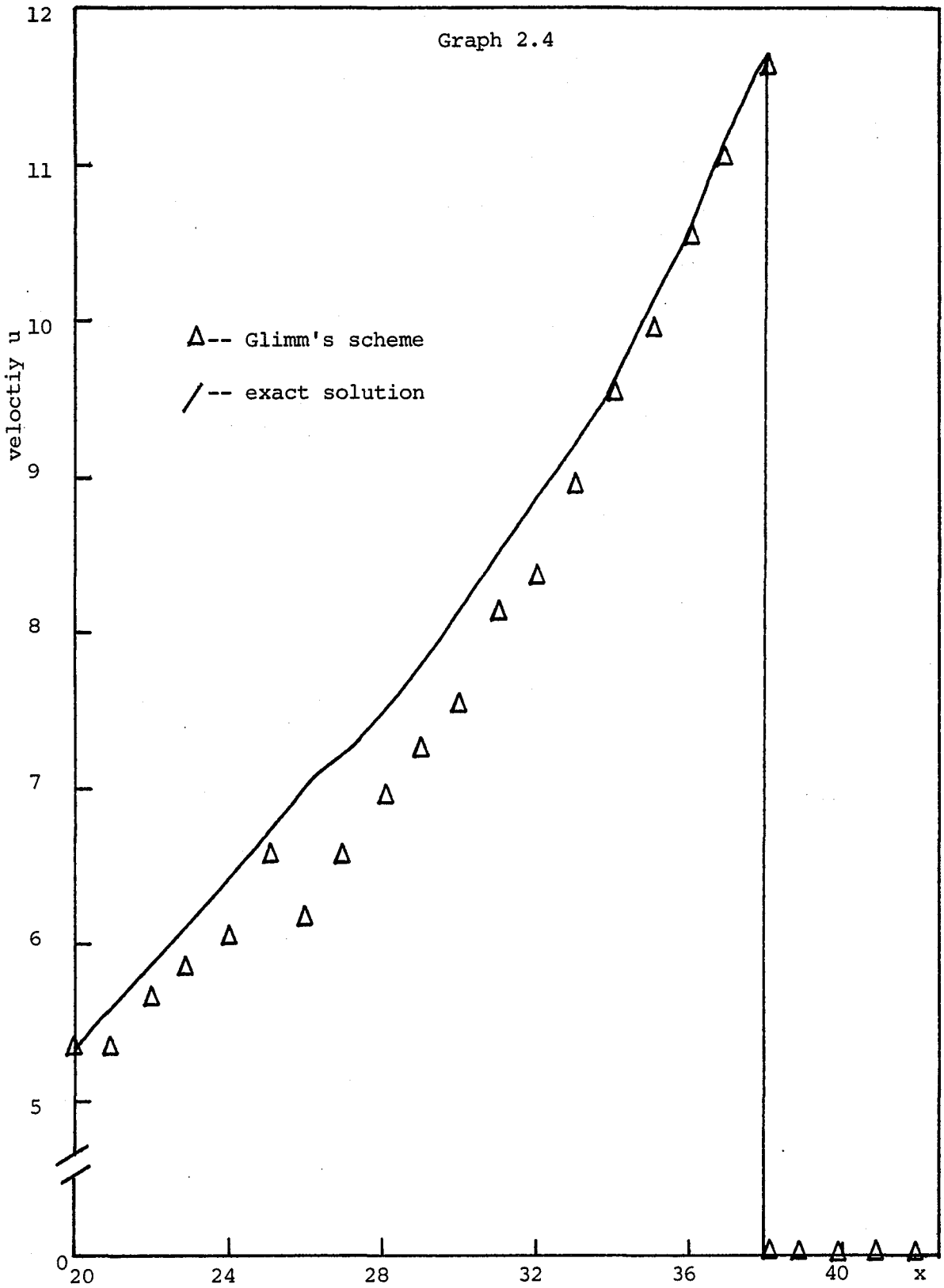
Graph 2.4
12
11
10
9
8
7
6
5
0
velocity u
Δ-- Glimm's scheme
/-- exact solution
20
24
28
32
36
40
x

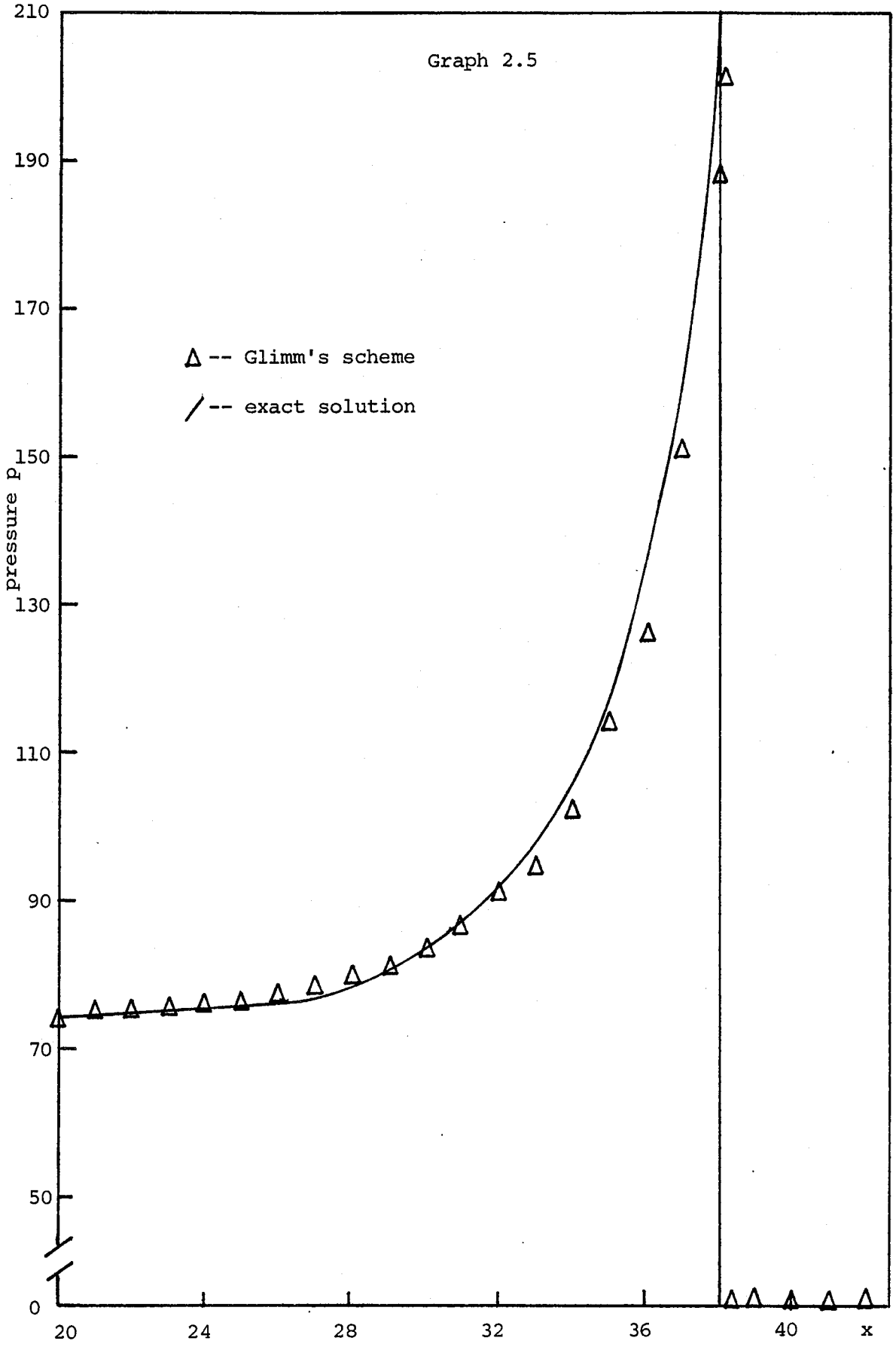
Graph 2.5
Δ -- Glimm's scheme
/ -- exact solution
pressure p
210
190
170
150
130
110
90
70
50
0
20
24
28
32
36
40
x

Figure 3.1

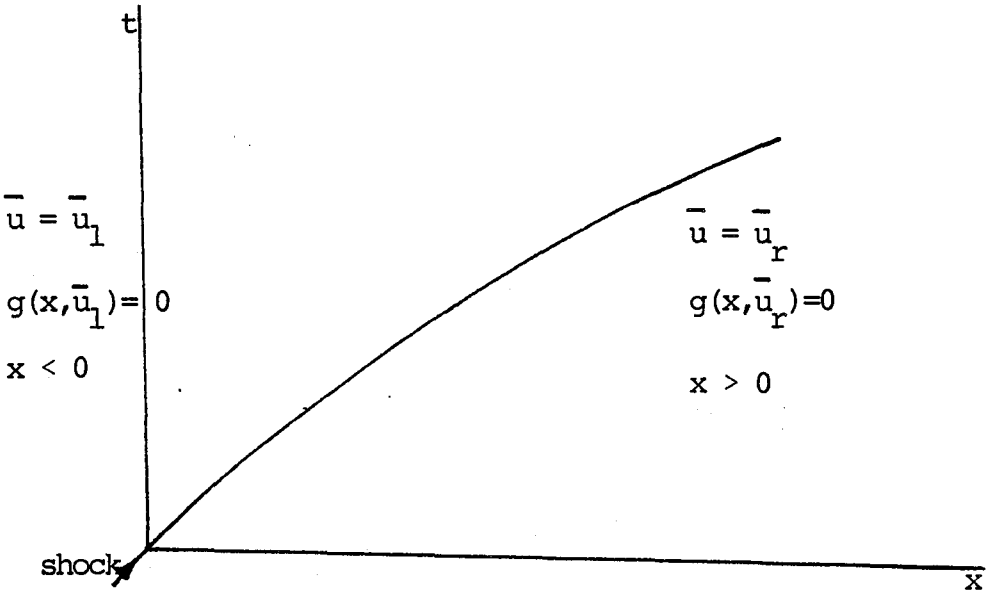

Figure 3.2

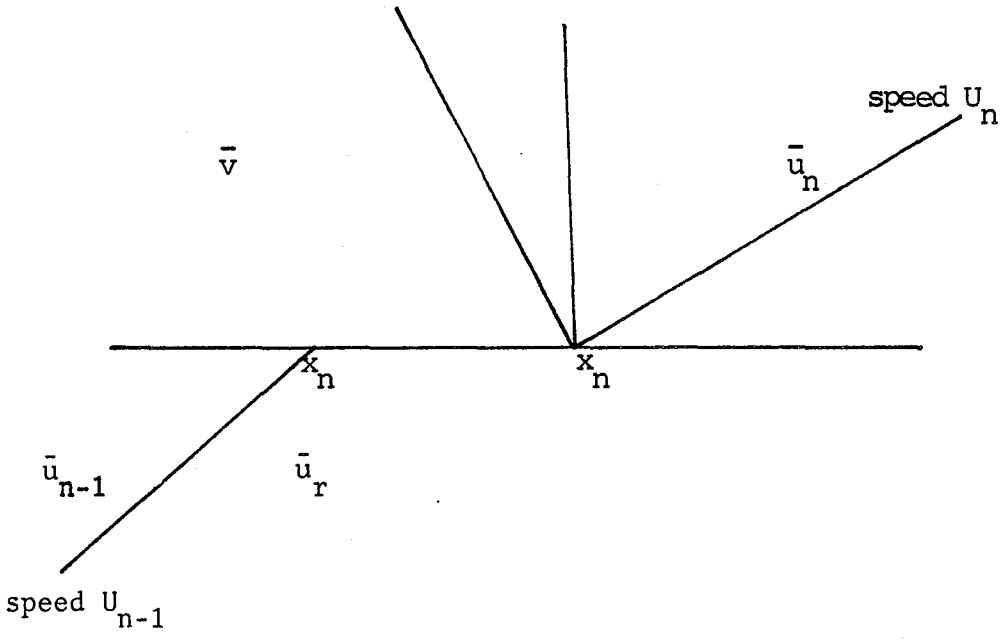

Table 3.1

** h = 0.04 **

	Chisnell's formula			Glimm's scheme		
x	M(x)	ρ(x)	u(x)	p(x)	ρ(x)	u(x)	p(x)
5.1	10.08	5.72	11.64	165.74	5.78	11.61	165.93
5.2	10.21	5.73	11.80	169.99	5.76	11.75	169.93
5.3	10.30	5.73	11.90	173.06	5.93	11.79	176.94
5.4	10.45	5.74	12.08	178.05	5.95	11.96	182.75
5.5	10.55	5.74	12.20	181.67	6.06	12.10	187.38
5.6	10.72	5.75	12.40	187.64	5.94	12.25	192.03
5.7	10.85	5.76	12.55	192.03	6.07	12.40	197.93
5.8	11.05	5.76	12.79	199.36	6.05	12.64	206.69
5.9	11.24	5.77	12.97	204.84	6.23	12.89	215.60

	Glimm's scheme with Chisnell's formula			Liu's scheme		
x	ρ(x)	u(x)	p(x)	ρ(x)	u(x)	p(x)
5.1	5.72	11.61	164.76	5.78	11.65	165.73
5.2	5.72	11.75	168.65	5.73	11.08	169.97
5.2	5.73	11.86	171.67	5.95	11.73	179.57
5.4	5.73	12.01	176.01	5.99	11.89	185.24
5.5	5.74	12.20	181.68	6.07	12.01	189.37
5.6	5.75	12.37	186.65	6.03	12.18	196.26
5.7	5.75	12.52	191.02	6.14	12.32	201.36
5.8	5.76	12.73	197.43	6.09	12.53	210.08
5.9	5.77	12.97	204.89	6.22	12.69	216.58

Table 3.2

** h = 0.02 **

	Chisnell's formula			Glimm's scheme		
x	M(x)	ρ(x)	u(x)	p(x)	ρ(x)	u(x)	p(x)
5.1	10.10	5.72	11.67	166.42	5.73	11.65	166.38
5.2	10.21	5.73	11.80	169.99	5.82	11.75	171.96
5.3	10.32	5.73	11.93	173.85	5.81	11.87	175.61
5.4	10.45	5.74	12.08	178.05	5.84	12.03	180.57
5.5	10.58	5.74	12.23	182.62	5.94	12.17	184.81
5.6	10.72	5.75	12.40	187.64	5.87	12.34	190.71
5.7	10.88	5.76	12.59	193.19	5.87	12.54	196.86
5.8	11.05	5.76	12.79	199.36	5.90	12.77	203.65
5.9	11.24	5.77	13.02	206.30	6.03	12.94	210.36

	Glimm's scheme with Chisnell's formula			Liu's scheme		
x	ρ(x)	u(x)	p(x)	ρ(x)	u(x)	p(x)
5.1	5.72	11.65	165.89	5.72	11.67	166.42
5.2	5.73	11.79	169.85	5.83	11.71	173.03
5.3	5.73	11.92	173.42	5.84	11.84	177.14
5.4	5.74	12.08	178.02	5.86	11.98	181.62
5.5	5.74	12.20	181.57	5.97	12.13	186.48
5.6	5.75	12.41	187.60	5.89	12.29	191.90
5.7	5.76	12.60	193.64	5.91	12.47	197.91
5.8	5.76	12.82	200.27	5.85	12.75	201.05
5.9	5.77	12.99	205.42	6.08	12.87	212.14

Table 3.3

Errors relative to Chisnell 's formula (%)

** h = 0.04 **

x	Glimm's scheme			Glimm's scheme with Chisnell's formula			Liu's scheme		
	ρ(x)	u(x)	p(x)	ρ(x)	u(x)	p(x)	ρ(x)	u(x)	p(x)
5.1	1.0	0.3	0.1	0.0	0.3	0.6	1.0	0.1	0.0
5.2	0.5	0.4	0.0	0.2	0.4	0.8	0.0	0.0	0.0
5.3	3.5	0.9	2.2	0.0	0.3	0.8	3.8	1.4	3.8
5.4	3.7	1.0	2.6	0.2	0.6	1.1	4.4	1.6	4.0
5.5	5.6	0.8	3.1	0.0	0.0	0.0	5.7	1.6	4.2
5.6	3.3	1.2	2.3	0.0	0.2	0.5	4.9	1.8	4.6
5.7	5.4	1.2	3.1	0.2	0.2	0.5	6.6	1.8	4.9
5.8	5.0	1.2	3.7	0.0	0.5	1.0	5.7	2.0	5.4
5.9	8.0	0.6	5.3	0.0	0.0	0.0	7.8	2.2	5.7

Table 3.4

** h = 0.02 **

5.1	0.2	0.2	0.0	0.0	0.2	0.3	0.0	0.0	0.0
5.2	1.6	0.4	1.2	0.0	0.1	0.1	1.7	0.8	1.8
5.3	1.4	0.5	1.0	0.0	0.1	0.2	1.9	0.8	1.9
5.4	1.7	0.4	1.4	0.0	0.0	0.0	2.1	0.8	2.0
5.5	3.5	0.5	1.2	0.0	0.2	0.6	4.0	0.8	2.1
5.6	2.1	0.5	1.6	0.0	0.1	0.0	2.4	0.9	2.3
5.7	1.9	0.4	1.9	0.0	0.1	0.2	2.6	1.0	2.4
5.8	2.4	0.2	2.2	0.0	0.2	0.5	1.6	0.3	0.8
5.9	4.5	0.6	2.0	0.0	0.2	0.4	5.4	1.2	2.8

Table 3.5

** h = 0.02 **

	Chisnell's formula			Glimm's scheme		
x	M(x)	ρ(x)	u(x)	p(x)	ρ(x)	u(x)	p(x)
6.1	10.21	5.73	11.80	169.99	5.76	11.75	169.93
6.2	10.45	5.74	12.08	178.05	5.95	11.96	182.75
6.3	10.72	5.75	12.40	187.64	5.94	12.25	192.03
6.4	11.05	5.76	12.79	199.36	6.05	12.64	206.69
6.5	11.46	5.78	13.27	214.18	6.38	13.08	222.73
6.6	11.97	5.80	13.87	233.82	6.23	13.66	247.93
6.7	12.67	5.82	14.69	261.83	6.38	14.41	283.18
6.8	13.72	5.84	15.92	307.12	6.72	15.67	352.92
6.9	15.72	5.88	18.27	403.45	8.56	16.45	494.84

	Glimm's scheme with Chisnell's formula			Liu's scheme		
x	ρ(x)	u(x)	p(x)	ρ(x)	u(x)	p(x)
6.1	5.72	11.75	168.65	5.73	11.80	169.97
6.2	5.74	12.01	176.01	5.98	11.89	185.24
6.3	5.75	12.37	186.65	6.03	12.18	196.26
6.4	5.76	12.73	197.43	6.09	12.53	210.08
6.5	5.78	13.27	214.17	6.45	12.95	227.58
6.6	5.80	13.81	231.06	5.87	13.85	233.49
6.7	5.82	14.64	260.07	5.92	14.68	261.44
6.8	5.85	15.98	309.49	6.00	15.90	306.20
6.9	5.88	17.94	389.32	7.89	17.46	449.93

Table 3.6

** h = 0.01 **

	Chisnell's formula				Glimm's scheme		
x	M(x)	ρ(x)	u(x)	p(x)	ρ(x)	u(x)	p(x)
6.1	10.21	5.73	11.80	169.99	5.82	11.75	171.96
6.2	10.45	5.74	12.08	178.05	5.84	12.03	180.57
6.3	10.72	5.75	12.40	187.64	5.87	12.34	190.71
6.4	11.05	5.76	12.79	199.36	5.90	12.77	203.65
6.5	11.46	5.78	13.27	214.18	5.95	13.17	218.88
6.6	11.97	5.80	13.87	233.82	6.01	13.76	240.73
6.7	12.67	5.82	14.69	261.83	6.11	14.50	271.00
6.8	13.72	5.84	15.92	307.12	6.17	15.99	323.31
6.9	15.72	5.88	18.27	403.45	6.16	18.00	406.95

	Glimm's scheme with Chisnell's formula			Liu's scheme		
x	ρ(x)	u(x)	p(x)	ρ(x)	u(x)	p(x)
6.1	5.73	11.79	169.85	5.83	11.71	173.03
6.2	5.74	12.08	178.02	5.86	11.98	181.62
6.3	5.75	12.41	187.60	5.89	12.29	191.90
6.4	5.76	12.82	200.27	5.85	12.75	201.05
6.5	5.78	13.25	213.72	5.81	13.26	214.03
6.6	5.80	13.88	234.41	5.84	13.86	233.65
6.7	5.82	14.69	261.75	5.87	14.67	261.38
6.8	5.84	15.99	309.82	5.92	15.90	306.54
6.9	5.88	17.99	391.44	5.88	18.21	401.09

Table 3.7

Errors relative to Chisnell's formula (%)

** h = 0.02 **

x	Glimm's scheme			Glimm's scheme with Chisnell's formula			Liu's scheme		
	ρ(x)	u(x)	p(x)	ρ(x)	u(x)	p(x)	ρ(x)	u(x)	p(x)
6.1	0.5	0.4	0.0	0.2	0.4	0.8	0.0	0.0	0.0
6.2	3.7	1.0	3.6	0.0	0.6	1.1	4.2	1.6	4.0
6.3	3.3	1.2	2.3	0.0	0.2	0.5	4.9	1.8	4.6
6.4	5.0	1.2	3.7	0.0	0.5	1.0	5.7	2.0	5.4
6.5	10.4	1.4	4.0	0.0	0.0	0.0	11.6	2.4	6.3
6.6	7.4	1.5	6.0	0.0	0.4	1.2	1.2	0.1	0.1
6.7	9.6	1.9	8.2	0.0	0.3	0.7	1.7	0.1	0.1
6.8	15.1	1.6	14.9	0.2	0.4	0.8	2.7	0.1	0.3
6.9	45.6	10.0	22.7	0.0	1.8	3.5	34.2	4.4	11.5

Table 3.8

** h = 0.01 **

6.1	1.6	0.4	1.2	0.0	0.1	0.1	1.7	0.8	1.8
6.2	1.7	0.4	1.4	0.0	0.0	0.0	2.1	0.8	2.0
6.3	2.1	0.5	1.6	0.0	0.1	0.0	2.4	0.9	2.3
6.4	2.4	0.2	2.2	0.0	0.2	0.5	1.6	0.3	0.8
6.5	2.9	0.8	2.2	0.0	0.2	0.2	0.5	0.1	0.1
6.6	3.6	0.8	3.0	0.0	0.1	0.3	0.7	0.1	0.1
6.7	5.0	1.3	3.5	0.0	0.0	0.0	0.9	0.1	0.2
6.8	5.7	0.4	5.3	0.0	0.4	0.9	1.4	0.1	0.2
6.9	4.8	1.5	0.9	0.0	1.5	3.0	0.0	0.3	0.6

Table 3.9

Averaged errors relative to Chisnell's formula (%)

** A'(x)/A(x) = -1/(7-x), xε(5,6] **

	Glimm's scheme			Glimm's scheme with Chisnell's formula			Liu's scheme		
	ρ(x)	u(x)	p(x)	ρ(x)	u(x)	p(x)	ρ(x)	u(x)	p(x)
h = 0.04	4.0	1.0	2.3	0.1	0.4	0.9	4.8	1.5	3.6
h = 0.02	2.2	0.4	1.4	0.0	0.1	0.3	2.4	0.7	1.8

** A'(x)/A(x) = -1/(7-x), xε(6.7] **

	Glimm's scheme			Glimm's scheme with Chisnell's formula			Liu's scheme		
	ρ(x)	u(x)	p(x)	ρ(x)	u(x)	p(x)	ρ(x)	u(x)	p(x)
h = 0.02	11.2	2.2	7.2	0.0	0.5	1.1	7.4	1.4	3.6
h = 0.01	3.3	0.7	2.2	0.0	0.3	0.6	1.3	0.4	0.9

Table 3.10

Execution time required by each numerical scheme

** $A'(x)/A(x) = -1/(7 - x)$, $x \in [5,6)$ **

	Glimm's scheme	Glimm's scheme with Chisnell's formula	Liu's scheme
h = 0.02	1.02	1.13	1.55
h = 0.04	0.31	0.35	0.49

** $A'(x)/A(x) = =1/(7 - x)$, $x \in [6,7)$ **

h = 0.01	3.90	4.36	6.26
h = 0.02	1.14	1.21	1.72

Table 3.11

** $A'(x)/A(x) = -1/(1 + x)$, $x \in [0,16)$ **

Glimm's scheme	Glimm's scheme with Chisnell's formula	Liu's scheme	Liu's scheme with Chisnell's formula
5.53	5.60	6.97	7.84

Graph 3.1a

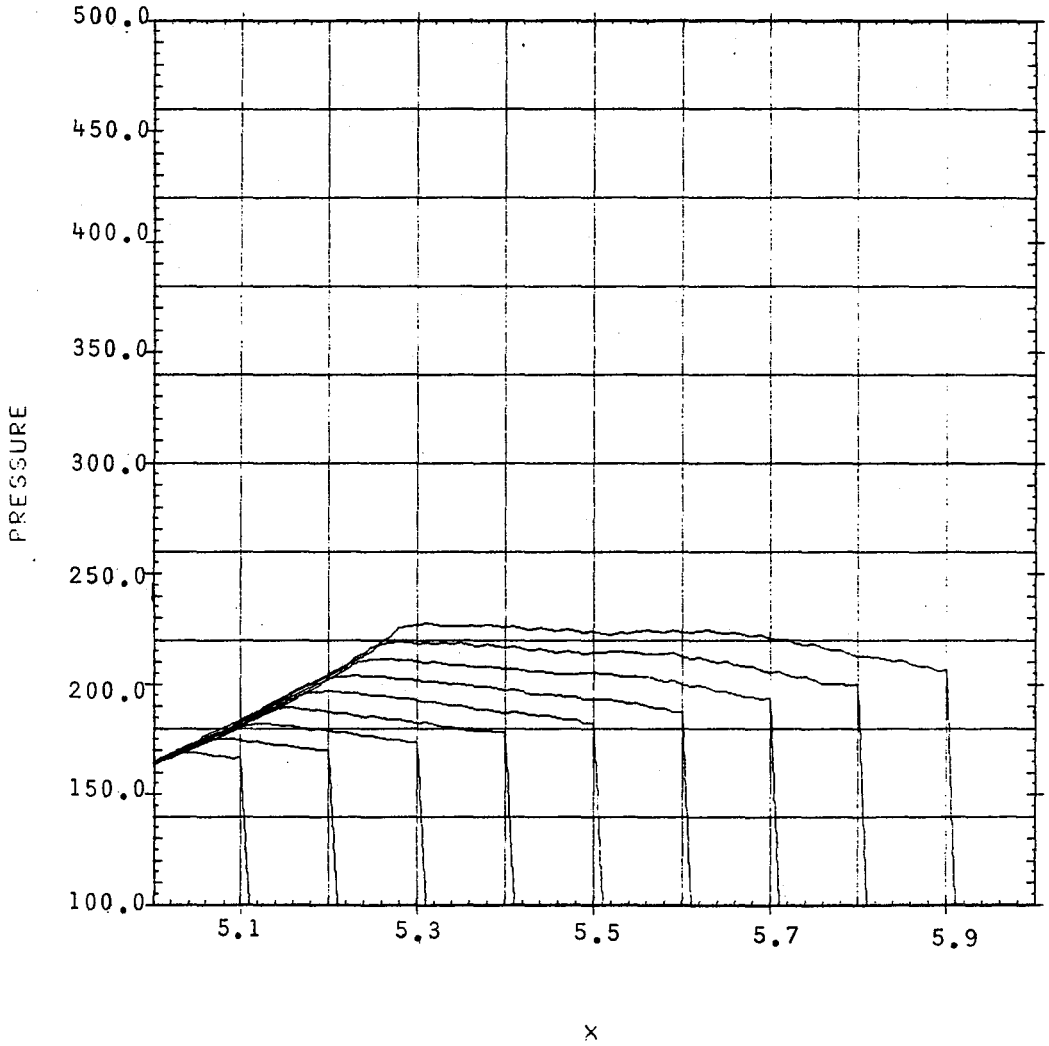
500.0
450.0
400.0
350.0
300.0
250.0
200.0
150.0
100.0
PRESSURE
5.1
5.3
5.5
5.7
5.9
X

Graph 3.2a

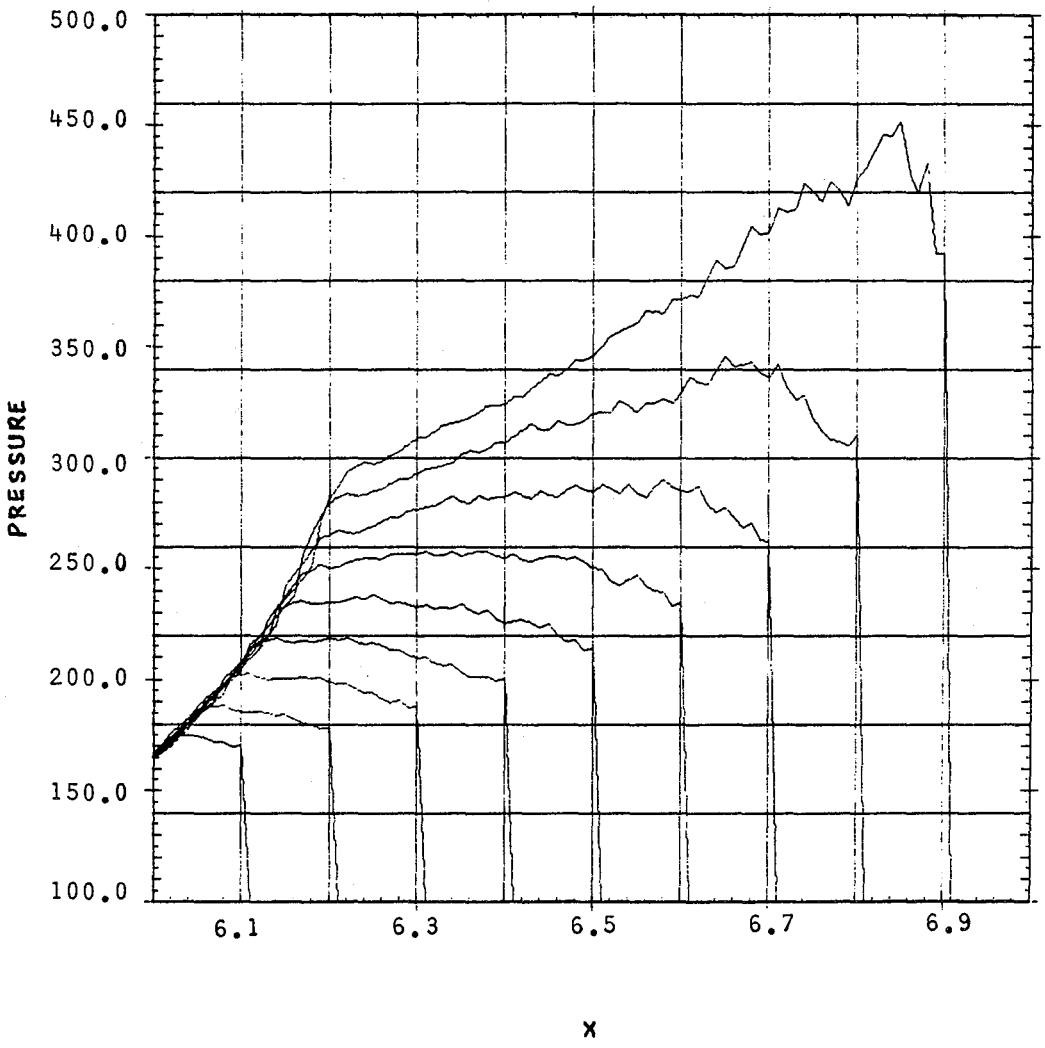
500.0
450.0
400.0
350.0
300.0
250.0
200.0
150.0
100.0
PRESSURE
6.1
6.3
6.5
6.7
6.9
X

Graph 3.1b

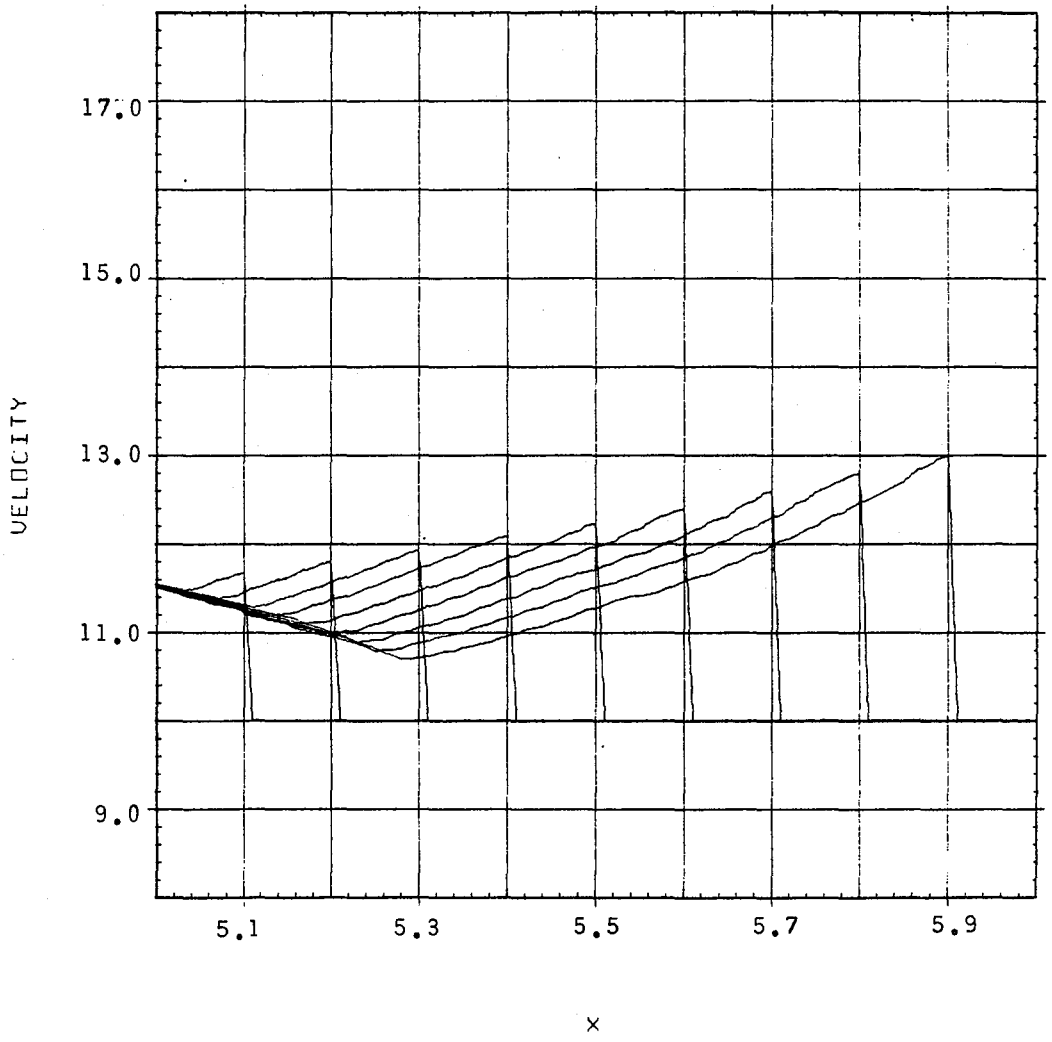

Graph 3.2b

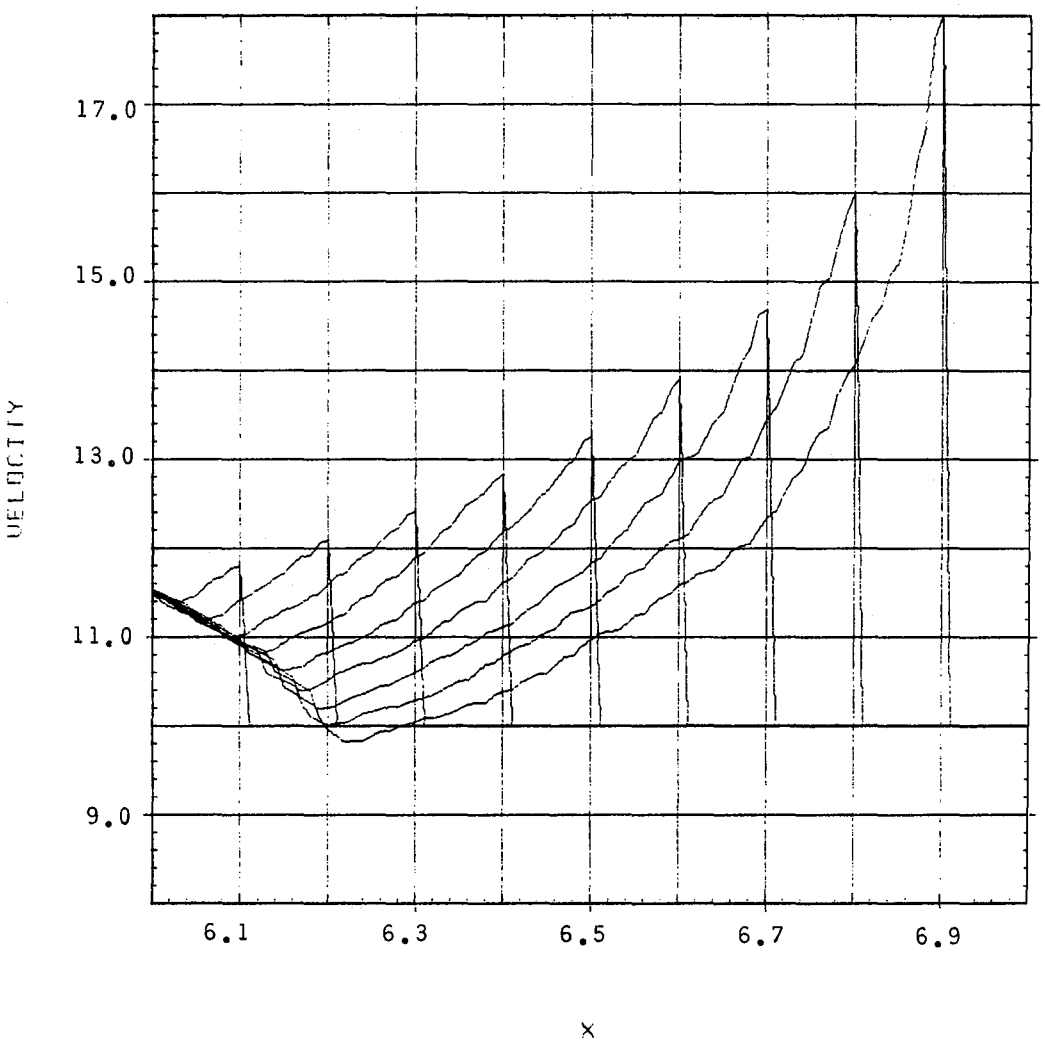

Graph 3.1c

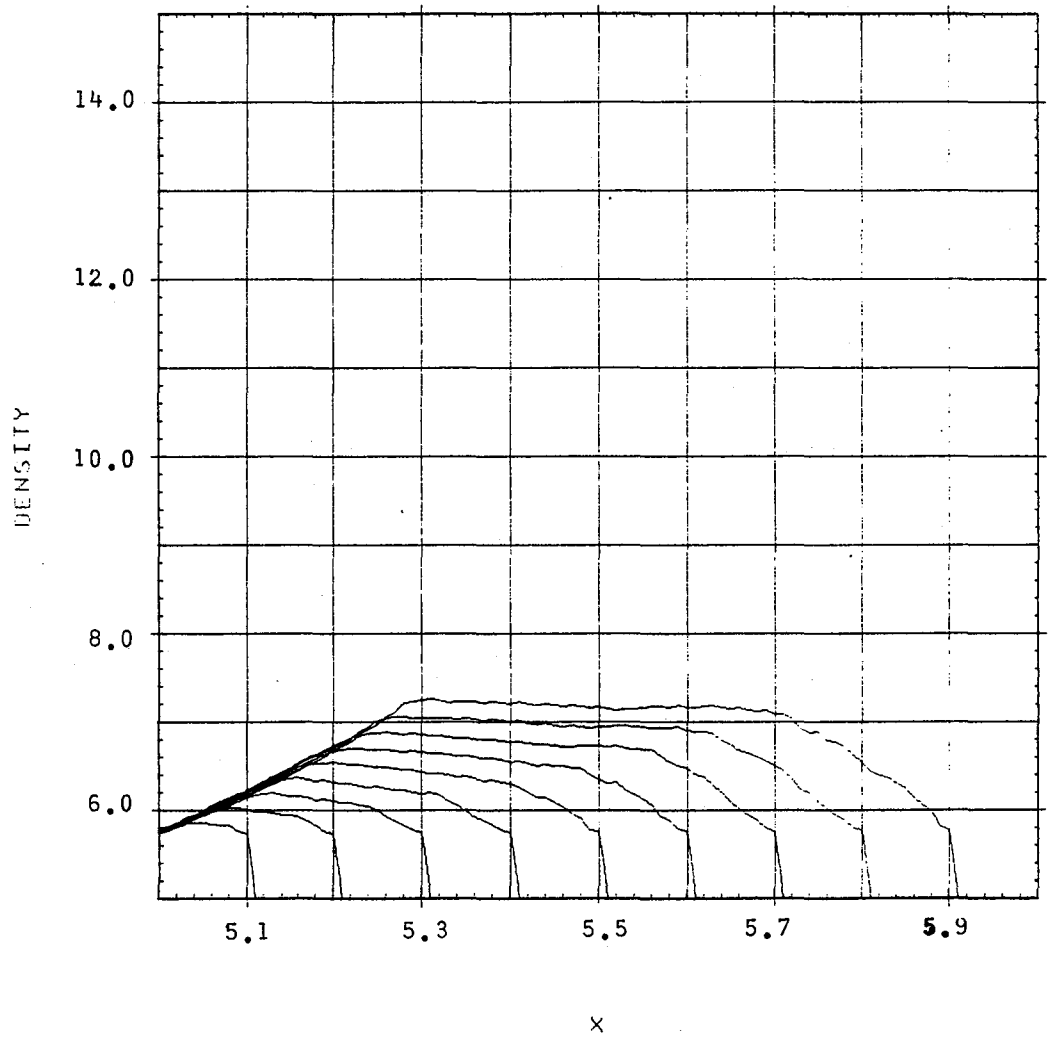

Graph 3.2c

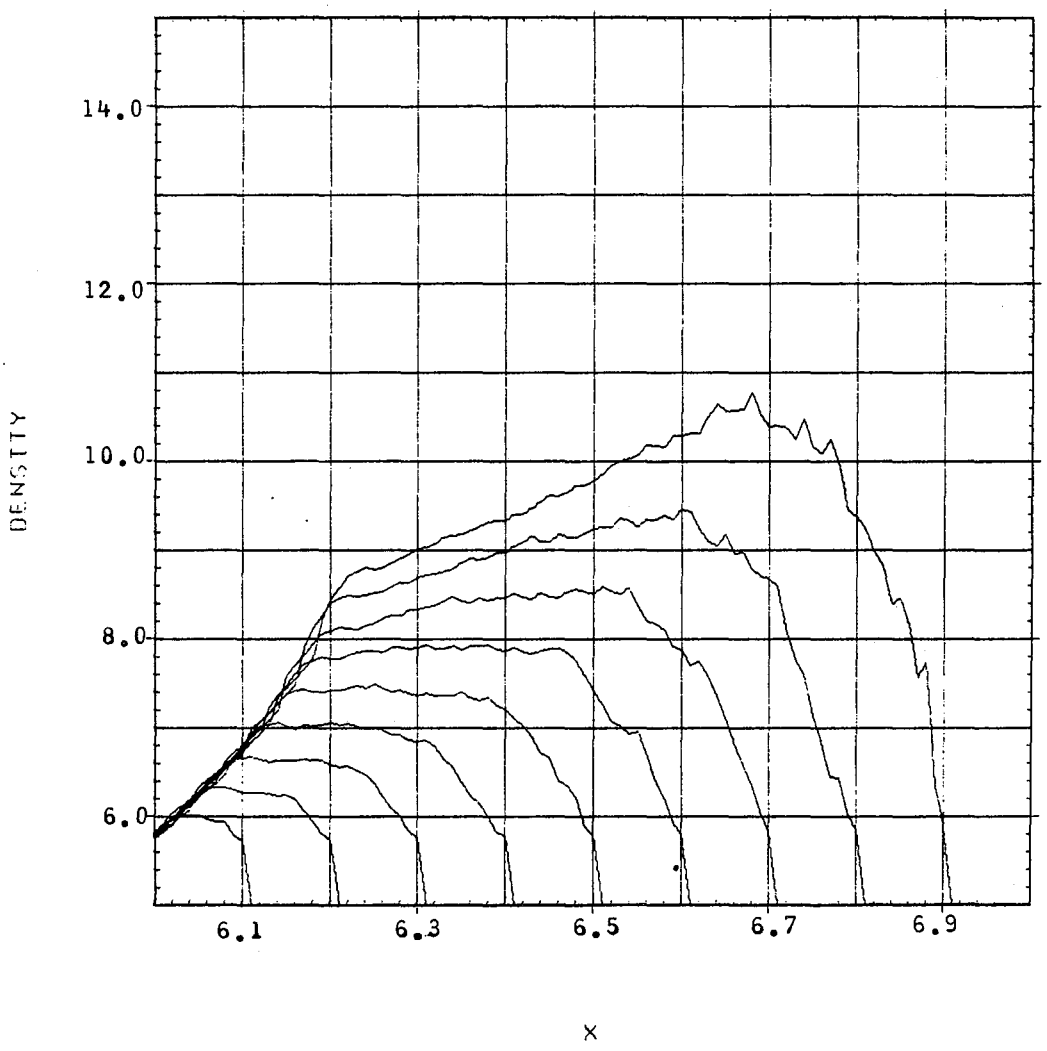

Graph 3.3a

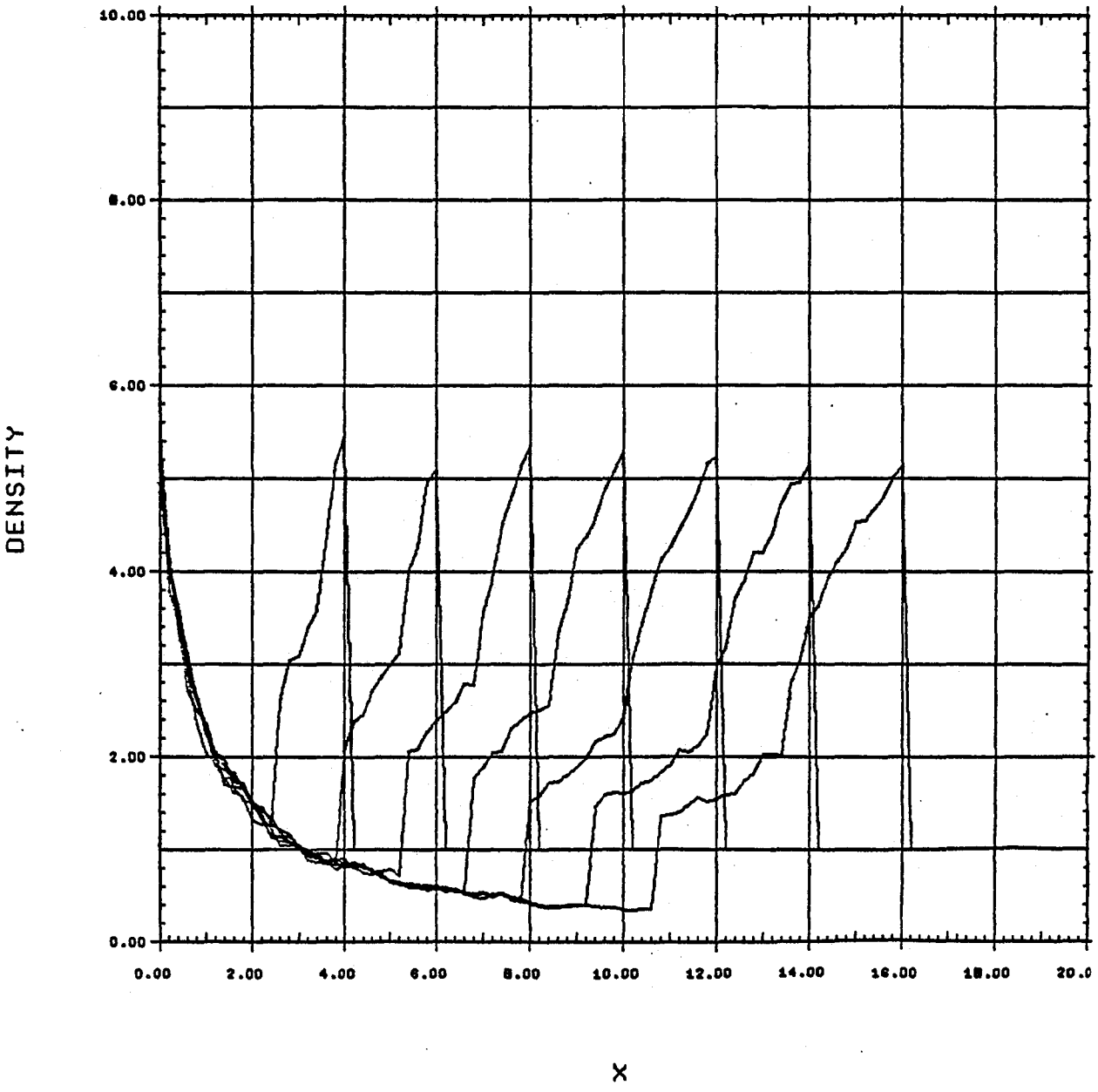
DENSITY
10.00
8.00
6.00
4.00
2.00
0.00
0.00
2.00
4.00
6.00
8.00
10.00
12.00
14.00
16.00
18.00
20.0
X

Graph 3.4a

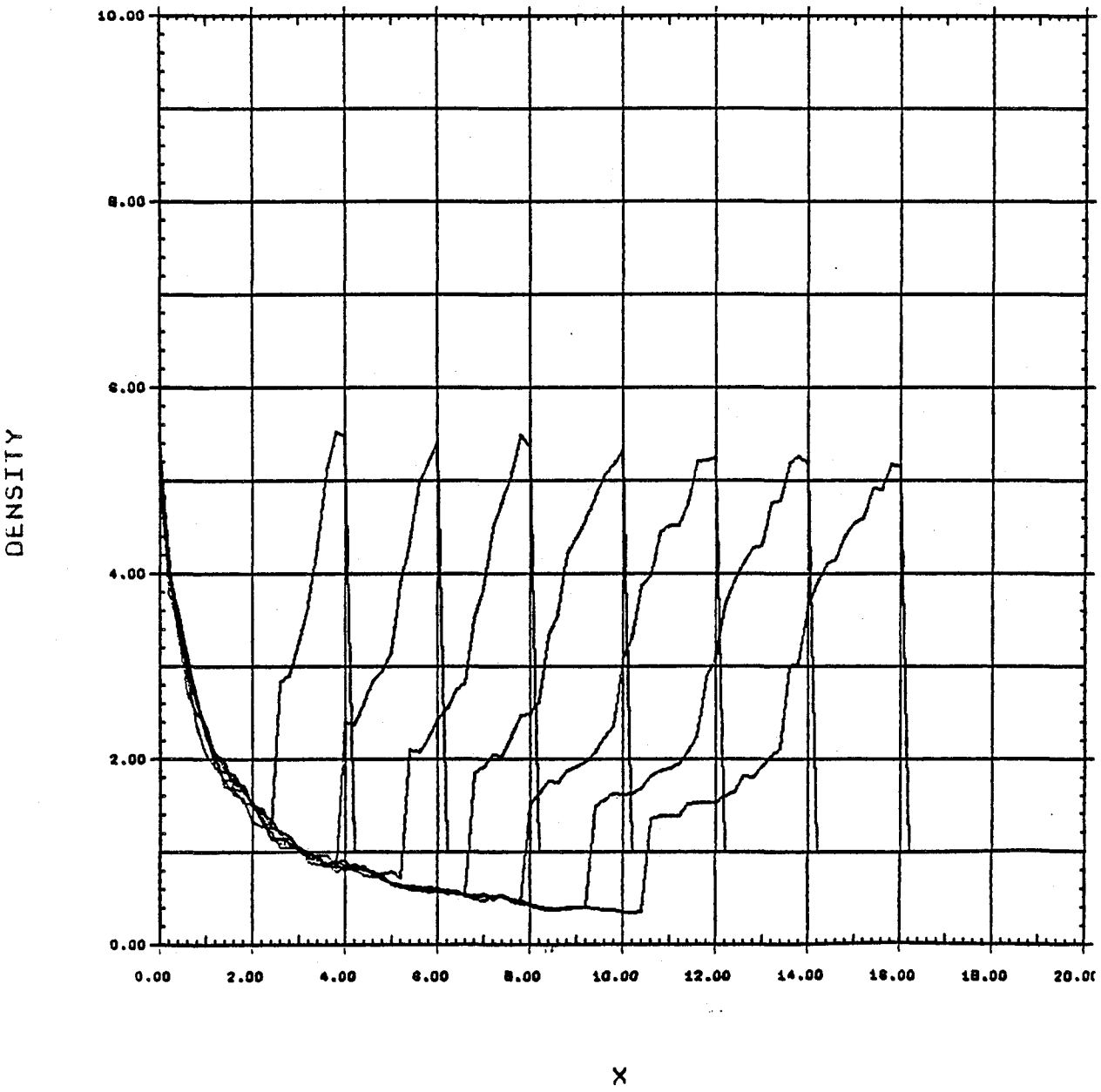
10.00
8.00
6.00
4.00
2.00
0.00
DENSITY
0.00
2.00
4.00
6.00
8.00
10.00
12.00
14.00
16.00
18.00
20.00
X

Graph 3.3b

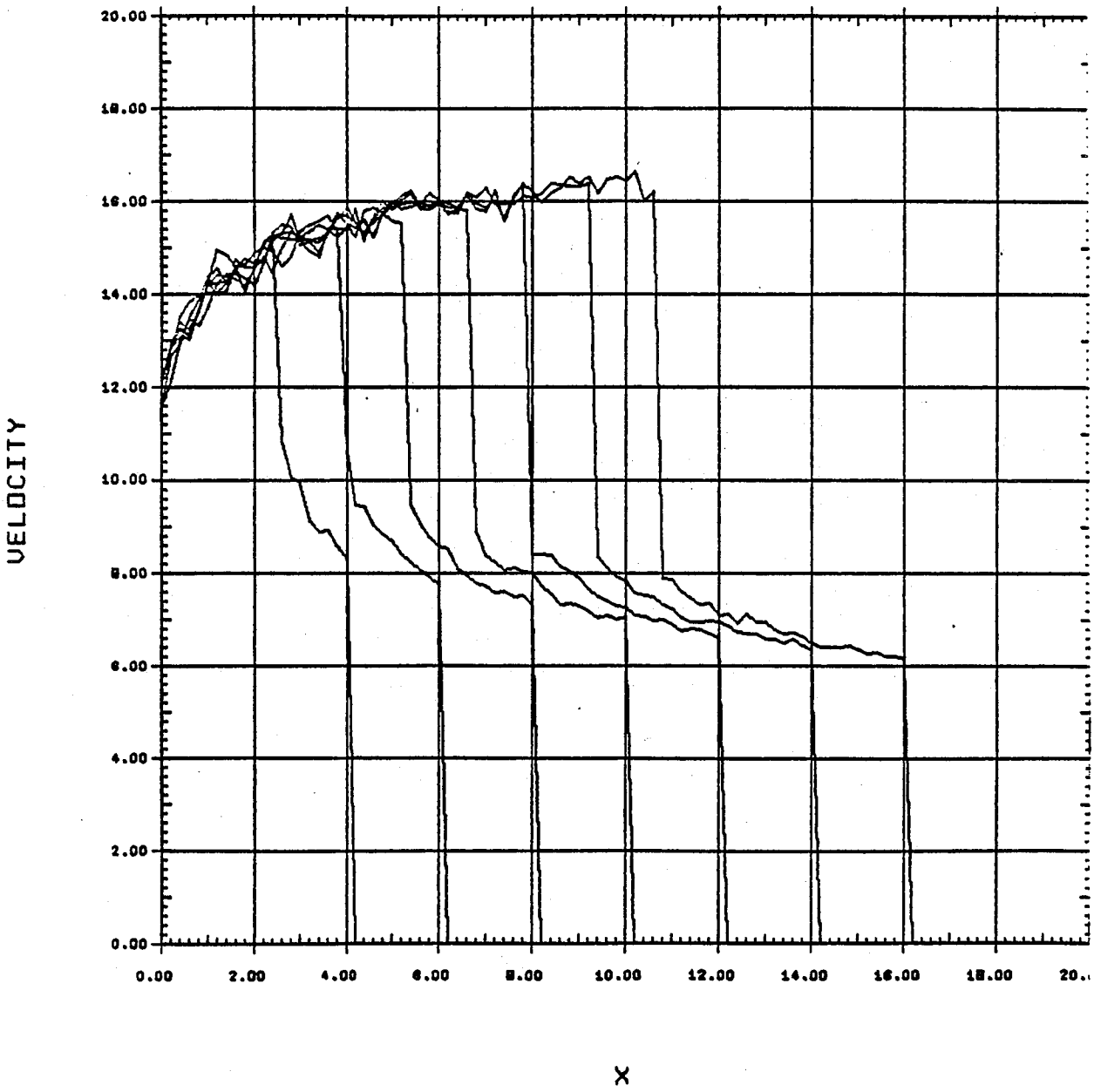
VELOCITY
20.00
18.00
16.00
14.00
12.00
10.00
8.00
6.00
4.00
2.00
0.00
0.00
2.00
4.00
6.00
8.00
10.00
12.00
14.00
16.00
18.00
X

Graph 3.4b

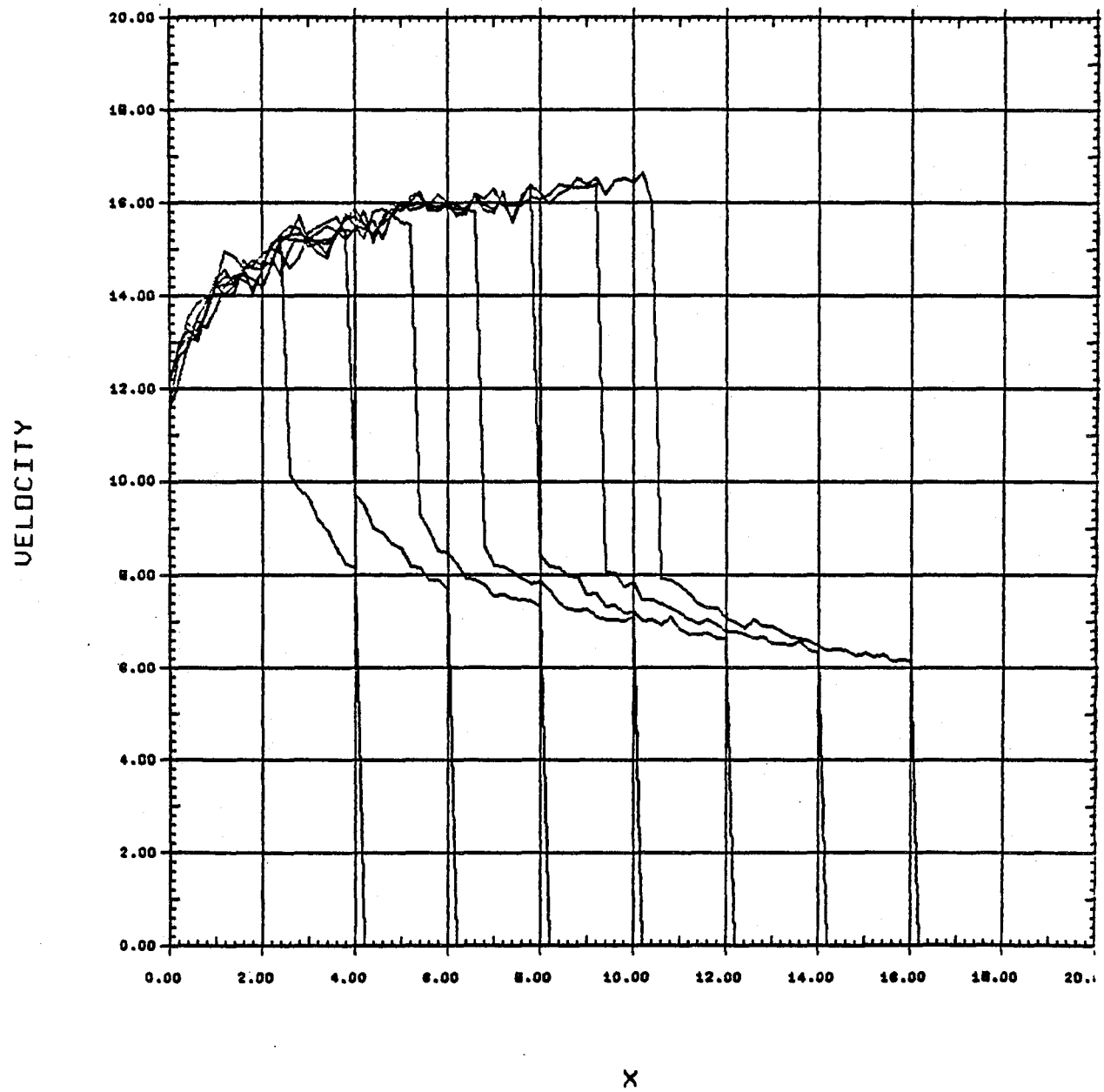
VELOCITY
20.00
18.00
16.00
14.00
12.00
10.00
8.00
6.00
4.00
2.00
0.00
0.00
2.00
4.00
6.00
8.00
10.00
12.00
14.00
16.00
18.00
X

Graph 3.3c

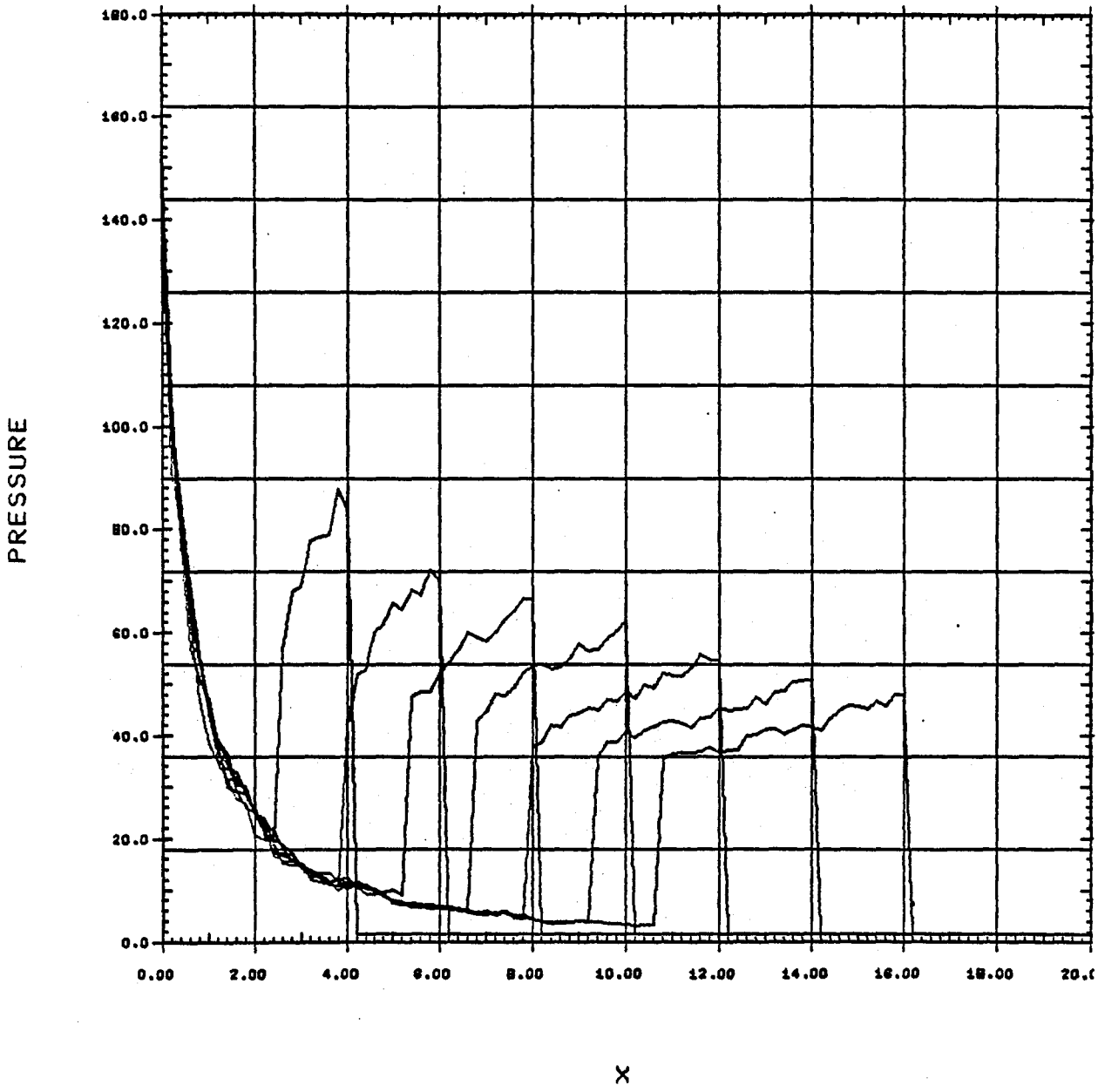
PRESSURE
180.0
160.0
140.0
120.0
100.0
80.0
60.0
40.0
20.0
0.0
0.00
2.00
4.00
6.00
8.00
10.00
12.00
14.00
16.00
X

Graph 3.4c

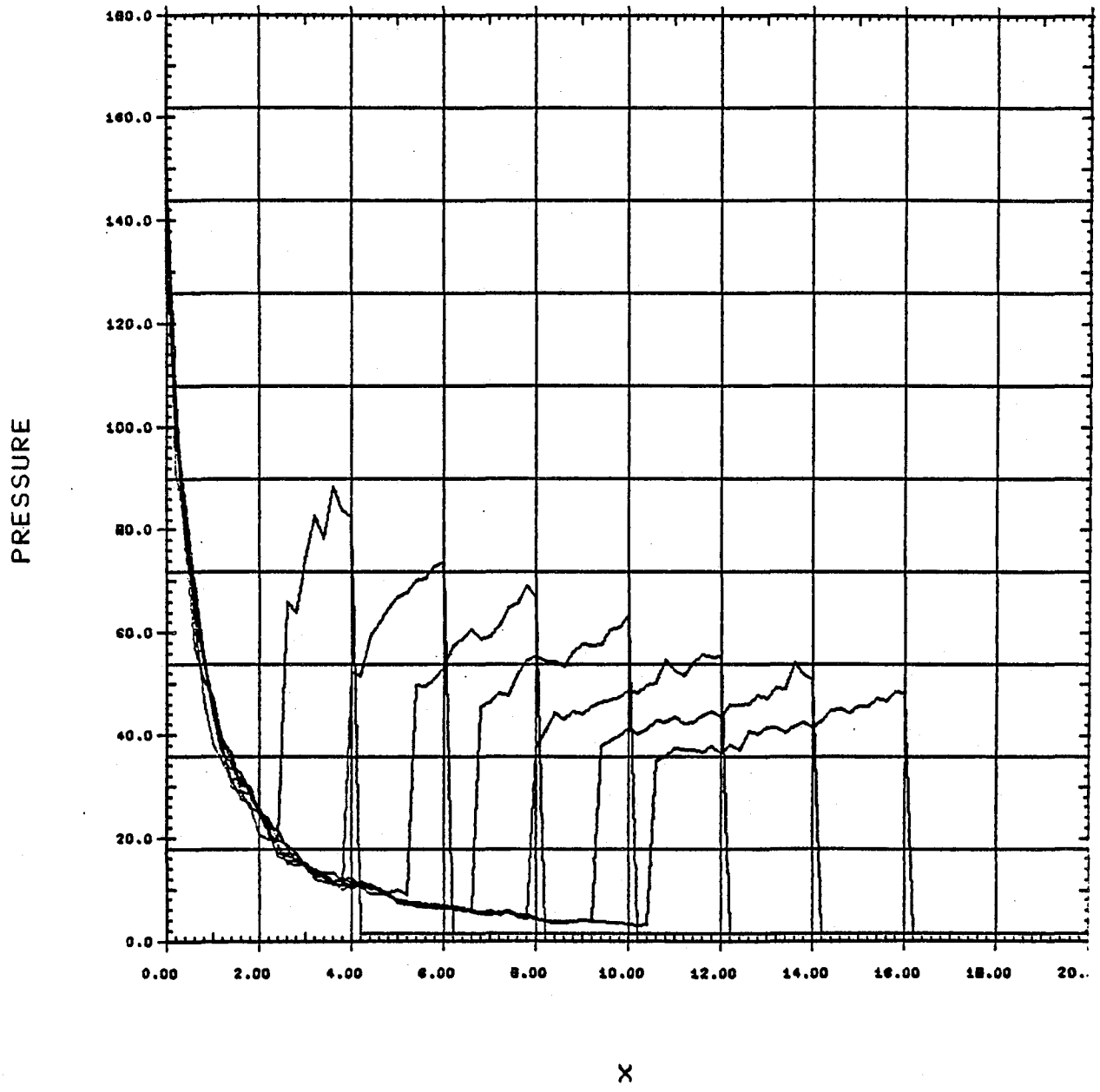
PRESSURE
180.0
160.0
140.0
120.0
100.0
80.0
60.0
40.0
20.0
0.0
0.00
2.00
4.00
6.00
8.00
10.00
12.00
14.00
16.00
18.00
20..
X

Graph 3.5a

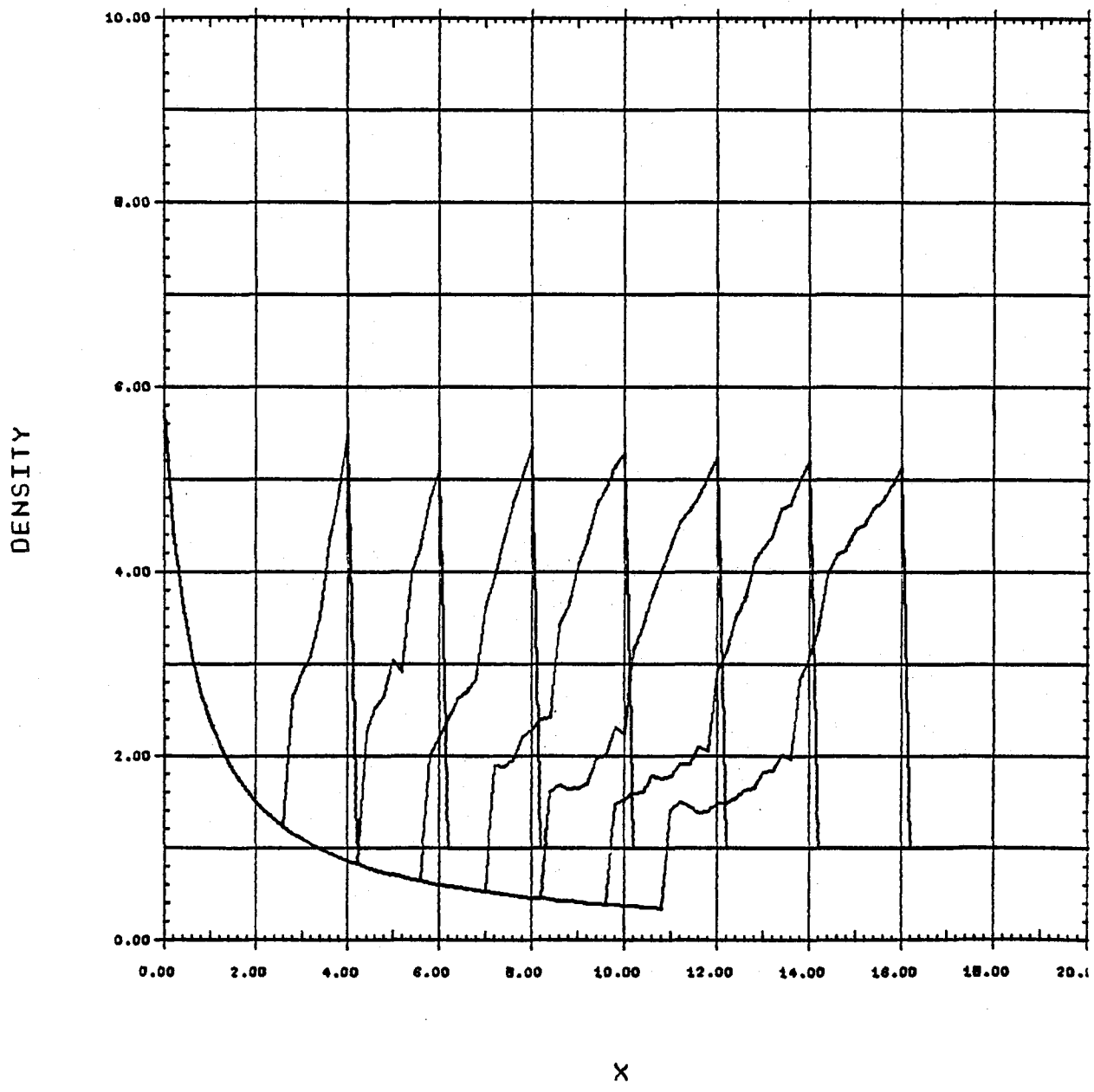
10.00
8.00
6.00
4.00
2.00
0.00
DENSITY
0.00
2.00
4.00
6.00
8.00
10.00
12.00
14.00
16.00
18.00
X

Graph 3.5b

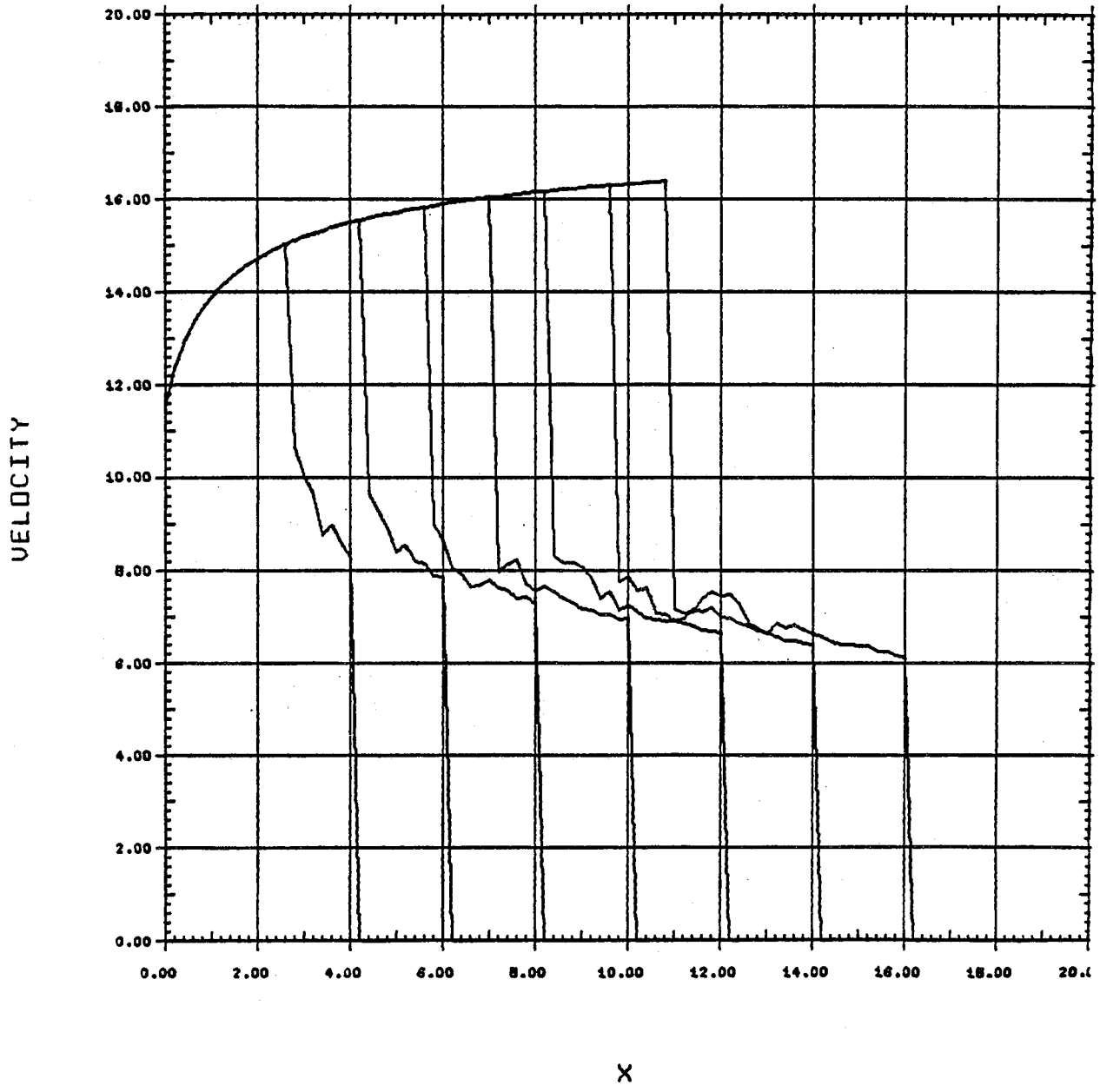
VELOCITY
20.00
18.00
16.00
14.00
12.00
10.00
8.00
6.00
4.00
2.00
0.00
0.00
2.00
4.00
6.00
8.00
10.00
12.00
14.00
16.00
18.00
X

Graph 3.5c

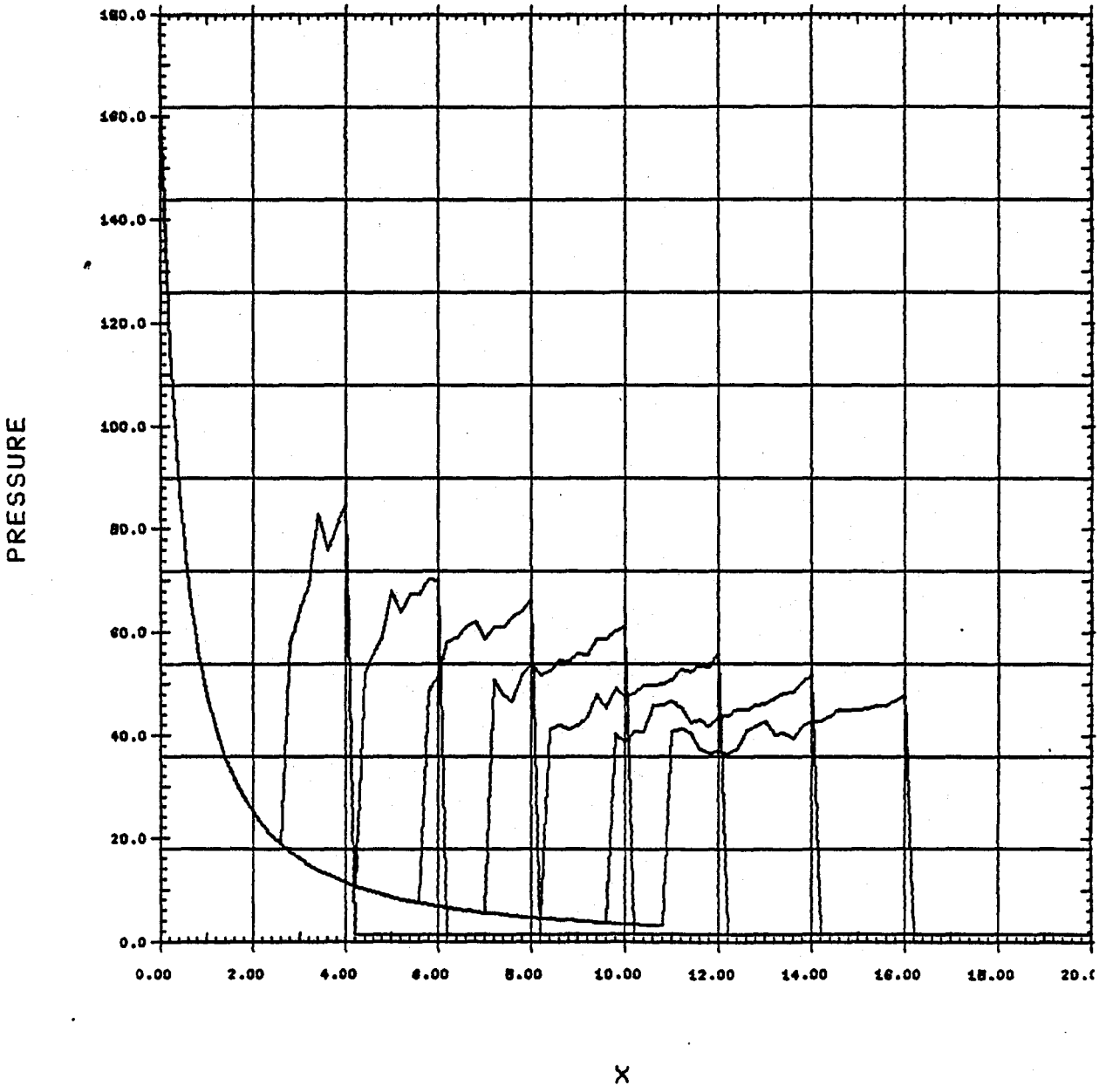
PRESSURE
180.0
160.0
140.0
120.0
100.0
80.0
60.0
40.0
20.0
0.0
0.00
2.00
4.00
6.00
8.00
10.00
12.00
14.00
16.00
18.00
X

Graph 3.6a

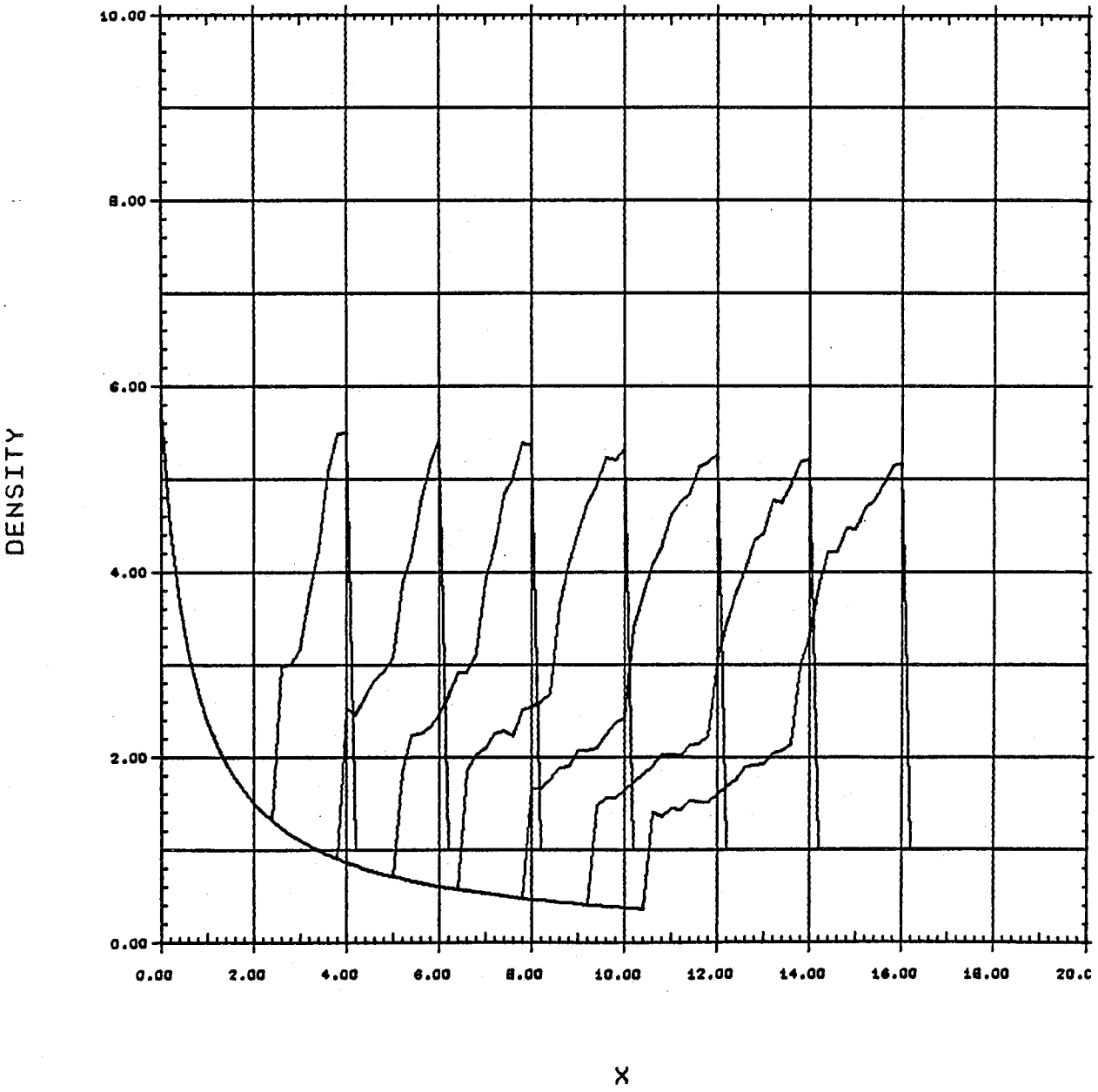
10.00
8.00
6.00
4.00
2.00
0.00
DENSITY
0.00
2.00
4.00
6.00
8.00
10.00
12.00
14.00
16.00
18.00
20.0
X

Graph 3.6b

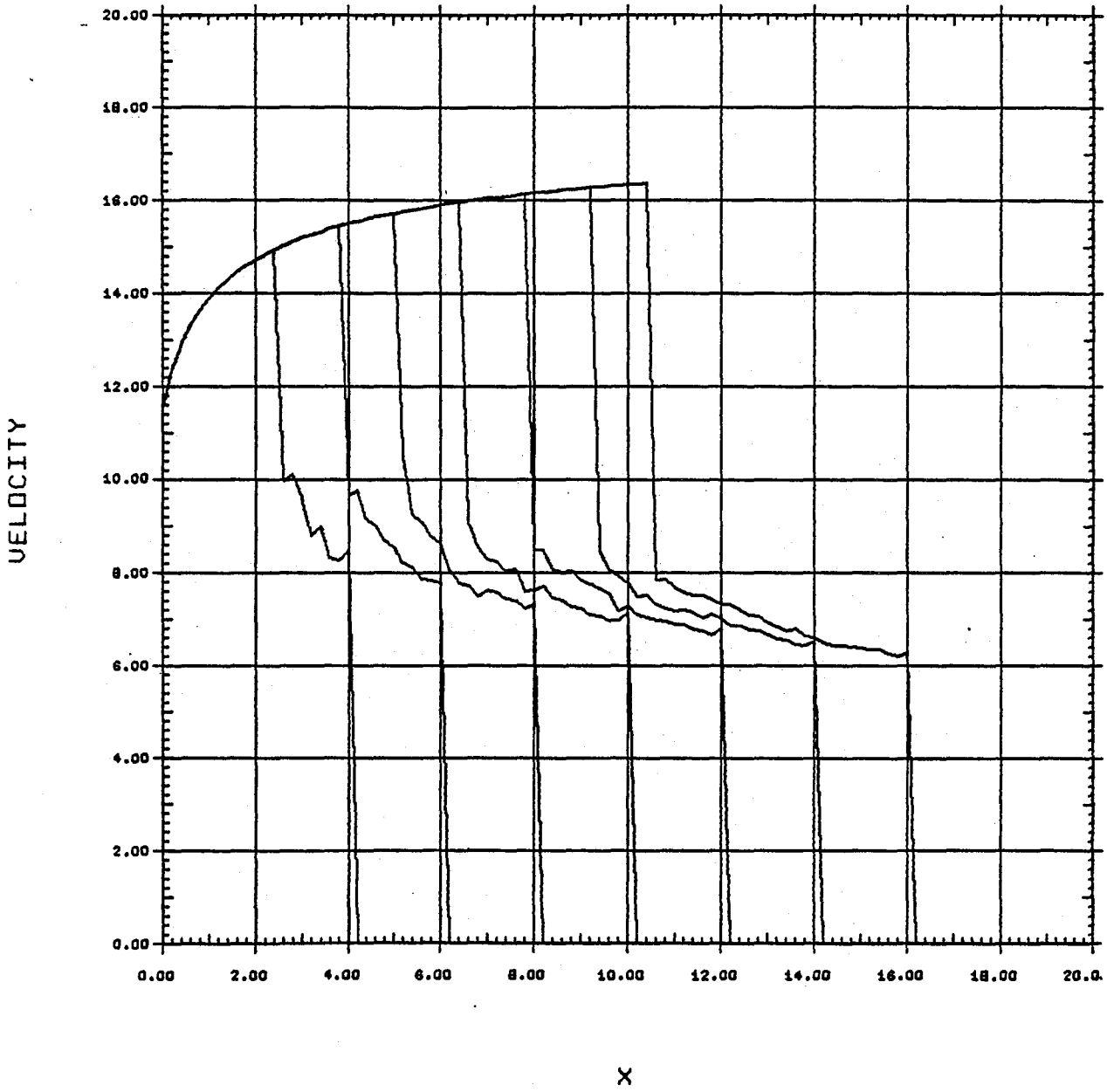
VELOCITY
20.00
18.00
16.00
14.00
12.00
10.00
8.00
6.00
4.00
2.00
0.00
0.00
2.00
4.00
6.00
8.00
10.00
12.00
14.00
16.00
18.00
20.0
X

Graph 3.6c

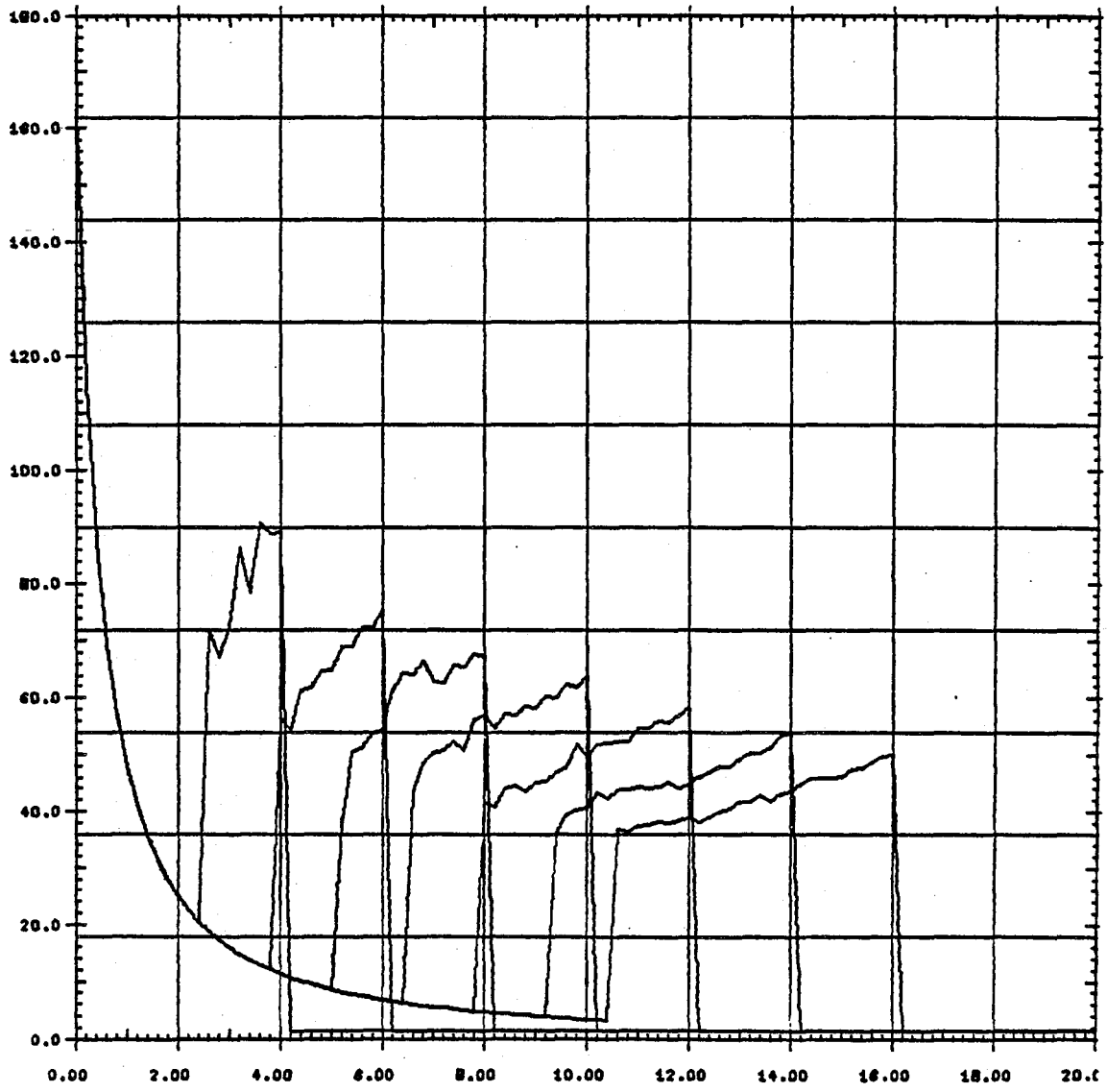
PRESSURE
180.0
160.0
140.0
120.0
100.0
80.0
60.0
40.0
20.0
0.0
0.00
2.00
4.00
6.00
8.00
10.00
12.00
14.00
16.00
18.00
X

Bibliography

1. Chisnell, R.F., "The Motion of a Shock Wave in a Channel with Applications to Cylindrical and Spherical Shock Waves," J. Fluid Mech. 2 pp. 286-298 (1957)

2. Chorin, A.J., "Random Choice Solution of Hyberbolic Systems," J. Comp. Phys. 22, pp. 517 (1976)

3. Collela, P., "An Analysis of the Effect of Operator Splitting and of the Sampling Procedure on the Accuracy of Glimm's Method," Report No. LBL-8774, Lawrence Berkeley Laboratory, University of California, Berkeley (1978)

4. Courant, R. and Friedrichs, K. O., Supersonic Flow and Shock Waves, Interscience, New York, 1948

5. Gear, C. W., Numerical Initial Value Problems in Ordinary Differential Equations, Prentice-Hall Inc., New Jersey, 1971

6. Glimm, J., " Solutions in the Large for Nonlinear Hyperbolic Systems of Equations," Comm. Pure Appl. Math. 18, pp. 697-715 (1965)

7. Dahlquist,G., and Bjork, A, Numerical Methods, Prentice-Hall Inc., New Jerssy, 1974

8. Lax, P. D., "Nonlinear Partial Differential Equations and Computing," Siam Rev. 11, pp. 7-19 (1969)

9. Liu, T. P., "Quasilinear Hyperbolic Systems," Comm. in Math. Physics 68, pp. 141-172 (1979)

10. Liu, T. P., "System of Quasilinear Hyperbolic Partial Differential Equations," Proceeding on Trends in Application of Pure Math. to Mech. (1979)

11. Liu, T. P., "Transonic Gas Flows in a Variable Area Duct," Preprint (1980)

12. Pereyra, V. and Lentini, M., PASVA3: An Adaptive Finite Difference FORTRAN program for First Order, Nonlinear, Ordinary Boundary Problems, Proc. Working Conf. on Codes for Boundary Value Problems in Ordinary Differential Equations, Houston, Texas, May 1978

13. Sod, G. A., "A Numerical Study of a Converging Cylindrical Shock," J. Comp. Phys. 27, pp. 1-31 (1978)

14. Taylor, G. I., "The Formation of a Blast Wave by a very Intense Explosion," Proc. Royal Soc. A201, pp.159-174, (1949)

15. Wendroff, B., "Shock propagation in Variable Area Ducts with Phase Changes: an Extension of Chisnell's Method," J. of Eng. Math., Vol. 11, No. 3, (1977)

16. Whitham,G. B., Linear and Nonlinear Waves, John-Wiley and Sons, New York (1974).